Jacek Wróbel

Mechanisms and modulation of NMDAR-dependent high-frequency oscillations in the rat olfactory bulb

PhD thesis

Completed in the Laboratory of Neuroinfromatics

of the Nencki Institute of Experimental Biology

Polish Academy of Sciences

SUPERVISOR:

Dr. Mark J. Hunt, Ph.D., D.Sc.

Warsaw, 2024

Acknowledgements

I would like to express my gratitude to all those who contributed to the completion of this thesis. In particular, I extend my thanks to:

Dr. Mark J. Hunt, Ph.D., D.Sc., my supervisor, for his guidance and scientific support.

Prof. Daniel K. Wójcik, Ph.D., D.Sc., head of the Laboratory of Neuroinformatics, for creating a friendly and stimulating scientific atmosphere in the Laboratory.

I am grateful to my **parents** for their constant support, and to my **brother** for his assistance with IT-related challenges.

My thanks go to all the individuals who offered their assistance and support along the way, with special gratitude to **Dr. Agnieszka Kępczyńska** for her expert help in processing the histological samples.

I would also like to thank the **National Science Centre (NCN)** for funding my research through grants: NZ4/03657, NZ4/03882, and NZ4/04051 (PI).

Abstract

NMDAR antagonists, particularly ketamine, have gained significant attention in clinical settings for their applications, especially in emerging treatments for depression, though their precise mechanisms of action remain incompletely understood. In preclinical research, NMDAR antagonists are used to model psychotic-like states, and are known to broadly influence brain rhythms in both animal and human models. Notably, NMDAR antagonists enhance the power of high-frequency oscillations (HFO), observed across species and in many brain regions. Recent studies have identified the olfactory bulb (OB) as a primary source of NMDAR-dependent HFO in the rat brain. This thesis builds on these findings to investigate the role of the OB in HFO generation, focusing on its input and output connections.

The starting point of my research was an observation that under ketamine-xylazine sedation in rats, HFO power in the OB attenuated when airflow to the nostrils was blocked. Building on this foundation, I investigated whether odours or enhanced intranasal airflow could influence HFO. My results showed that increased nares air pressure, but not odours, drove HFO in the OB. Next, to overcome the limitations of ketamine-xylazine sedation, I shifted the subsequent experiments to freely moving animals. In these experiments, I found that naris block attenuated NMDAR-dependent HFO power in the OB, as well as in the prefrontal cortex and ventral striatum. Additionally, fast sniffing entrained NMDAR-dependent HFO. Having shown that nasal input drives HFO in the OB, I next examined these oscillations in the piriform cortex (PC), the major projection pathway of the OB. I demonstrated that reversible inhibition of the OB attenuated NMDAR-dependent HFO power, both locally in the OB and in the PC. Given that the PC sends feedback projections to the OB, I inhibited the PC and observed a gradual reduction in NMDAR-dependent HFO power locally in the PC, with no changes in the OB. This suggests that the OB is the primary generator of NMDAR-dependent HFO, and that HFO observed in the PC, relies on this primary generator. The OB serves as the initial processing station in the olfactory pathway, where olfactory information is processed and dopamine plays a key role in this process. Therefore, I investigated the effects of D1R and D2R stimulation or inhibition on NMDAR-dependent HFO in the OB. My results show that the generation of NMDAR-dependent HFO is dopamine-independent; however, exogenous stimulation of D2R reduces both the power and frequency of this rhythm.

The results presented in this thesis underscore the critical role of the OB and nasal respiration in generating HFO following NMDAR antagonist administration. While NMDAR antagonists, particularly ketamine, are recognized for their neuropsychiatric effects, the underlying neuronal networks influenced by these compounds remain only partially understood. My findings indicate that, in the context of HFO, the OB is a key brain region impacted by NMDAR antagonists, which, along with downstream effects on corticostriatal areas, may at least partially contribute to the neuropsychiatric effects of these compounds.

Key words: HFO, olfactory bulb, NMDA receptor, dopamine receptor, ketamine, MK801

Streszczenie

Antagoniści receptora NMDA, w szczególności ketamina, są obiektem wzmożonego zainteresowania w badaniach klinicznych ze względu na swoje zastosowania, zwłaszcza w leczeniu depresji, chociaż ich dokładne mechanizmy działania nadal nie są wyjaśnione. Związki te, wykorzystywane są w badaniach przedklinicznych w celu modelowania stanów podobnych do stanów psychotycznych. Znany jest również ich wpływ na rytmy mózgowe, zarówno w modelach zwierzęcych, jak i u ludzi. Cechą charakterystyczną tych związków jest nasilanie mocy oscylacji wysokoczęstotliwościowych (HFO), które można zarejestrować u różnych gatunków zwierząt i w wielu obszarach mózgu. Ostatnie badania pozwoliły na zidentyfikowanie opuszki węchowej jako głównego źródła HFO nasilonych przez antagonistów receptora NMDA. Niniejsza dysertacja bazując na tych odkryciach, eksploruje rolę opuszki węchowej w generacji tych oscylacji, ze szczególnym uwzględnieniem jej połączeń wejściowych i wyjściowych.

Rozpocząłem swoje badania od obserwacji, że moc HFO ulega zanikowi w opuszce węchowej po zablokowaniu przepływu powietrza przez nozdrza szczura w stanie sedacji ketaminowo-ksylazynowej. Bazując na tej obserwacji, sprawdziłem czy prezentacja zapachów i nasilenie przepływu powietrza przez nozdrza wpływa na moc badanych oscylacji. Uzyskane rezultaty pokazały, że to zwiększone ciśnienie w nozdrzach, a nie zapachy napędzały badany rytm, zwiększając jego moc. Wszystkie następne eksperymenty przeprowadziłem na swobodnie poruszających się szczurach, aby uniknąć ograniczeń wynikających ze stanu sedacji. W tych eksperymentach pokazałem, że blokada nozdrzy skutkuje zanikiem mocy nasilonych HFO nie tylko w opuszce węchowej, ale również w korze przedczołowej i brzusznej części prążkowia, a przyśpieszone węszenie napędza badany rytm w opuszce. W następnych eksperymentach skupiłem się na HFO w korze gruszkowatej, która stanowi główny cel projekcji neuronalnych z opuszki węchowej. Pokazałem, że odwracalne zahamowanie aktywności opuszki, prowadzi do zaniku nasilonych HFO lokalnie w opuszce, jak i w korze gruszkowatej. Mając na uwadze, że kora gruszkowata wysyła połączenia zwrotne do opuszki, zahamowałem również aktywność kory gruszkowatej i zaobserwowałem stopniowy zanik mocy nasilonych HFO lokalnie w korze oraz brak zmian HFO w opuszce. Ten rezultat sugeruje, że opuszka jest głównym generatorem nasilonych HFO, a rytm ten występujący w korze gruszkowatej, zależy od aktywności głównego generatora w opuszce. Opuszka węchowa jest główną stacją przekaźnikową na szlaku węchowym, gdzie odbywa się procesowanie informacji węchowej. Dopamina odgrywa w tym procesie kluczową rolę, dlatego następnie zbadałem efekty stymulacji i hamowania receptorów dopaminowych na nasilone HFO rejestrowane w tej strukturze. Z uzyskanych rezultatów wynika, że generacja nasilonych HFO jest niezależna od dopaminy, jednak egzogenna stymulacja D2R redukuje moc i częstość tego rytmu.

Wyniki przedstawione w tej dysertacji, podkreślają krytyczną rolę opuszki węchowej i oddychania nosowego w generacji HFO po podaniach antagonistów receptora NMDA. Związki te, w szczególności ketamina, wywołują efekty neuropsychiatryczne, jednak nie jest do końca jasne jakie sieci neuronowe biorą udział w tym procesie. Moje rezultaty pokazują, że w kontekście HFO, opuszka węchowa jest kluczowym obszarem mózgu na który oddziałują antagoniści receptora NMDA, co biorąc pod uwagę ich dodatkowy wpływ na regiony kory i prążkowia, może przynajmniej częściowo, przyczyniać się do występowania efektów neuropsychiatrycznych.

Słowa kluczowe: HFO, opuszka węchowa, receptor NMDA, receptor dopaminowy, ketamina, MK801

Abbreviations

AMPH – (S)-amphetamine
ANOVA – analysis of variance
APO – R-(–)-apomorphine
ARI – aripiprazole
CFC – cross frequency coupling
D1R – dopamine D1 receptor
D2R – dopamine D2 receptor
DA – dopamine
DMSO – dimethyl sulfoxide
ECoG – electrocorticography
EEG – electroencephalography
ETI – eticlopride
Hal – haloperidol
HFO – high frequency oscillations
i.p. – intraperitoneal
inf. – infusion
Ket – (±)-ketamine
LFPs – local field potentials
LMA – locomotor activity
musc – muscimol
NAc – nucleus accumbens
NMDAR – N-methyl-D-aspartate receptor
OB – olfactory bulb
ON – olfactory nerve
OSN – olfactory sensory neurons
PC – piriform cortex
PFC – prefrontal cortex
Q – (–)-quinpirole
RIS – risperidone
SCH – R(+)-SCH23390
SKF – (R)-(+)-SKF38393
TTX – tetrodotoxin
VS – ventral stiatum
Xyl – xylazine

Contents

1 Introduction **1**
- 1.1 Psychopharmacology of NMDAR antagonists . . . 1
  - 1.1.1 NMDAR hypofunction model of psychotic-like states . . . 1
  - 1.1.2 Ketamine – NMDAR antagonist used in clinical practice . . . 3
  - 1.1.3 Ketamine affects brain activity . . . 4
- 1.2 Electrophysiology . . . 6
  - 1.2.1 Local field potentials . . . 6
  - 1.2.2 High frequency oscillations (HFO) . . . 7
  - 1.2.3 Pharmacology of NMDAR-dependent HFO . . . 8
  - 1.2.4 Basic characteristics of NMDAR-dependent HFO . . . 11
  - 1.2.5 NMDAR-dependent HFO in experimental animals . . . 11
  - 1.2.6 NMDAR-dependent HFO in various brain structures . . . 12
  - 1.2.7 NMDAR-dependent HFO and other brain rhythms . . . 13
  - 1.2.8 HFO in the olfactory bulb (OB) . . . 14
- 1.3 The OB network . . . 14
  - 1.3.1 The OB . . . 15
  - 1.3.2 Inputs and outputs of the OB . . . 18

2 Rationale and aims of the thesis **21**
- 2.1 Rationale . . . 21
- 2.2 Aims . . . 22

3 Methods **24**
- 3.1 Experimental animals . . . 24
- 3.2 Stereotaxic surgery . . . 25
- 3.3 Experimental procedures . . . 26
- 3.4 Brain preparation and histological analysis . . . 29
- 3.5 Signal processing and data analysis . . . 31
- 3.6 Statistical analysis and data visualization . . . 31

4 Results **33**
- 4.1 Role of nasal input in NMDAR-dependent HFO . . . 33
  - 4.1.1 Increased air pressure enhances Ket\Xyl-dependent HFO . . . 34
  - 4.1.2 Odour does not affect Ket\Xyl-dependent HFO . . . 35
  - 4.1.3 Ketamine triggers fast sniffing behaviour in rats . . . 37

4.1.4 Relationship between ketamine-dependent HFO and behaviour in rats . . . 39
4.1.5 Nasal respiration drives ketamine-dependent HFO in multiple brain regions . . . 41
4.2 The OB drives NMDAR-dependent HFO in the piriform cortex (PC) 41
4.2.1 MK801-dependent HFO in the OB and PC . . . 43
4.2.2 Reversible inhibition of the OB reduces MK801-dependent HFO in the OB and PC . . . 45
4.2.3 Reversible inhibition of the PC does not affect MK801-dependent HFO in the OB . . . 46
4.3 Role of DA receptors in NMDAR-dependent HFO in the OB . . . 48
4.3.1 Systemic DA receptor stimulation reduces MK801-dependent HFO frequency in the OB . . . 49
4.3.2 Local D2R, but not D1R, stimulation affects MK801-dependent HFO in the OB . . . 51
4.3.3 Local blockade of D1R or D2R antagonists does not affect MK801-dependent HFO in the OB . . . 53
4.3.4 Systemic blockade of D1R and D2R does not affect MK801-dependent HFO in the OB . . . 54
4.4 Exploratory investigations . . . 56
4.4.1 Local blockade of NMDAR in the OB increases HFO power . 56
4.4.2 Differential effects of a 2^{nd} and 3^{rd} generation antipsychotic drug on MK801-dependent HFO in the OB . . . 58

5 Discussion **60**
5.1 NMDAR-dependent HFO in the brain . . . 60
5.2 Generation of NMDAR-dependent HFO in the OB . . . 61
5.3 NMDAR-dependent HFO and nasal input . . . 63
5.4 D2R stimulation affects NMDAR-dependent HFO . . . 64
5.5 NMDAR-dependent HFO and behaviour . . . 66
5.6 Limitations of the study . . . 68
5.7 Functional relevance and future work . . . 69

6 Summary and conclusions **70**

A HFO review table **72**

B Bibliography **76**

C Publications of the PhD candidate **92**

List of Figures

1.1 Classification of glutamate receptors . . . 2
1.2 Ketamine blocks NMDAR . . . 4
1.3 Ketamine-dependent HFO in the OB . . . 9
1.4 Olfactory layers and cells in the OB . . . 16

3.1 OB section showing electrode tracks . . . 30

4.1 The power of Ket/Xyl-dependent HFO in the OB is enhanced by incerased airflow to the naris . . . 35
4.2 The power of Ket/Xyl-dependent HFO in the OB is not enhanced by four different odours . . . 36
4.3 Ketamine induces fast sniffing behaviour, which is reversed by haloperidol . . . 38
4.4 Ketamine increases the power of HFO in the OB which correlates with fast sniffing and LMA . . . 40
4.5 Naris blockade reduces the power of ketamine-dependent HFO in the OB, VS and PFC in freely moving rats . . . 42
4.6 Comparison of the power and modulation of MK801-dependent HFO recorded in the OB and PC in freely moving rats . . . 44
4.7 Effect of muscimol infusion to the OB on the power of MK801-dependent HFO in the OB and PC in freely moving rats . . . 46
4.8 Effect of muscimol or TTX infusion to the PC on the power of MK801-dependent HFO in the OB and PC in freely moving rats . . . 47
4.9 Systemic DA receptor stimulation reduces MK801-dependent HFO frequency, but not power, in the OB *via* a D2R mechanism . . . 50
4.10 Local infusion of quinpirole, but not SKF38393 to the OB reduces the power and frequency of MK801-dependent HFO in freely moving rats . . . 52
4.11 Examples of fluorescent SKF83566-green infusion to the OB . . . 53
4.12 Local OB infusion of SCH23390 or eticlopride does not affect the power or frequency of MK801-dependent HFO in freely moving rats . . . 54
4.13 Systemic coadministration of SCH23390 and eticlopride does not affect MK801-dependent HFO power and frequency, but reduces LMA . . . 55
4.14 Systemic vs local NMDAR blockade in the OB: effects on MK801-dependent HFO power and LMA . . . 57
4.15 Risperidone, but not aripiprazole, reduces MK801-dependent HFO frequency and LMA . . . 59

Chapter 1

Introduction

The research presented in this thesis integrates the fields of experimental psychopharmacology and *in vivo* electrophysiology, with a specific focus on the olfactory bulb. This introduction will provide an overview of these three core topics, laying the groundwork for the subsequent chapters.

1.1 Psychopharmacology of NMDAR antagonists

Research in psychopharmacology provides critical insights into the effects of drugs on higher brain functions. Additionally, these studies play a crucial role in improving existing medications and creating new treatments for psychiatric disorders like anxiety, depression, and psychosis (Simola, 2022). The research in this thesis focuses on the effects of N-methyl-D-aspartate receptor (NMDAR) blockade on brain activity, a topic that will be further elaborated in the following section, with particular emphasis on ketamine as a key representative of NMDAR antagonists.

1.1.1 NMDAR hypofunction model of psychotic-like states

Glutamatergic neurotransmission in the central nervous system is controlled by metabotropic and ionotropic glutamate receptors (see Figure 1.1).

Among the ionotropic receptors, NMDAR functions as a ligand-gated ion channel that permits the flow of cations. NMDAR is characterized by a voltage-dependent

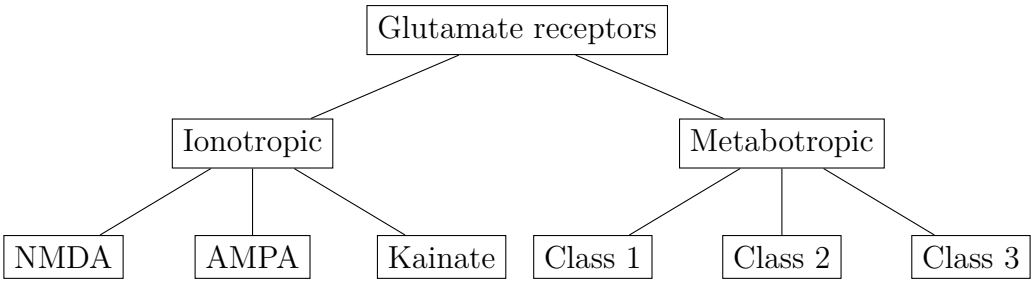

Figure 1.1: **Classification of glutamate receptors.**

Mg^{2+} block, high permeability to Ca^{2+}, and the requirement for the co-agonists glycine and glutamate to bind simultaneously for activation. These distinctive features set NMDAR apart from other glutamatergic ionotropic AMPA and kainate receptors (collectively known as non-NMDAR), and significantly influence their physiological functions in the central nervous system (Hansen et al., 2017). NMDAR is a large multi-subunit complex organized into heteromeric assemblies consisting of four homologous subunits selected from a repertoire of over 10 types: 8 GluN1 isoforms, 4 GluN2 subunits (A–D), and 2 GluN3 subunits (A and B) (Paoletti, 2011).

Several compounds block NMDAR channel through use-dependent and voltage-dependent mechanisms. These compounds include dissociative anaesthetics such as phencyclidine (PCP), dizocilpine (MK801) and ketamine (Monaghan and Jane, 2009). In experimental psychopharmacology, all these NMDAR antagonists are employed as pharmacological models for studying psychotic-like states (Mouri et al., 2007; Manahan-Vaughan et al., 2008; Frohlich and Van Horn, 2014), supporting the hypothesis that the glutamatergic system is underactive in schizophrenia (Javitt, 1987). This concept developed into the NMDAR hypofunction model of schizophrenia after the identification of NMDAR involvement (Olney and Farber, 1995) and was further substantiated by molecular evidence demonstrating reduced expression of specific NMDAR subunits, such as NR1 and NR2C, in *post-mortem* brains of individuals with schizophrenia (Weickert et al., 2013).

Two meta-analyses highlight the utility of NMDAR antagonists in modeling schizophrenia-like symptoms in both experimental animals and humans. Lee and Zhou demonstrated that NMDAR antagonists elicit a comprehensive spectrum of

behaviors corresponding to schizophrenia symptoms, with particularly pronounced effects on behaviors related to negative and cognitive symptoms. Notably, some behavioral deficits induced by NMDAR antagonists were reversed by antipsychotic drug administration (Lee and Zhou, 2019). Similarly, a meta-analysis conducted by Beck encompassing 36 studies with 725 healthy participants found that acute ketamine administration, compared to placebo, significantly increased positive and negative psychotic symptoms as assessed by the Brief Psychiatric Rating Scale or the Positive and Negative Syndrome Scale in both healthy individuals and patients with schizophrenia (Beck et al., 2020). These findings underscore the relevance of NMDAR antagonists as valuable tools in preclinical and clinical neuropsychiatric research.

1.1.2 Ketamine – NMDAR antagonist used in clinical practice

Ketamine is the most commonly used NMDAR antagonist in clinical settings and has a wide range of applications. Initially, it was used primarily as an anaesthetic (Miyasaka et Domino, 1968); however, its use in this role has diminished due to its psychosis-mimetic properties. Today, ketamine is also employed in the treatment of various psychiatric conditions, including obsessive-compulsive disorder and post-traumatic stress disorder (Rodriguez et al., 2011; Bandeira et al., 2022), with its most significant clinical application being in the treatment of depression (Yavi et al., 2022; Krystal et al., 2024).

The growing body of research on ketamine's antidepressant effects (Nikolin et al., 2023) stems from its initial discovery of efficacy in patients with treatment-resistant depression following intravenous administration at subanesthetic doses (Berman et al., 2000). Clinical trials have consistently demonstrated its rapid and effective reduction of depressive symptoms (Mandal et al., 2019; Bahji et al., 2022), likely due to its unique modulation of the glutamatergic system, which distinguishes it from traditional pharmacological treatments (Krystal et al., 2024).

Additionally, ketamine's availability as a nasal spray (marketed as Spravato) offers a convenient alternative to oral or injectable administration for patients (Bahr et al., 2019). Spravato contains the S-(+)-enantiomer of ketamine, which has shown greater efficacy compared to the R-(–)-enantiomer (Bonaventura et al., 2021). This formulation provides rapid onset of action compared to traditional antidepressants (Daly et al., 2019). However, patients must first demonstrate resistance to at least two conventional antidepressants before qualifying for ketamine-based treatment.

1.1.3 Ketamine affects brain activity

Ketamine primarily targets NMDAR, acting as a non-competitive antagonist by binding to a unique site within the receptor's pore, thereby inhibiting ion flow across the membrane (Orser et al., 1997) (see Figure 1.2). Although ketamine can also interact with AMPA and kainate receptors, its affinity for these is much lower compared to NMDAR (Mion and Villevieille, 2013). Under normal conditions, the NMDAR channel is blocked by Mg^{2+} ions, which prevent activation. Upon depolarization, Mg^{2+} ions are displaced, permitting the passage of Na^{+}, K^{+}, and Ca^{2+} ions. Other compounds, such as PCP and MK801, also block NMDAR, eliciting effects similar to those induced by ketamine (Contreras et al., 1987; Kovacic and Somanathan, 2010).

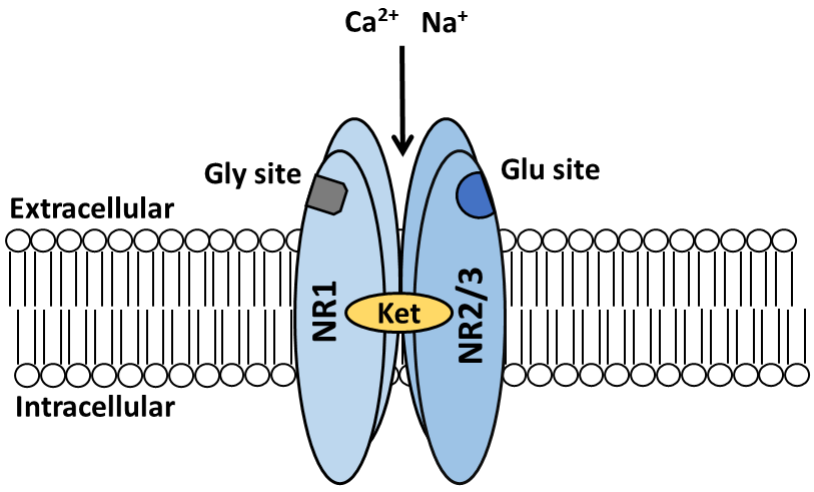

Figure 1.2: **Ketamine blocks NMDAR.** Ketamine as a non-competitive antagonist blocks pore of the NMDAR. Legend: Ket - ketamine, Gly - glycine, Glu - glutamate.

The pharmacology of ketamine is highly complex, stemming from its ability to interact not only with glutamate receptors, but also with various other receptor types, ion channels, and enzymes (Sleigh et al., 2014). Beyond its well-known effects on glutamatergic receptors, ketamine engages with delta (δ), kappa (κ), and mu (μ) opioid receptors (Grunebaum et al., 2020), as well as muscarinic (Durieux, 1995) and nicotinic acetylcholine receptors (Harper et al., 2020). It modulates serotonin 5-HT3 receptors, acting as a potentiator (Peters et al., 1991), and interacts with other serotonin receptors, including 5-HT1A and 5-HT2A, along with dopamine (DA) D2 receptors (D2R) (Martin et al., 1982; Kapur and Seeman, 2002). Additionally, ketamine acts as an antagonist at neurokinin-1 receptors, blocking the binding of the neuropeptide substance P (Yamaguchi et al., 2017), and inhibits neuronal acetylcholine receptor subunit alpha-7 activity (Kohrs and Durieux, 1998). It has also been demonstrated that cyclic nucleotide-gated channels, which are activated by hyperpolarization and play a crucial role in various physiological functions (Sartiani et al., 2017), mediate some of the effects of ketamine. Previous research have identified these channels as targets of ketamine's action (Chen et al., 2009; Zhang et al., 2016), and other groups have suggested that antagonism of these channels is critical for the functional effects of ketamine (Subramanian et al., 2022). This is supported by findings showing that ketamine has a significantly weaker impact on knockout animals in which these channels are inactive (Cai et al., 2023).

Additionally, ketamine can inhibit several enzymes, including cholinesterase (Schuh, 1975), and act as an inhibitor of the sodium-dependent noradrenaline transporter (López-Gil et al., 2019). It has been shown that after ketamine administration, brain-derived neurotrophic factor, a protein crucial for synaptic plasticity, and mammalian target of rapamycin, an enzyme essential for translation, are upregulated (Silva Pereira et al., 2017), which is linked with neuroplasticity processes (Zhou et al., 2014). Furthermore, their expression can be influenced by cyclic nucleotide-gated channels (Ni et al., 2020), suggesting that ketamine may exert its effects by targeting different components of the same molecular pathways.

1.2 Electrophysiology

Electrophysiology is the study of the electrical properties of cells, including membrane potentials, action potentials, and the ion channels and proteins that give cells their electrical characteristics. Electrophysiology techniques, which allow direct measurement of electrical phenomena, facilitate understanding of the nervous system, as electrical signalling forms the basis of neural communication (Carter et al., 2022).

Intracellular and whole cell patch-clamp electrophysiology techniques involve measuring voltage and/or current across a cell membrane. These methods provide insights into the molecular and cellular mechanisms that enable different neurons to exhibit unique physiological properties. Extracellular electrophysiology techniques, such as single-unit recording, multi-unit recording, and local field potentials (LFPs), along with electroencephalography (EEG), electrocorticography (ECoG), and magnetoencephalography, are employed to explore system-level questions. These techniques help investigate the functions of neurons within neural circuits, their roles in regulating behaviour, and the importance of synchronized neuronal activity (Wickenden, 2014; Carter et al., 2022).

The research presented in this thesis is based on extracellular recordings of LFPs. To provide a clearer understanding, the next section will introduce the LFPs.

1.2.1 Local field potentials

LFPs measurement is a valuable technique in neuroscience for capturing brain oscillations and understanding the neural dynamics underlying various brain processes (Herreras, 2016). This technique involves the insertion of microelectrodes into neural tissue, allowing for the recording of electrophysiological signals from deep brain structures, such as the basal ganglia (Brown and Williams, 2005). LFPs represent the extracellular electrical potential, reflecting the combined activity of many neurons within a localized area, typically a few hundred micrometers to several millimeters from the electrode tip (Łęski et al., 2010; Hunt et al., 2011; Kajikawa and

Schroeder, 2011). While LFPs offer insights into specific brain regions and broader network dynamics, they lack the spatial resolution to distinguish individual neuron activity (Buzsáki, 2012).

LFPs capture oscillatory activity across a broad frequency spectrum, which can be divided into bands linked to various cognitive and behavioral functions (Buzsáki and Watson, 2012). Slower oscillations, like delta (0.5-4 Hz), are associated with restorative processes and memory consolidation (Kim et al., 2019), while theta (4-8 Hz) is linked to spatial navigation and memory retrieval (Herweg et al., 2020). Faster oscillations, such as alpha (8-12 Hz) and beta (12-30 Hz), are connected to attention and concentration (Pitchford and Arnell, 2019), while gamma (30-100 Hz) and oscillations above 100 Hz are believed to support higher cognitive functions (Başar et al., 2013). LFPs are widely used to investigate the role of brain oscillations in various cognitive and sensory processes (Belitski et al., 2010; Wimmer et al., 2016) and allow to analyze the power and phase relationships of oscillations in different frequency bands to understand how brain regions communicate and synchronize (Murthy and Fetz, 1996; Gallego-Carracedo et al., 2022).

Because LFPs contain signals from multiple sources, filtering techniques are essential to isolate specific frequency bands (Geddes et al., 2020). This approach allows researchers to focus on specific oscillatory activity and differentiate meaningful neural signals from noise (Magri et al., 2012). However, LFPs recordings are susceptible to artifacts, such as those arising from muscle movements, eye blinks, or cardiac activity, as well as electrical noise from surrounding equipment (Hammer et al., 2022). These artifacts can be minimized using advanced signal processing techniques, which enhance the quality of the recorded data and improve the reliability of the findings (Debarros et al., 2020).

1.2.2 High frequency oscillations (HFO)

The categorization of HFO in the literature is often subjective, with varying definitions for terms like high-gamma (Ray et al., 2008a, b), leading to inconsistent

and not fully established terminology. However, distinct types of high-frequency oscillatory activity can still be identified. For instance, oscillations faster than high gamma originating from the somatosensory cortex (>300 Hz) can be divided into early and late bursts, which respond differentially to glutamatergic receptor antagonists (Ozaki and Hashimoto, 2011), and indicates that these distinct high-frequency oscillatory patterns may reflect specific neural mechanisms influenced by the modulation of glutamatergic signalling. Additionally, hippocampal recordings reveal specific high-frequency activity during slow-wave sleep, such as oscillations in the 150–200 Hz range (Olivia et al., 2018) or around 200 Hz "ripples" (Wilson and McNaughton, 1994; Siapas and Wilson, 1998), which are crucial for episodic memory and planning (Buzsáki, 2015). Furthermore, high-frequency activity in the 80–500 Hz range is associated with cortical seizure-like states and can be observed in seizure-generating limbic areas in animal models (e.g., rats made epileptic *via* intra-hippocampal injection of kainic acid) as well as in patients with mesial temporal lobe epilepsy (Bragin et al., 1999; Park and Hong, 2019).

The primary focus of this thesis is a type of HFO, typically observed in the 130–180 Hz range, whose power is enhanced after NMDAR antagonists. This activity is referred to throughout the thesis as NMDAR-dependent HFO.

1.2.3 Pharmacology of NMDAR-dependent HFO

In 2006, MJ Hunt observed that the power of HFO in a specific band around 150 Hz, recorded from the rat nucleus accumbens (NAc), was enhanced following ketamine (10, 25, and 50 mg/kg) administration in a dose-dependent manner. Ketamine produced an inverted U-shaped dose-response for HFO, with doses up to 25 mg/kg leading to progressively greater increases in HFO power, while higher doses produced biphasic effects (Hunt et al., 2006). In many brain regions, HFO exist as a low-amplitude, spontaneous endogenous rhythm, and ketamine enhances this activity rather than inducing it (Figure 1.3). This suggests that HFO play a more significant role in pathophysiological conditions than in physiological states.

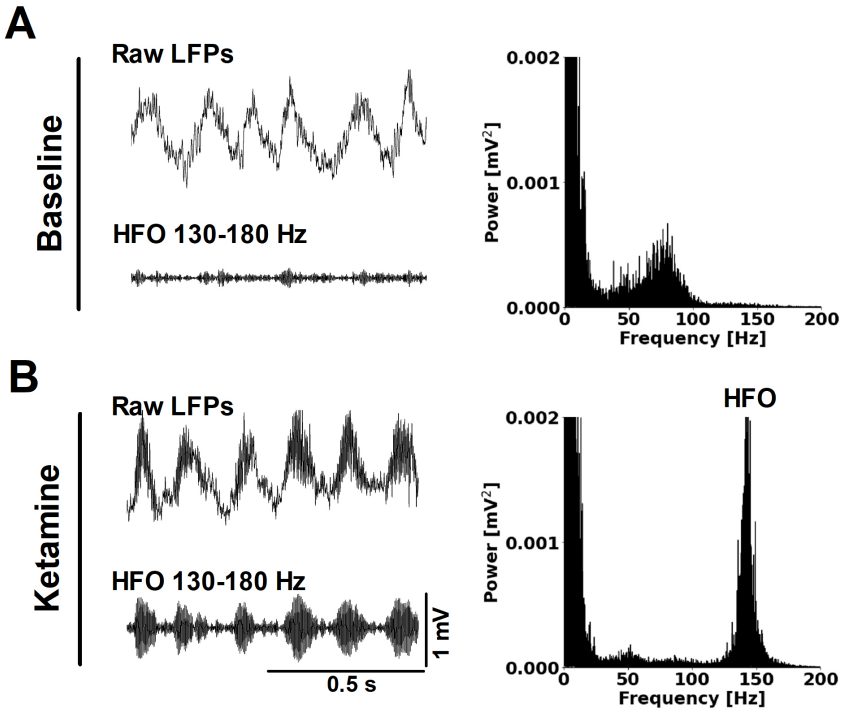

Figure 1.3: **Ketamine-dependent HFO in the OB.** Fragments of raw LFPs and 130-180 Hz filtred signal and corresponding power spectra (60s) for **(A)** baseline and **(B)** after systemic injection of 20 mg/kg ketamine. The increase in HFO power following NMDAR antagonists administration is evident across multiple brain structures (for further details, see the Table A.1 in Appendix A).

The increase in HFO power following ketamine administration has been consistently observed across multiple independent research groups worldwide (e.g., Hakami et al., 2009; Nicolas et al., 2011; Philips et al., 2012; Kulikova et al., 2012). Other non-competitive NMDAR antagonists like MK801 and PCP have also been shown to enhance HFO power in the brain (Hunt et al., 2006; Hakami et al., 2009; Philips et al., 2012; Hiyoshi et al., 2014). The dose-dependent effect of NMDAR antagonists on HFO has been confirmed for ketamine (e.g., Nicolas et al., 2011; Caixeta et al., 2013; Hansen et al., 2019), MK801, and PCP (e.g., Hakami et al., 2009; Hiyoshi et al., 2014; Hunt et al., 2015; Amat-Foraster et al., 2019), with a biphasic effect observed at higher doses (Hiyoshi et al., 2014; Flores et al., 2015).

MK801, a more selective NMDAR antagonist, induces a prolonged increase in HFO (Hakami et al., 2009), due to its higher binding affinity at NMDAR (Bresink et al., 1995). The temporal effects of ketamine and PCP also differ, with ketamine effects peaking earlier than those of PCP (Amat-Foraster et al., 2019). Evidence

on memantine's (other NMDAR antagonist) effects on HFO is mixed: one study reported an increase in HFO power with memantine (Hiyoshi et al., 2014), whereas another found no effect (Mao et al., 2020). One study demonstrated that the competitive NMDAR antagonist SDZ 220,581 produces a comparable increase in HFO power to that observed with non-competitive NMDAR antagonists (Phillips et al., 2012).

The essential role of NMDAR in HFO generation is highlighted by studies showing that ketamine administration significantly increases cortical HFO power in Sp4 hypomorphic mice, which have reduced NR1 protein expression (Ji et al., 2013). Pittman-Polletta and colleagues further demonstrated that specific NMDAR subunits contribute to HFO modulation: the NR2A-preferring antagonist (NVP-AAM077) can replicate the cortical HFO power changes observed after MK801, whereas the NR2B antagonist (Ro25-6985) does not (Pittman-Polletta et al., 2018). Additionally, the importance of NMDAR subunit specificity is underscored by findings in GluN2D knockout mice, which exhibit exaggerated ketamine-induced HFO power relative to controls (Sapkota et al., 2016; Mao et al., 2020).

It is also notable that previous studies have shown that serotonergic agents, primarily acting through 5-HT2 receptor agonism – such as lysergic acid diethylamide, 2,5-Dimethoxy-4-iodoamphetamine, TCB-2, and CP 80910 – enhance HFO in the brain. However, the HFO power and frequencies induced by these agents are generally lower than those triggered by NMDAR antagonists (Goda et al., 2013; Hansen et al., 2019; Brys et al., 2023). Serotonergic psychedelics, unlike their non-psychedelic counterparts, appear to reduce NMDAR currents, which may play a role in their impact on HFO power (Arvanov et al., 1999). Nonetheless, this thesis specifically focuses on HFO whose power is enhanced by NMDAR antagonists.

1.2.4 Basic characteristics of NMDAR-dependent HFO

A prominent effect of NMDAR antagonists is increased locomotor activity (LMA) (Liljequist et al., 1991). HFO increases typically emerge at doses that also induce locomotion changes, and most studies report positive correlations between HFO power and LMA (e.g., Hakami et al., 2009; Caixeta et al, 2013; Ye et al, 2018). However, NMDAR-dependent HFO is unlikely to be causally related to locomotion (Hunt et al., 2006; Hansen et al., 2019). For example, cataleptic doses of DA antagonists attenuate LMA increases, but do not affect HFO increases following NMDAR antagonism (Matulewicz et al., 2010; Ye et al., 2018). Additionally, amphetamine, which increases LMA, does not significantly affect HFO (Hunt et al., 2006; Hansen et al., 2019; Brys et al., 2023). Antipsychotics that induce catalepsy also do not reduce the power of NMDAR-dependent HFO (Olszewski et al., 2013b).

An anaesthetic dose of ketamine is associated with attenuation of HFO, which rebounds as the animal's righting reflex recovers (Hunt et al., 2006, 2019; Średniawa et al., 2021). NMDAR-dependent HFO is generally considered a wake-dependent rhythm, as it does not induce increases in HFO power in animals under other anaesthetics, such as isoflurane, pentobarbital, urethane, or propofol (Hunt et al., 2009; Średniawa et al., 2021). However, that under ketamine-xylazine (Ket/Xyl) sedation, HFO can still be recorded (Średniawa et al., 2021), that shares key features with wake-related activity, though its frequency is substantially lower.

1.2.5 NMDAR-dependent HFO in experimental animals

The most commonly used experimental animals used in studies examining NMDAR-dependent HFO are rodents, particularly rats (e.g., Hunt et al., 2006; Flores et al., 2015; Pittman-Polletta et al., 2018; Bowman et al., 2022) and mice (e.g., Hunt et al., 2015; Sapkota et al., 2016; Maheshwari et al., 2017; Mao et al., 2020; Sokolenko et al., 2019). Large amplitude HFO can also be recorded under Ket/Xyl sedation in cats (Średniawa et al., 2021), which was later confirmed in awake cats after ketamine by another research group (Castro-Zaballa et al., 2024). Notably, HFO

power in cats recorded in both sedative and awake conditions was sensitive to naris blockade, consistent with findings from rodent studies (Hunt et al., 2019; Średniawa et al., 2021). Ketamine-induced increases in fast oscillations have also been observed in the large mammal sheep, with a frequency around 100 Hz (Nicol and Morton, 2020). One study employing ECoG in monkeys reported an increase in HFO power in cortical areas following ketamine administration (Yan et al., 2022), while another study yielded inconclusive results (Skoblenick et al., 2016).

Recently, Nottage and colleagues reported that both ketamine and d-cycloserine induced broadband increases in HFO rhythm in frontal and parietal EEG recordings, with the increase occurring during the peak of ketamine exposure (Nottage et al., 2023). This is the only study to date reporting HFO following ketamine administration in humans. Altogether, these results demonstrate that NMDAR-dependent HFO can be recorded across different species, suggesting that they are an inter-species phenomenon, however further studies using deep electrode recordings are warranted.

1.2.6 NMDAR-dependent HFO in various brain structures

Since the initial observation of ketamine-dependent HFO in the NAc (Hunt et al., 2006), this brain region has remained a primary focus of research (Hunt et al., 2006, 2008, 2010, 2015; Lee et al., 2017; Ye et al., 2021). However, many laboratories have reported NMDAR-dependent HFO in various other brain regions (see Table 1.1), including both cortical and subcortical areas (e.g., Hakami et al., 2009; Nicolas et al., 2011; Cordon et al., 2015). Other areas where ketamine-induced HFO has been consistently observed, albeit generally with lower amplitude than in the NAc, include the prefrontal cortex (Lee et al., 2017; Amat-Foraster et al., 2019; Hansen et al., 2019; Sokolenko et al., 2019), other cortical regions such as motor cortex, visual cortex (Cordon et al., 2015; Flores et al., 2015; Pittman-Polletta et al., 2018; Ye et al., 2018;), hippocampus (Hunt et al, 2010; Caixeta et al, 2013; Lee et al., 2017), subcortical structures such as caudate (Nicolas et al, 2011; Olszewski et al, 2013a;

Cordon et al, 2015), thalamus (Hansen et al, 2019) or striatum (Ye et al., 2018). Frontostriatal structures were often targeted as they broadly fitted the networks that might be associated with ketamine's psychoactive effects. However, in 2019, we unexpectedly observed that ketamine-dependent HFO could also be recorded in the olfactory bulb (OB), at an order of magnitude larger than in any other area reported at that time (Hunt et al., 2019).

Publication	**NMDAR antagonist**	**Structures**
Hunt et al., 2006	Ket, MK801	NAc
Hakami et al., 2009	Ket, MK801	basal ganglia
Hunt et al., 2011	Ket	NAc, Hip, striatum
Cordon et al., 2015	Ket	basal ganglia
Maheshwari et al, 2016	MK801	SomCtx
Sapkota et al, 2016	Ket	RetCtx
Kealy et al, 2017	PCP, Ket, MK801	Hip, striatum
Hunt et al, 2019	Ket	OB, VS
Wróbel et al, 2020	Ket	OB, PFC, VS
Ye et al, 2021	Ket	NAc, striatum, MotCtx
Cui et al., 2022	MK801	PFC, Hip
Georgiou et al, 2022	Ket, MK801	FrCtx
Castro-Zabala et al, 2024	Ket	OB, PFC, ParCtx

Table 1.1: **Examples of brain structures in which NMDAR-dependent HFO have been recorded.** Legend: FrCtx – frontal cortex, Hip – hippocampus, Ket – ketamine, MotCtx – motor cortex, NAc – nucleus accumbens, PFC – prefrontal cortex, RetCtx – retrospenial cortex, SomCtx – somatosensory cortex, VS – ventral striatum. For a more detailed review, refer to the Table A.1 in Appendix A.

1.2.7 NMDAR-dependent HFO and other brain rhythms

Cross-frequency coupling (CFC) refers to the correlation between the phase or amplitude of oscillations in one frequency band with those in another bands e.g. theta-gamma (Lisman and Jensen, 2013; Tort et al., 2009). This interaction is essential for coordinating neural activity and facilitating brain information processing (Canolty and Knight, 2010).

NMDAR antagonists have been shown to modulate CFC between low rhythms and HFO. For instance, studies have reported that NMDAR antagonism enhances delta-HFO coupling in the striatum (Ye et al., 2018), while other work observed theta phase modulation of HFO in the hippocampus (Caixeta et al., 2013). Additionally, MK801 potentiates theta-HFO coupling, while NR2A antagonism reduces

it (Pittman-Polletta et al., 2018). Other groups reported decreases in theta with HFO emergence and a reduction in beta activity associated with increased HFO after NMDAR antagonist administration (Zepeda et al., 2022; Amat-Foraster et al., 2019). Overall, these results demonstrate that slow rhythms can modulate NMDAR-dependent HFO in various ways across different brain structures.

1.2.8 HFO in the olfactory bulb (OB)

In 2019, our research group identified the OB as a primary source of NMDAR-dependent HFO. Simultaneous recordings in the OB and the ventral striatum (VS), which includes regions such as the NAc (Cansler et al., 2020), showed that ketamine-dependent HFO were significantly stronger in the OB (around 10 fold) than in the VS in freely moving rats. Furthermore, Granger causality analysis revealed that ketamine-enhanced HFO in the OB preceded those occurring in the VS, suggesting that the HFO generator in the OB drives the HFO observed in the VS. This finding was further supported by experiments in which intra-bulbar infusion of a GABA-A agonist muscimol attenuated HFO power locally in the OB and also reduced HFO in the VS (Hunt et al., 2019). In experiments using anaesthetic doses of ketamine (200 mg/kg) or Ket/Xyl sedation (Ket: 100 mg/kg+Xyl: 10 mg/kg), HFO exhibited a lower frequency ($\sim$115 Hz). It was shown that HFO rhythms – those arising during recovery from ketamine anaesthesia and Ket/Xyl-dependent HFO – are sensitive to airflow through the nares. Blocking airflow in one naris resulted in a reduction of HFO power on the ipsilateral side of the OB, while the contralateral OB remained unaffected (Hunt et al., 2019; Średniawa et al., 2021).

1.3 The OB network

Given that all the experiments conducted by me and presented in this thesis are related to the OB, the following sections will provide a characterization of the OB, including its inputs and outputs.

1.3.1 The OB

The OB serves as the first relay station for olfactory information in the brain, where sensory input is processed and integrated, leading to the formation of olfactory representations (Mori et al., 1999). It is a neuroanatomically well-isolated and evolutionarily conserved structure (Tufo et al., 2022), composed of several distinct layers. Olfactory nerve layer is the outermost layer, where the axons of olfactory sensory neurons (OSN) enter the OB and make initial contact (Aroniadou-Anderjaska et al., 1997). Glomerular layer contains spherical structures called glomeruli, which are essential for processing and integrating olfactory information (Su et al., 2009). Within the glomerular layer, collateral inhibition, where the activity of a neuron is weakened by neighbouring neuron, plays a crucial role in sharpening odour representations and enhancing odour discrimination (Shao et al., 2012). The mitral cell layer contains the cell bodies of mitral cells (and some tufted cells), which receive input from OSN *via* the glomeruli and project to higher olfactory centers (Economo et al., 2016). External plexiform layer and internal plexiform layer surround the mitral cell layer and are rich in interneurons that contribute to collateral inhibition and further processing of olfactory signals (Burton et al., 2017). Granule cell layer, the innermost layer of the OB, contains the cell bodies of granule cells, which receive input from mitral and tufted cells and provide feedback inhibition *via* dendro-dendritic synapses, playing a key role in shaping the spatial and temporal patterns of mitral and tufted cell output (Egger et al., 2003).

Since the 1970s, it has been known that each layer of the OB contains specific types of cells (Price and Powell, 1970a, b). Nagayama et colleagues provided a more detailed classification of OB cell types, describing three main categories: juxtaglomerular, mitral/tufted, and granule cells (Nagayama et al., 2014). Juxtaglomerular cells can be subdivided into three types: periglomerular, external tufted and superficial short-axon cells. Molecular heterogeneity allows for a more detailed classification within these groups, such as periglomerular type I and II, external tufted cells with or without secondary dendrites, and short-axon cells categorized

into classic and HT+/GAD67+ types. Mitral and tufted cells can be divided into subclasses based on dendritic and axonal characteristics. Mitral cells are classified into type I and II, while tufted cells are further divided into middle and internal subtypes. Granule cells can be classified into types I–V and type-S, reflecting morphological and functional diversity. Additionally, deep short-axon cells are classified based on their location within the layers of the OB, including glomerular, external plexiform and granule cell layer (Nagayama et al., 2014). For a schematic representation of the connections between these cells and their localization in specific layers, see Figure 1.4.

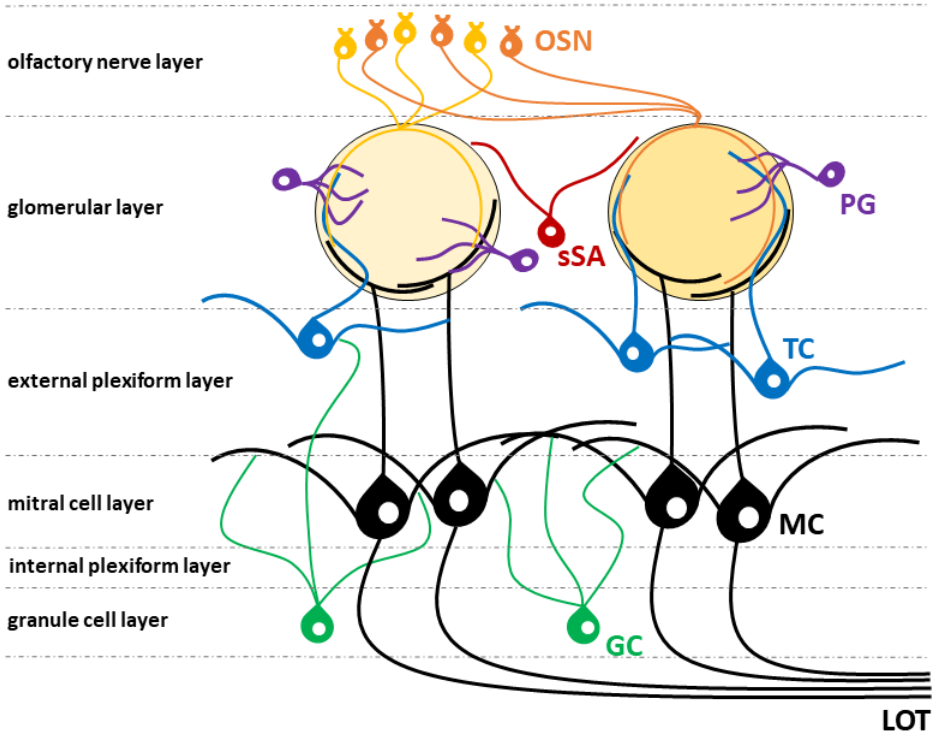

Figure 1.4: **Olfactory layers and cells in the OB.** The OB, composed of multiple olfactory layers, contains distinct types of cells specialized for processing sensory input. Legend: GC - granule cell, LOT - lateral olfactory tract, MC - mitral cell, OSN - olfactory sensory neurons, PG - periglomerular cell, sSA - superficial short-axon cell, TC - tufted cell (based on Nagayama et al., 2014).

The OB's activity is periodically modulated by respiration; the phasic activity of bulbar neurons is closely linked to nasal airflow (Ravel et al., 1987). This modulation means that the rate of olfactory perception is influenced by the generation and maintenance of the respiratory rhythm, so respiratory-driven oscillations play a crucial role in the temporal organization of olfactory processing in the OB and

other structures (Sheriff et al., 2021). These is associated with the rat's behavioural state, such as during odour discrimination or exploration of novel odorants, and correspond to different sniffing rates - slow or fast sniffing (Kepecs et al., 2007).

The OB, like other brain regions, exhibits oscillatory activity across various brain rhythms (Kay et al., 2009). Neuronal oscillations' synchronization is believed to play a crucial role in coordinating information flow between distant brain regions (Ward, 2003), with numerous examples of such coordination between the OB and other brain structures. For example, Gourévitch and colleagues showed strong unidirectional coupling from the OB to dorsal and ventral hippocampus, indicating that, during odour processing, beta oscillations in the hippocampus are driven by the OB (Gourévitch et al., 2010). This was supported by research by Lockmann and colleagues has demonstrated that the OB and hippocampus exhibit synchronized oscillations in this frequency range. This synchrony supports communication between these two structures, potentially enhancing the integration of olfactory and memory-related information (Lockmann et al., 2018). In other research it has been shown that OB drives neuronal and network activity in the lateral entorhinal cortex, and also subsequently, hippocampus and prefrontal cortex *via* long-range projections from mitral cells to hippocampal-projecting entorhinal cortex neurons in neonatal development (Kostka et al., 2023).

An example of a faster brain rhythm that has been extensively studied in the OB is the gamma rhythm (Mori et al., 2013). Gamma activity in the OB arises from interactions between excitatory mitral cells and inhibitory granule cells at the dendro-dendritic reciprocal synapse, which play a central role in generating these oscillations (Rojas-Líbano and Kay, 2008). Most research suggests that the frequency of gamma oscillations is heavily influenced by the decay time of inhibitory inputs from granule cells, which shapes the dynamics of the network. However, alternative mechanisms have been proposed, such as the interaction of subthreshold oscillations in the membrane potential of mitral cells with the inhibitory effects of granule cells, contributing to the emergence of gamma rhythms in the OB (Brea

et al., 2009). Gamma oscillations in the OB are thought to play a key role in fine odour discrimination (Beshel et al., 2007; Lepousez and Lledo, 2013).

It has been proposed that gamma activity in the OB can be categorized into two distinct types based on their behavioural associations and synaptic origins (Kay, 2003): Type I (high gamma, 65-100 Hz) which is correlated with the sniff cycle and typically begins at the peak of inhalation, the most prominent during exploratory behaviour, but also present during resting states and trained odour discrimination tasks. High gamma is believed to support the encoding of olfactory information during active sensing; Type II (low gamma, 35-65 Hz), in contrast, is not strongly linked to the sniff cycle and is inhibited by the onset of sniffing. It becomes more prominent during states of alert immobility, suggesting a different functional role from high gamma (Kay, 2003). Gamma oscillations in the OB have also been shown to couple with gamma activity in other brain regions, such as the entorhinal cortex (Salimi et al., 2021) and the hippocampus (Leung et al., 2024), which may facilitate the integration of olfactory information with memory-related processes.

1.3.2 Inputs and outputs of the OB

The main olfactory input to the OB is provided by the olfactory nerve (ON), whose terminals form direct connections with cells located in the glomerular layer (Greer, 1991). The primary role of the ON is to transfer odour information from the odorant receptors to the OB (Mathews, 1974). These receptors are located on the cilia of OSN, which are bipolar cells with small-diameter, unmyelinated axons originating from the olfactory epithelium (Purves et al., 2001). OSN generate diverse response patterns, thereby enhancing the dimensionality of the olfactory coding space (Kim et al., 2023). OSN can detect two distinct types of stimuli: chemical and mechanical. Mechanical responses are directly correlated with the intensity of pressure and exhibit characteristics similar to those induced by chemical odorants, such as onset latency, reversal potential, and adaptation to repeated stimulation (Grosmaitre et al., 2007). This ability to respond to multiple stimulus modalities highlights the

complexity and versatility of olfactory sensory processing at the earliest stage of the olfactory pathway.

Additionally, the OB receives feedback connections known as centrifugal fibres from cortical and subcortical brain regions (Matsutani and Yamamoto, 2008). These connections provide a pathway for ongoing information from other brain areas to influence and modulate early olfactory information processing, thereby shaping the perception and processing of odours based on cognitive and contextual factors (Wang et al., 2023).

The OB sends direct projections to other olfactory structures as well as to non-olfactory structures: the anterior olfactory nucleus, anterior and posterior piriform cortex (PC), olfactory tubercle, lateral entorhinal cortex, medial amygdaloid nucleus, anterior and posterolateral cortical amygdaloid nucleus (Imamura et al., 2020); however, the primary output of the OB is directed towards the PC. Given its significance for the research presented in this thesis, the PC will be described in detail below.

The PC is the main cortical station in olfactory processing (Kumar et al., 2018) and is involved in the higher-order processing of olfactory information, including odour discrimination, recognition, and memory formation (Blazing and Franks, 2020). The PC consists of 3 layers (Bekkers and Suzuki, 2013). Layer I, known as the molecular layer, is the outermost layer of the PC. It is rich in dendrites, axons, and synaptic connections, because receives input from the OB *via* the lateral olfactory tract. Layer II (outer pyramidal layer), contains pyramidal neurons whose cell bodies are arranged parallel to the surface of the cortex. It sends output to other brain regions involved in olfactory processing, such as the entorhinal cortex and amygdala (Johnson et al., 2000). Layer III (internal pyramidal layer) contains pyramidal neurons similar to those in layer II, but with more diverse orientations which project to other cortical and subcortical areas (Bekkers and Suzuki, 2013). Layers II and III contain pyramidal neurons which are the primary excitatory cells of the PC and transmit olfactory information to other brain regions (Bathellier et al.,

2009). The second type of cells in the PC are interneurons, which express different calcium-binding proteins such as parvalbumin, calbindin, and calretinin. Each of these types is differentially localized within the three layers of the PC, contributing to various aspects of local circuit modulation (Gavrilovici et al., 2010). The PC has feedback connections to the OB, allowing for bidirectional communication and modulation of information processing (Trejo et al., 2023), which is important in the context of research included in this thesis.

Chapter 2

Rationale and aims of the thesis

2.1 Rationale

The main objective of my PhD project was to explore NMDAR-dependent HFO in the OB, focusing on their dependence on both input and output pathways, as well as the influence of DA receptor activity on these oscillations.

My research builds upon previous findings from our laboratory, which demonstrated that the OB is a primary source of ketamine-dependent HFO in the rat brain during the waking state (Hunt et al., 2019). Early in my time with the team, I contributed to a project revealing that HFO can also be recorded in the OB during Ket/Xyl sedation (Średniawa et al., 2021). This work, conducted under Ket/Xyl sedation, was a part of Dr. Władysław Średniawa's PhD thesis and is not included in the results presented in my thesis. Both studies emphasized the crucial role of unobstructed nasal respiration in driving this rhythm within the OB. Indeed, nasal respiration is crucial for olfaction, allowing rodents to receive sensory cues from the environment (Alberts and May, 1980). The olfactory epithelium contains OSN (Mombaerts, 1999), which have receptors that respond to both odorant molecules and mechanostimulation (Grosmaitre et al., 2007). However, previous studies have not clarified whether HFO is driven by odours, pressure, or other factors, leaving their specific influence on HFO uncertain.

Experiments under Ket/Xyl sedation have limitations, as sedation alters physio-

logical processes and suppresses typical brain function, restricting natural behaviours like exploration, and learning - activities known to shape neural activity in freely moving animals (Sorrenti et al., 2021). Thus, an important question arises: does nasal respiration also play a role in HFO generation during wakefulness, when the rat is free to explore its environment without the confounding effects of sedation?

The OB projects to several brain regions, with its most prominent projection targeting the PC (Haberly and Bower, 1989). The PC, another critical olfactory structure, sends reciprocal projections back to the OB, thus modulating its neuronal activity (Boyd et al., 2012). Whether NMDAR-dependent HFO can be recorded in the PC remains an open question. Additionally, if NMDAR-dependent HFO are present in the PC, it is unclear how they relate to HFO in the OB.

The OB's primary function is to process olfactory information (Mori et al., 1999), and DA is the one of a key neurotransmitter in this process (Escanilla et al., 2009). DA acts in part through presynaptic D2R located on the ON terminals (Gutièrrez-Mecinas et al., 2005), which release glutamate to activate OB cells (Berkowicz and Trombley, 2000). Given DA's known effects on olfactory circuits (Liu, 2020), I was motivated to explore its potential role in NMDAR-dependent HFO. To pursue this, I applied for and received a grant to conduct independent research on this research topic.

2.2 Aims

This thesis builds on previous work demonstrating the occurrence of aberrant HFO in the rat brain following administration of ketamine and other NMDAR antagonists. The research presented here focuses on addressing the following aims:

1. **To examine the role of nasal input on the generation of NMDAR-dependent HFO.** To do this, I examined nasal respiration rhythm (using thermocouples), odours presentation, and changes in nasal air pressure to determine which factor(s) may drive this rhythm.

2. **To examine whether the OB can drive NMDAR-dependent HFO in the PC.** To do this, I examined the relationship between NMDAR-dependent HFO in the OB and PC, and whether reversible inhibition of the OB affects this rhythm in the PC.

3. **To investigate the influence of DA on NMDAR-dependent HFO in the OB.** To do this, I examined the effect of D1R/D2R agonists and antagonists (administered systemically, and locally in the OB) on NMDAR-dependent HFO.

Chapter 3

Methods

3.1 Experimental animals

All experiments were conducted on male Wistar rats, which were housed in the Animal House at the Institute of Experimental Biology in Warsaw. A total of 88 animals were used in the experiments presented in this thesis. Their health and well-being were closely monitored by the experimenters and the Animal House staff, who ensured that the animals' living conditions were optimal. The rats, weighing approximately 250 g, were housed in groups of 3 to 5 per cage, each cage measuring 59.5 x 38 x 20 cm. To promote environmental enrichment and stimulate natural behaviours, the cages contained materials such as nesting items, wooden blocks, and aspen tunnels.

To reduce potential aggression, rats from different litters were not mixed, thus maintaining existing social hierarchies and minimizing the risk of conflict. The cages were made of polysulfone and equipped with stainless steel feeders, providing the animals with *ad libitum* access to water and food. Lignocel Select litter (poplar wood fibers, 3.5 mm) was used for bedding. The animals were kept in a controlled environment with a 12-hour light/dark cycle (light from 7:00 AM to 7:00 PM), a temperature range of 21-23°C, and humidity levels maintained between 50-60%.

All experimental procedures were conducted in full compliance with the European Community guidelines for the Care and Use of Laboratory Animals

(86/609/EEC) and received approval from the 1st Local Ethics Committee for Animal Experiments in Warsaw, Poland. Additionally, all practices adhered to the ARRIVE guidelines to ensure the welfare of the animals and the scientific integrity of the research.

3.2 Stereotaxic surgery

For surgery, rats (250–300 g) were anesthetized with inhaled isoflurane, with anaesthesia depth monitored throughout the procedure using the corneal reflex. After anaesthesia induction, animals received intraperitoneal (i.p.) premedication for analgesia and anti-inflammatory effects, as well as local anaesthetic at the surgical site. Each animal was then placed in a stereotaxic apparatus. The head was shaved, and an incision was made to expose the skull, where holes were drilled based on coordinates from the rat brain atlas for precise electrode or electrode-cannula placement (see Table 3.1). Stabilizing screws were affixed to the skull, with one serving additionally as a ground and reference electrode. Electrodes or electrode-cannula assemblies and screws were secured with dental cement, forming a protective socket for stability. During surgery, body temperature was maintained with a heating mat, and fluid needs were met with subcutaneous saline injections. Eyes were lubricated to prevent dryness.

All rats were bilaterally implanted with stainless steel twisted-wire electrodes in the OB, with cannulas added as necessary. For the thermocouple experiment, rats (N=8) were additionally implanted bilaterally in both nares with thermocouples (respiratory sensors). For the naris block experiment, additional bilateral electrodes were implanted in the PFC and VS (n=7). For the OB-PC experiments, unilateral electrodes were implanted in the PC (n=16). For detailed experimental procedures, please refer to the section below (3.3).

Once implantation was complete, the incision around the electrodes was sutured. Post-surgery, each animal was placed in a separate cage to prevent interference with sutures by other rats. Recovery care included 3 additional doses of an analgesic

and anti-inflammatory, with further analgesic provided in water *via* a soluble tablet. Animals were monitored multiple times daily during a 3-day recovery period, after which they were returned to a group cage to reduce stress associated with isolation.

Structure	**AP [mm]**	**ML [mm]**	**DV [mm]**
OB	+6.7-7.5	±0.5	−3.0-3.5
PFC	+3.2	±0.5	−3.0
VS	+1.6	±1.0	−7.0
PC	+0.5	±4.5	−8.0

Table 3.1: **The coordinates used for implantation.** Legend: OB – olfactory bulb, PC – piriform coretx, PFC – prefrontal cortex, VS – ventral striatum, AP – anterior-posterior, DV – dorsal/ventral, ML – medial/lateral. Coordinates based on The Rat Brain in Stereotaxic Coordinates (Paxinos and Watson, 1998).

3.3 Experimental procedures

One week after surgery, rats were placed in an arena (44 × 50 × 42 cm) for recording. LFPs (and thermocouple) signals were recorded through a JFET preamplifier, amplified 1000×, filtered at 0.1–1000 Hz (A-M Systems, USA), and digitized at 5 kHz (Micro1401, CED, Cambridge, UK). In experiments requiring the assessment of LMA, horizontal LMA was measured using photocell beam breaks (Columbus Instruments, USA). Rats were recorded for 2 days prior to the main experiment to habituate them to the recording chamber. All experiments followed a Latin square design, where each animal received each drug, dose or stimulus in a pseudorandomized order to minimize the number of animals used. A minimum washout period of 3 days was maintained between consecutive experiments involving the same rats.

Below is an overview of the various types of experiments conducted as part of this PhD thesis. A summary of these experiments can be found in Table 3.2.

1. **Air pressure experiment (N=7):** After Ket/Xyl sedation (Ket: 100 mg/kg+Xyl: 10 mg/kg), a tube was inserted into one rat nostril, and air was pumped through it at either low (0.1 l/hour) or high pressure (1.0 l/hour) for 10 seconds. A control measurement was also performed without airflow. All stimuli (with random order) were presented with at 3 min. intervals

for all rats. **Odour experiment (N=7):** After Ket/Xyl sedation (Ket: 100 mg/kg+Xyl: 10 mg/kg), rats were presented with individual odours - (+)-carvone, 2-hexanone, (R)-(+)-limonene, (+)-α-pinene, or control saline - at the nares for 10 seconds each, with 3-min. intervals between presentations. Each odor was delivered by positioning a cotton bud soaked in the selected substance near the nostrils. To prevent cross-contamination, each odour was removed from the anaesthetic setup using vacuum suction after presentation. LFPs were continuously recorded from the OB throughout all experimental procedures.

2. **Thermocouple experiment (N=8):** Each rat received two pseudorandomized injection of either 20 mg/kg ketamine or saline. A subgroup of rats (N=5) was pre-injected with 1 mg/kg haloperidol, followed 15 min. later by 20 mg/kg ketamine. LMA and LFPs and were continuously recorded from the OB alongside nasal theromocouple recordings throughout all experimental procedures.

3. **Naris blockade experiment (N=7):** Occlusion was achieved using a silicon occluder. Each rat was baselined for 20 min., then briefly anesthetized with isoflurane to allow occluder insertion. After a 60-min. recording period to allow isoflurane washout, rats were injected with 20 mg/kg ketamine. LMA and LFPs were continuously recorded from the OB, PFC and VS throughout all experimental procedures.

4. **OB-PC experiments:** Rats were baselined for 20 min. and then injected with 0.15 mg/kg MK801. 30 min. after i.p. injection of MK801, animals were disconnected from the recording equipment and gently restrained for substance infusion through implanted cannulas *via* an infusion pump (Harvard Apparatus, USA). A 28-gauge infusion needles (Bilaney, Germany) were manually lowered 1 mm below the cannulas tip. 1-min. infusion proceeded at 0.5 μl/min, delivering either muscimol (0.5 μg/side) or saline to the OB (N=8) or PC (N=10). Additionally, a subgroup of the PC group (N=6) received TTX

(10 ng/side) following the MK801 injection. LMA and LFPs were continuously recorded from the OB and PC throughout all experimental procedures.

5. **Non-selective DA agonists experiment (N=7):** Rats were baselined for 20 min. and then injected (i.p.) with 0.15 mg/kg MK801 followed, 25 min. later, by injection of: 2 mg/kg amphetamine, 2 mg/kg apomorphine, or control saline. LFPs were continuously recorded from the OB throughout all experimental procedures.

6. **Selective D1R and D2R agonists experiment (N=7):** Rats were baselined for 20 min. and then injected (i.p.) with 0.15 mg/kg MK801 followed, 25 min. later, by injection of: 1 mg/kg quinpirole or 1 mg/kg SKF38393. LFPs were continuously recorded from the OB throughout all experimental procedures.

7. **DA antagonist and antipsychotics experiments (N=7):** Rats were baselined for 20 min. and then injected (i.p.) with 0.15 mg/kg MK801 followed, 30 min. later, by injection of: 1 mg/kg eticlopride+1 mg/kg SCH23390, 3 mg/kg risperidone, 3 mg/kg aripiprazole and control saline or dimethyl sulfoxide (DMSO). LMA and LFPs were continuously recorded from the OB throughout all experimental procedures.

8. **MK801 infusion experiment (N=7):** After a 20-min. baseline, a 28-gauge infusion needles (Bilaney, Germany) were lowered 1 mm below the cannulas tip in the OB, and infusion were administered at a rate of 0.5 μl/min for 1 min. Either MK801 (4 μg/side) or saline was infused into the OB. LMA and LFPs were continuously recorded from the OB throughout all experimental procedures.

9. - 12. **DA agonist/antagonist infusion experiments (N=29):** Rats were baselined for 20 min. Briefly, 30 min post i.p. injection of 0.15 mg/kg MK801 a 28 gauge infusion needles (Bilaney, Germany) were inserted bilaterally and

descended 1 mm below the tip of the cannulas implanted in the OB. Infusions were carried out at a rate of 0.5 μl/min. for 1 minute. DA agents or saline were infused to the OB. Four separate groups of rats were used. Each group received an infusion of saline control and only one agonist or antagonist at two doses: D1R agonist SKF38393 at 2.5 μg/side or 5 μg/side (N=7); D2R agonist quinpirole at 2.5 μg/side or 12.5 μg/side (N=8); D1R antagonist SCH23390 at 1 μg/side or 6 μg/side (N=7); or D2R antagonist eticlopride at 2.5 μg/side or 12.5 μg/side (N=7). LMA and LFPs were continuously recorded from the OB throughout all experimental procedures.

Compounds: (+)-MK-801 hydrogen maleate (MK801), muscimol, TTX, (S)-amphetamine hemisulfate (AMPH), R-(–)-apomorphine hydrohloride hemihydrate (APO), (R)-(+)-SKF-38393 hydrochloride (SKF38393), (–)-quinpirole hydrochloride (Q), R(+)-SCH-23390 hydrochloride (SCH23390) and CA200773 CellAura fluorescent D1 antagonist SKF83566-green were dissolved in saline, whereas haloperidol (HAL), risperidone (RIS), aripiprazole (ARI) in dimethyl sulfoxide (DMSO, >99.9%). (±)-Ketamine (100 mg/ml), xylazine (20 mg/ml), (+)-carvone (96%), 2-hexanone (98%), (R)-(+)-limonene (98%), and (+)-α-pinene (98%) were originally prepared in solution form. All drugs were purchased from Sigma (Poland), except for fluorescent SKF83566-green, which was obtained from Hello Bio (Ireland) as well as ketamine and xylazine, which were obtained from Biowet (Poland).

3.4 Brain preparation and histological analysis

At the end of the experiments, rats were euthanized using an overdose of anaesthetic or pentobarbital. Electrolytic lesions were made for all electrodes (9V, 10 seconds). The brains were then fixed in 4% paraformaldehyde (Sigma, Poland) and preserved in 30% sucrose (Sigma, Poland). They were frozen on dry ice at approximately -80°C before being prepared for cryostat sectioning.

Ex.	Rationale	Drug and dose	N
1	Do naris air pressure or odours affect HFO?	Ket+Xyl: 100+10mg/kg	7
2	Are HFO related to sniffing? Does Hal reverse Ket-induced sniffing?	Ket: 20mg/kg Hal+Ket: 1+20mg/kg	8 5
3	Does naris block attenuate HFO?	Ket: 20mg/kg	7
4	Does OB inhibition affect HFO in OB? Does PC inhibition affect HFO in PC?	MK801: 0.15mg/kg + musc: 0.5μg/side MK801: 0.15mg/kg + musc: 0.5μg/side + TTX: 10ng/side	8 10$\star$ 6
5	Do DA rec. non-select. agonists affect HFO?	MK801: 0.15mg/kg + AMPH: 2mg/kg + APO: 2mg/kg	7*
6	Do DA rec. select. agonists affect HFO?	MK801: 0.15mg/kg + Q: 1mg/kg + SKF: 1mg/kg	7
7	Do DA rec. antagonists affect HFO? Do 2^{nd} and 3^{rd} generation APD affect HFO?	MK801: 0.15mg/kg + (ETI+SCH: 1+1mg/kg) MK801: 0.15mg/kg + RIS 3mg/kg + ARI: 3mg/kg	7
8	Local OB NMDAR block: HFO effect?	MK801: 4μg/side	7
9	Does local D1R block. in OB affect HFO?	MK801: 0.15mg/kg + SCH: 1, 6μg/side	7
10	Does local D2R block. in OB affect HFO?	MK801: 0.15mg/kg + ETI: 2.5, 12.5μg/side	7
11	Does local D1R stim. in OB affect HFO?	MK801: 0.15mg/kg + SKF: 2.5, 5μg/side	7
12	Does local D2R stim. in OB affect HFO?	MK801: 0.15mg/kg + Q: 2.5, 12.5μg/side	8

Table 3.2: **Summary of the experimental procedures.** Legend: AMPH – amphetamine, APO – apomorphine, ARI – aripiprazole, ETI – eticlopride, Hal – haoperidol, Ket – ketamine, musc – muscimol, RIS – risperidone, SCH – SCH23390, SKF – SKF38393, TTX – tetradotoxin, Q – quinpirole, Xyl – xylazine. Ex. – experiment. * – all rats for these experiments were taken from Ex. 2. $\star$ – 2 rats were also used from Ex. 3.

Frozen brains were mounted on a cryostat stage (Leica Microsystems, Germany) and sectioned into 35-40 μm thick slices, which were placed on gelatin-coated slides. The slides were left to dry for at least 24 hours. Electrode or cannula placements were determined on Cresyl violet-stained sections using the Nissl method (Figure 3.1).

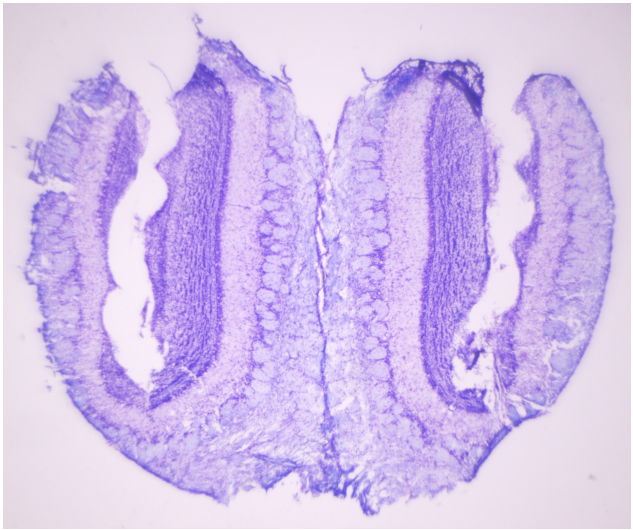

Figure 3.1: **OB section showing electrode tracks.** An example of an OB section with visible tracks from twisted-wire electrodes, cut on a cryostat (35 μm thickness) and stained using Nissl method.

3.5 Signal processing and data analysis

LFPs recordings, stored in Spike2 format, were imported into Python for analysis using the Spike2IO class from the Neo library. Signal processing was performed with the SciPy Signal and NumPy libraries, primarily applying bandpass filtering with Butterworth filters. To eliminate narrowband noise, additional notch filters were applied as necessary. Spectrogram analysis, based on a Fourier Transform with 4096 points, was performed on 30-second windows to assess power in the dominant frequency and within specific frequency ranges.

Thermocouple signals (1–10 Hz) were used to identify the dominant sniffing frequency and quantify the proportion of fast (4–10 Hz) sniffing behaviour. For analysis of HFO, data were filtered within the following ranges: 130-180 Hz for ketamine experiments, 80-180 Hz for Ket/Xyl experiments, and 130-200 Hz for MK801 experiments. A 120-200 Hz range was used to capture reductions in HFO frequency below 130 Hz after apomorphine i.p. injection (Figure 4.9 C). Please note that HFO range was expanded because DA drugs affected the dominant frequency of this rhythm.

For the analysis of HFO power and frequency following quinpirole local infusion (Figure 4.10 F and G), the LFPs signal was divided into five batches: fragment 0 (pre-infusion) and fragments 1-4 (post-infusion, each lasting 10 min.). For comparisons of frequencies in Figure 4.4 G power spectra were computed from 60s segments taken 5 min. after injection. For comparisons of frequencies in Figures 4.9 D, G and 4.14 G, H power spectra were computed from 60s segments taken 40 min. after injection.

3.6 Statistical analysis and data visualization

Data normality was assessed using the Shapiro–Wilk test. Data are presented as mean±SEM or median±interquartile range, depending on the distribution of the data. For normally distributed data, statistical comparisons were made using 1-way ANOVA or 2-way ANOVA followed by Bonferroni's post-hoc test or paired/unpaired

Student's t-test. For non-normally distributed data, the Kruskal–Wallis test with Dunn's multiple comparison test or the Wilcoxon test were used. Differences were considered significant when $p \leq 0.05$. Spearman's rank correlation coefficient was used to examine the relationships between sniffing, LMA, and oscillatory activity. A p-value of ≤ 0.05 was considered statistically significant. All graphs were prepared in GraphPadPrism (GraphPad Software, San Diego, USA), taken from Spike2 or generated in Python.

Chapter 4

Results

4.1 Role of nasal input in NMDAR-dependent HFO

At the beginning of my PhD research, I contributed to a project investigating HFO under Ket/Xyl sedation. The primary results from this project were published in a co-authored article (Średniawa et al., 2021). In this study, we demonstrated that HFO could be reliably recorded in the OB under Ket/Xyl sedation, providing a more manageable experimental condition compared to the challenges of working with freely moving rats. Our findings indicated that blocking naris airflow attenuates Ket/Xyl-dependent HFO. The studies presented in subsections 4.1.1 and 4.1.2 build on this research by evaluating which factor – pressure changes in the nares or odour exposure – primarily drives this effect.

Experiments conducted under Ket/Xyl sedation have limitations, as sedation significantly alters physiological processes and suppresses normal brain function, thereby preventing natural behaviors such as exploration, social interaction, and learning, which influence neural activity in freely moving animals (Sorrenti et al., 2021). To address these limitations, subsequent experiments were performed in freely moving rats to preserve natural physiological and behavioural states.

In the second part of this chapter, I examined the relationship between ketamine

administration and sniffing behaviour (4.1.3), assessed whether ketamine-dependent HFO in the OB correlates with sniffing and LMA (4.1.4), and investigated whether unobstructed nasal airflow is essential for ketamine-dependent HFO generation in freely moving rats to determine if findings from Ket/Xyl-sedated conditions hold under natural, active conditions (4.1.5). The findings from freely moving rats experiments have been published in Scientific Reports (Wróbel et al., 2020).

4.1.1 Increased air pressure enhances Ket\Xyl-dependent HFO

To assess the impact of increased naris airflow on HFO, it was necessary to anesthetize the rats. In the initial phase of the experiment, rats implanted bilaterally with electrodes in the OB (N=7) received i.p. injection of Ket/Xyl at a sedative dose (Ket: 100 mg/kg+Xyl: 10 mg/kg). Adequate anesthesia was confirmed by the absence of a corneal reflex, after which the animals were placed in an experimental chamber and connected to the electrophysiological recording apparatus. Once baseline Ket/Xyl-dependent HFO recordings were obtained, the experimental phase commenced.

For this, a tube was inserted into one rat nostril, and air was pumped through it at either low (0.1 l/hour) or high pressure (1.0 l/hour) for 10s. A control measurement was also performed without airflow. All stimuli (with random order) were presented with at 3 min. intervals for all rats. Figure 4.1 illustrates the changes in Ket/Xyl-dependent HFO power in the control (A), low-pressure (B), and high-pressure (C) conditions, as recorded from the OB on the same side as the nostril receiving airflow. Figures 4.1 D, E, and F display the corresponding Ket/Xyl-dependent HFO measurements from the contralateral OB. Results showed that only high-pressure airflow enhanced Ket/Xyl-dependent HFO, affecting both the ipsilateral and contralateral OBs, with a more pronounced increase in Ket/Xyl-dependent HFO power observed in the ipsilateral OB. 1-way ANOVA showed significance for high air pressure (for ipsilateral p=0.0035, for contralateral p=0.0125). Bonfer-

roni's *post hoc* test revealed a significant effect for air vs +20s, $p<0.01$; air vs +10s, air vs -10s and air vs -20s, $p<0.05$. For control and low air pressure conditions 1-way ANOVA was not significant (for control: ipsilateral $p=0.1332$, contralateral $p=0.6204$; for low air pressure: ipsilateral $p=0.4702$, contralateral $p=0.1763$).

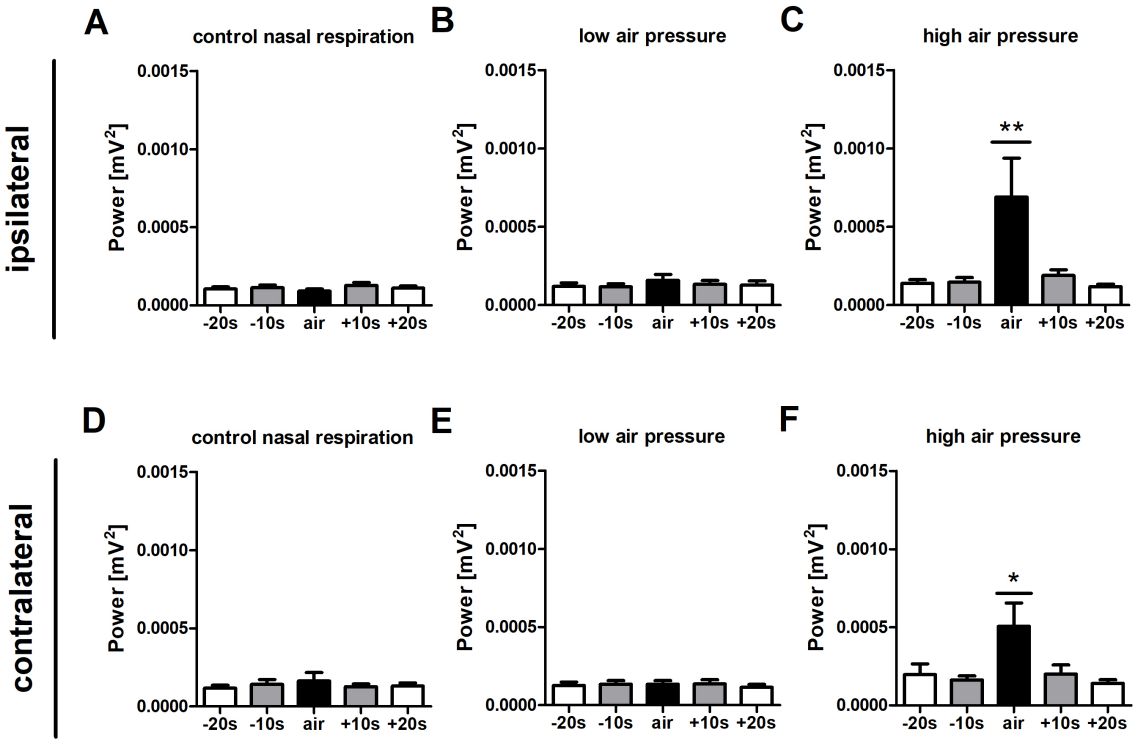

Figure 4.1: **The power of Ket/Xyl-dependent HFO in the OB is enhanced by incerased airflow to the naris.** Bar charts presenting power of Ket/Xyl-dependent HFO (80-180 Hz) before (10-20s, 0-10s), after (0-10s, 10-20s) and during (airflow for 10s) for **(A)** control condition (no air pressure), **(B)** low air pressure **(C)** high air pressure for ipsilateral OB and **(D)** control condition, **(E)** low air pressure, **(F)** high air pressure for contralateral OB. 1-way ANOVA was significant only for high air pressure (for ipsilateral $^{**}p<0.01$, for contralateral $^{*}p<0.05$). Note that the increase in Ket/Xyl-dependent HFO power occurred in the contralateral OB, likely because the nostrils are connected, and air pressure affected both nostrils.

4.1.2 Odour does not affect Ket\Xyl-dependent HFO

In the following experiment, I aimed to determine whether Ket/Xyl-dependent HFO is responsive to specific odours. For this purpose, four odours were selected: (+)-carvone, 2-hexanone, (R)-(+)-limonene and (+)-α-pinene.

After administering a sedative dose of Ket/Xyl (Ket: 100 mg/kg+Xyl: 10 mg/kg), odours were presented individually to the rats' nostril for a duration of

10s, with intervals of 3 min. between presentations. After each presentation, odours were removed using vacuum suction from the anaesthetic equipment. All rats (N=7) were presented with each odour in a randomized order. Figure 4.2 illustrates the changes in Ket/Xyl-dependent HFO power following the presentation of each odour as well as a saline control (no odour). None of the tested odours produced any significant effect on Ket/Xyl-dependent HFO power. 1-way ANOVA showed no significance for all conditions for both bulbs (for control: ipsilateral p=0.5164, contralateral p=0.5054; for carvone: ipsilateral p=0.8569, contralateral p=0.8905; for hexanone: ipsilateral p=0.9437, contralateral p=0.6404; for limonene: ipsilateral p=0.2610, contralateral p=0.2003; for pinene: ipsilateral p=0.8331, contralateral p=0.6826).

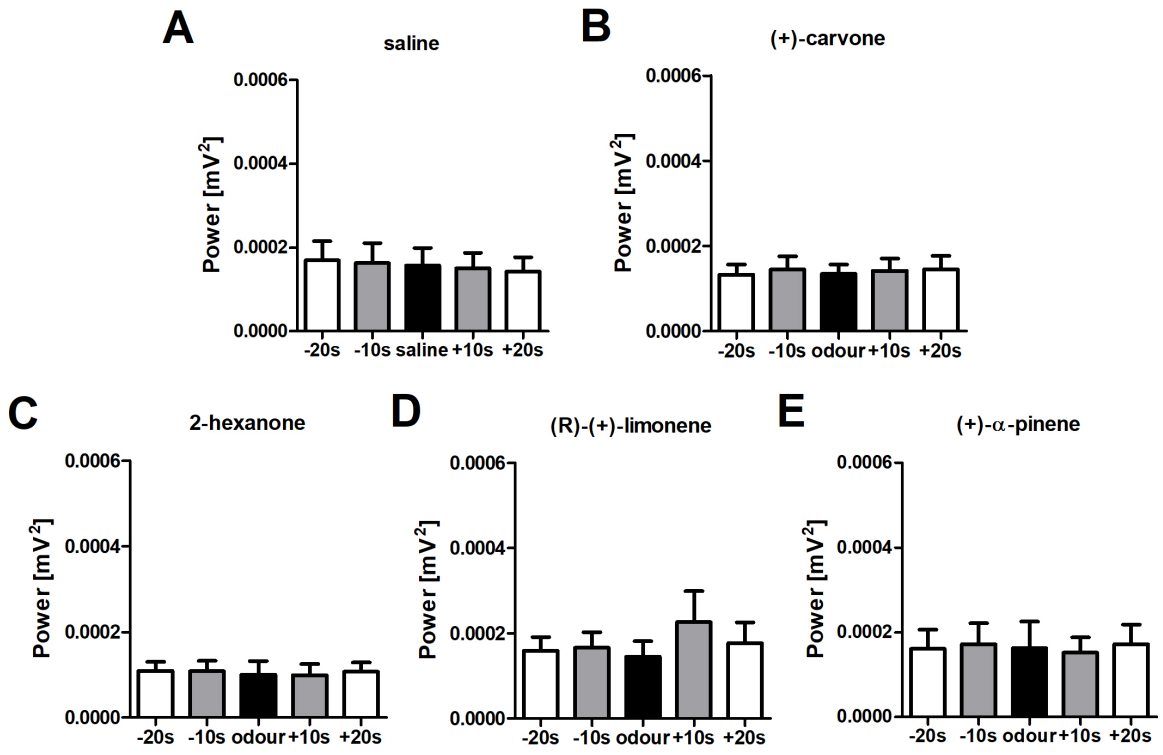

Figure 4.2: **The power of Ket/Xyl-dependent HFO in the OB is not enhanced by four different odours.** Bar charts presenting power of Ket/Xyl-dependent HFO (80-180 Hz) before (10-20s, 0-10s), after (0-10s, 10-20s) and during (10s) presentation of **(A)** control saline (no odour), **(B)** (+)-carvone, **(C)** 2-hexanone, **(D)** (R)-(+)-limonene and **(E)** (+)-α-pinene. 1-way ANOVA revealed no significant differences across all conditions. All plots display results from the ipsilateral OB.

4.1.3 Ketamine triggers fast sniffing behaviour in rats

In this experiment, thermocouples were used as respiratory sensors to enable direct detection of respiration. Rats (N=8) with bilateral OB electrode implants and thermocouples received i.p. injection of either 20 mg/kg ketamine or saline. Additionally, 5 rats from this group received 1 mg/kg antipsychotic haloperidol prior to ketamine injection. Nasal respiration patterns were categorized into two primary modes: slow sniffing (1–3 Hz), associated with resting states, and fast sniffing (4–10 Hz), linked to active exploratory behaviour, aligning with prior findings (Wesson et al., 2009). Representative thermocouple signals and corresponding power spectra following control saline, ketamine, and ketamine with haloperidol pretreatment are shown in Figure 4.3 A1 and A2.

After ketamine administration, the rats demonstrated prolonged and nearly continuous fast sniffing, which subsided around 15 min. post-injection. During this period, the median sniffing frequency was approximately 6 Hz, compared to around 2 Hz under saline conditions. Figures 4.3 B and 4.3 C illustrate the time-course data for the dominant sniffing frequency ($p=0.001$, Kruskal–Wallis, Dunn's *post hoc*) and the proportion of fast sniffing (4–10 Hz) ($p<0.0001$, 1-way ANOVA, Bonferroni's *post hoc*) during the first 15 min. after ketamine administration. An elevation in fast sniffing was also observed following saline injection, but this effect was short-lived and declined to slow sniffing levels within 2 min.

This sustained behaviour coincided with increased LMA (Figure 4.3 D). Adjacent plot illustrates beam breaks for each rat for the first 15 min. post-injection showing a significant increase of LMA after ketamine ($p<0.0001$, 1-way ANOVA, Bonferroni's *post hoc*). There was a significant positive correlation between LMA, as measured by beam breaks, and the proportion of fast sniffing (Spearman $r=0.7366$; $p<0.0001$) within the first 15 min. following ketamine administration. Analysis of individual rats showed significant correlations in 7 out of 8 cases ($p<0.001$), with the exception of one rat (Figure 4.3 E).

This experiment also aimed to assess whether blocking rat LMA would impact

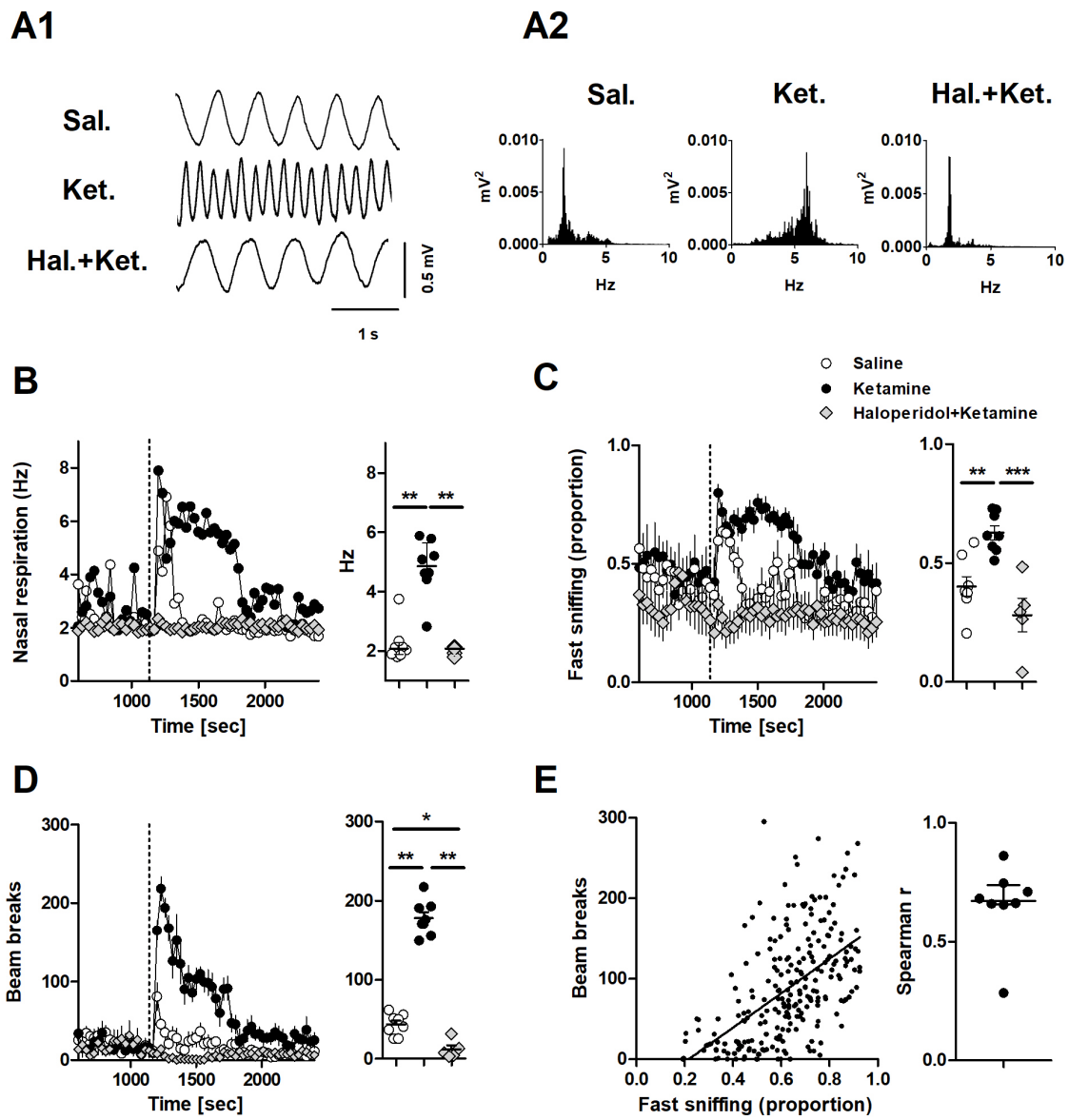

Figure 4.3: **Ketamine induces fast sniffing behaviour, which is reversed by haloperidol.** **(A1)** Traces of nasal respiration for saline (Sal.), ketamine (Ket.), and haloperidol+ketamine (Hal.+Ket.) directly after injection. **(A2)** Power spectra (60s) show the dominant sniffing frequency for each condition. **(B)** Time-course presents the median dominant sniffing frequency post-injection for Sal., Ket. (N=8), and Hal.+Ket. (N=5). Adjacent plot shows a significant increase of sniffing frequency after ketamine, p=0.001. **(C)** Time-course of the proportion of fast sniffing (4–10 Hz) post-injection of Ket., Sal. and Hal.+Ket. Adjacent plot displays individual rats, showing a significant difference in the proportion of fast sniffing among conditions, p<0.0001. **(D)** Time-course shows Ket.-induced hyperlocomotion. Adjacent plot presents beam breaks for each rat (first 15 min. post-injection) showing a significant increase of LMA after Ket., p<0.0001. **(E)** A significant correlation between the proportion of fast sniffing and beam breaks (first 15 min. post-injection), p<0.0001. The adjacent plot shows the Spearman's rank correlation scores, with a significant correlation in 7 of the 8 rats, p<0.001; *p<0.05, **p<0.001, ***p<0.0001.

ketamine-induced increases in fast sniffing. To achieve this, I used the antipsychotic haloperidol, known to induce catalepsy in a dose-dependent manner between 0.03

and 10 mg/kg (Campbell et al., 1988). Pretreatment with 1 mg/kg haloperidol (gray symbols) effectively blocked the ketamine-induced increase in fast sniffing (Figures 4.3 B and C) as well as the associated hyperlocomotion (Figure 4.3 D).

4.1.4 Relationship between ketamine-dependent HFO and behaviour in rats

Next, in the same rats, I analyzed the oscillatory activity within LFPs recordings from the OB. Representative raw and filtered (130-180 Hz) LFPs signals following saline and ketamine administration are presented in Figures 4.4 A and C, while corresponding spectrograms are displayed in Figures 4.4 B and D.

Ketamine administration led to a rapid and around 15 min. increase in HFO power. The time-course of HFO changes following ketamine injection is depicted in Figure 4.4 E. 2-way ANOVA revealed a significant time×group interaction ($F_{(132,1848)}$=8.95, p<0.0001). Bonferroni's *post hoc* test revealed a significant effect for saline vs ketamine, p<0.0001. A paired-sample analysis for each rat comparing the mean HFO power between saline and ketamine conditions over the 15 min. post injection revealed a significant increase in HFO power after ketamine administration (p=0.0078, paired t-test) (Figure 4.4 F). Comparison of power spectra indicated a prominent ketamine-dependent HFO peak at around 150 Hz (Figure 4.4 G).

I also found a significant correlation between HFO power, the proportion of fast sniffing and enhanced LMA (both p<0.0001) during the first 15 min. post-ketamine injection. Analyses of individual rats indicated that the correlation between HFO power and fast sniffing was significant in 7 out of 8 rats, while the correlation between HFO power and beam breaks was significant in all 8 rats. The individual correlation coefficients are presented in Figure 4.4 H.

Next, I analyzed thermocouple and LFPs signals to identify potential periods where HFO aligned with respiration. Figures 4.4 I, J, and K present examples of simultaneous thermocouple (blue) and LFPs signals (1–10 Hz in red and 130–180 Hz HFO bursts in black) recorded at three intervals: baseline, the early phase post-

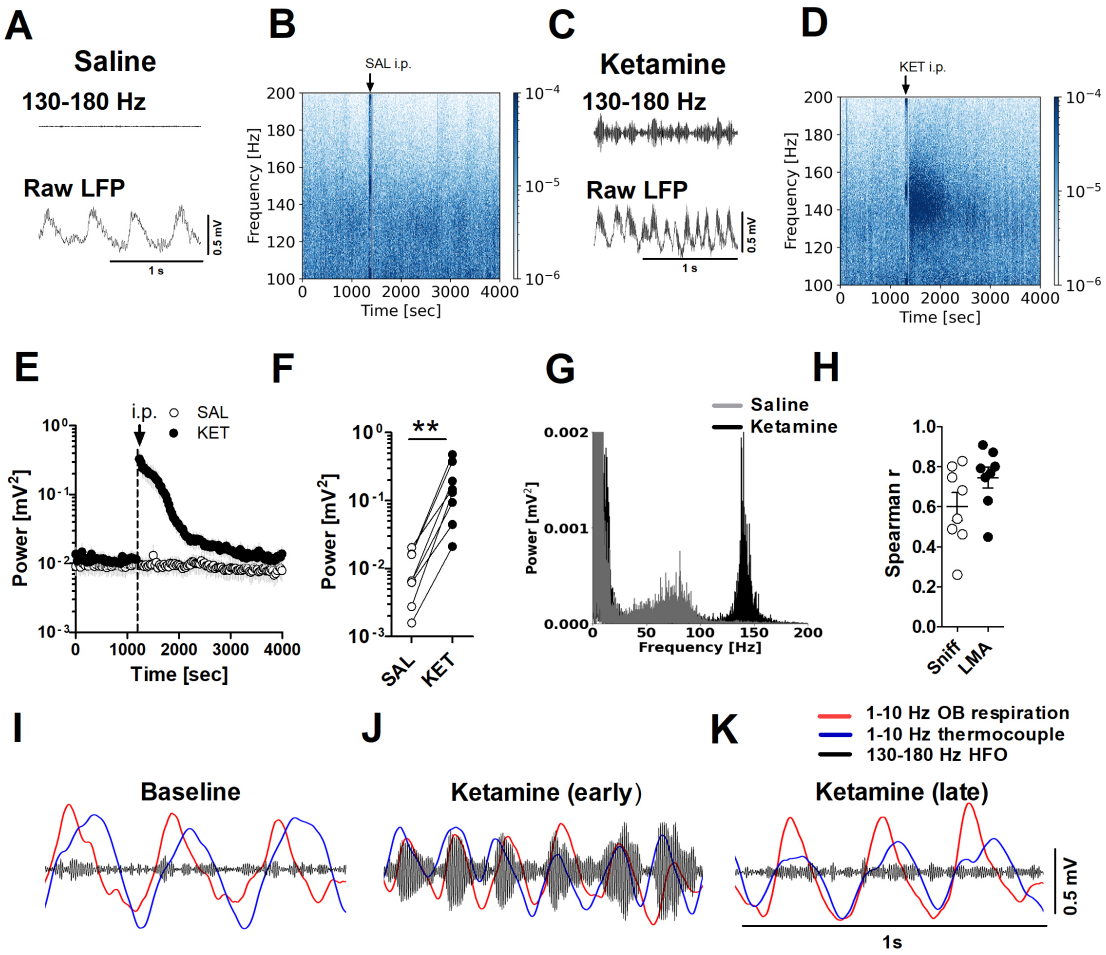

Figure 4.4: **Ketamine increases the power of HFO in the OB which correlates with fast sniffing and LMA.** **(A, C)** Example of OB filtered (130-180 Hz) and raw LFPs signals after saline or 20 mg/kg ketamine injection. **(B, D)** Example of spectrograms after saline and ketamine injection. **(E)** Time-course presents a significant increase of HFO power after ketamine injection (N=8), $p<0.0001$. **(F)** Before-after plot shows average HFO power for first 15 min. post saline or ketamine injection for individual rats, $p<0.01$. **(G)** Power spectrum shows ketamine-dependent HFO peak around 150 Hz. **(H)** Spearman r correlation for individual rats between ketamine-dependent HFO and fast sniffing (Sniff) and increased LMA, $p<0.0001$. **(I)** Example of baseline, **(J)** early after ketamine injection, and **(K)** at the end of the recording, showing filtered (1-10 Hz) thermocouple signal (blue), filtered (1-10 Hz) OB LFPs signal (red), and filtered (130-180 Hz) HFO bursts (black); $^{**}p<0.01$.

ketamine injection and toward the end of the session, when ketamine's effects had diminished. Notably, HFO bursts were entrained to the 1-10 Hz rhythm detected by thermocouples and in the OB, but only during the early phase following ketamine injection.

4.1.5 Nasal respiration drives ketamine-dependent HFO in multiple brain regions

Our previous studies (Hunt et al., 2019; Średniawa et al., 2021) established that naris occlusion reduces HFO power in the OB during recovery from ketamine anaesthesia and during Ket/Xyl sedation. To investigate whether naris occlusion similarly affects ketamine-dependent HFO power under freely moving conditions, a separate group of rats (N=7) was implanted with electrodes in the OB, but also in the prefrontal cortex (PFC), and ventral striatum (VS) to additionally assess the impact of naris blockage across cortical and subcortical structures. These structures were selected based on previous studies demonstrating ketamine-dependent HFO in these regions (e.g., Hunt et al., 2006; Lee et al., 2017; Hansen et al., 2019).

In the initial phase of the experiment, the rats underwent unilateral naris blockade while under isoflurane anaesthesia, followed by an i.p. injection of 20 mg/kg ketamine 1 hour later. We assessed the quality of the naris blockade by observing the desynchronization of the raw LFPs with the respiratory rhythm. The results indicated that unilateral naris occlusion led to a decrease in HFO power on the ipsilateral OB after ketamine administration, whereas ketamine-dependent HFO levels on the contralateral OB remained unaffected (Figures 4.5 A, B, and C). 2-way ANOVA analysis revealed a significant interaction effect between time and group for the OB ($F_{(59.590)}$=2.52, p<0.0001), VS ($F_{(59.708)}$=2.52, p<0.0001), and PFC ($F_{(59.708)}$=2.52, p<0.0001).

4.2 The OB drives NMDAR-dependent HFO in the piriform cortex (PC)

In previous sections, I presented results examining input to the OB, demonstrating that nasal respiration, rather than odours, contributes to ketamine-dependent HFO generation. Here, I focus on the primary output pathway of the OB, the PC, which

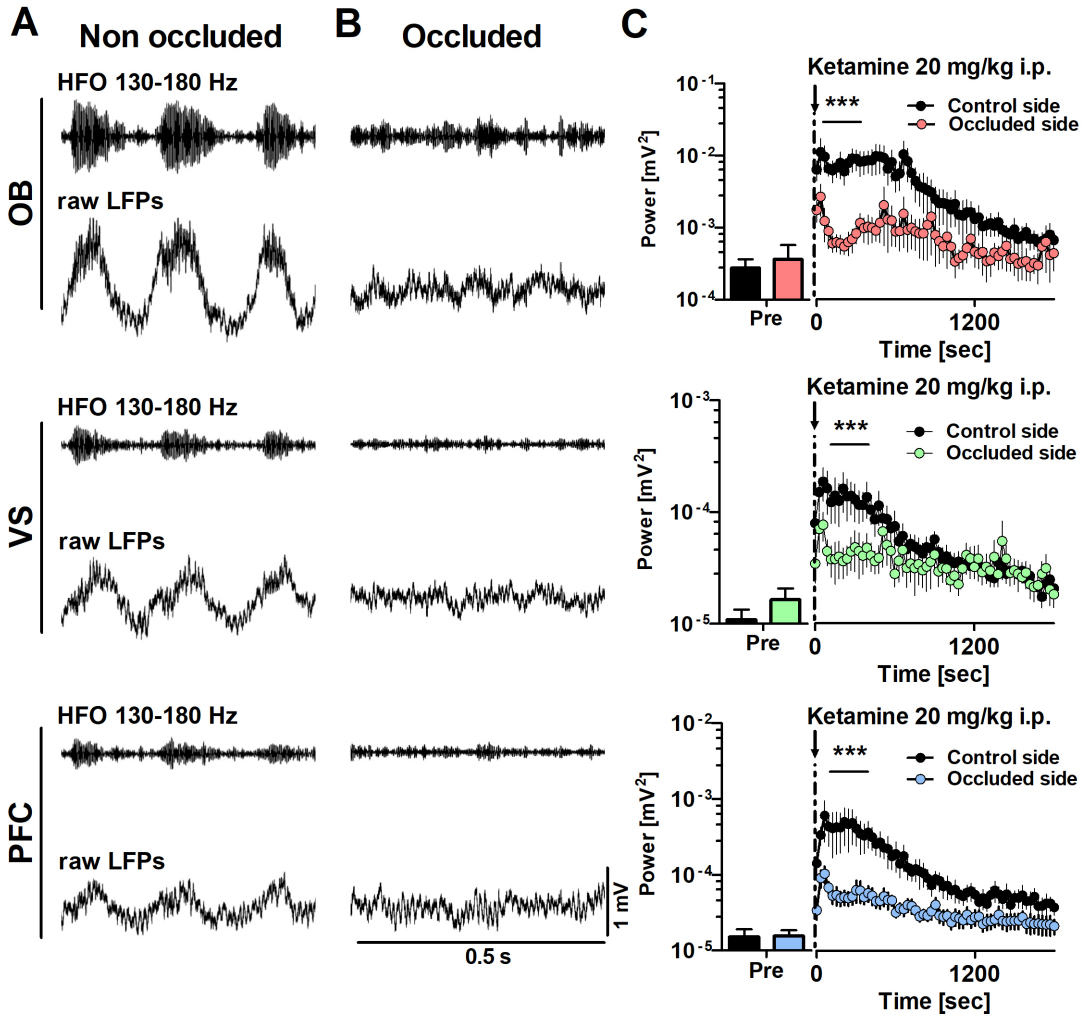

Figure 4.5: **Naris blockade reduces the power of ketamine-dependent HFO in the OB, VS and PFC in freely moving rats.** **(A)** Examples of filtred HFO (130-180 Hz) and raw LFPs signals in the olfactory bulb (OB), ventral striatum (VS) and prefrontal cortex (PFC) without naris occlusion and **(B)** after naris occlusion. **(C)** Time-courses showing reduction of ketamine-dependent HFO power on the occluded side in the OB, VS and PFC respectively (N=7); ***p<0.0001. The Y-axes in the plots differ in magnitude across structures.

serves as a major target of OB projections (Haberly and Bower, 1989) and provides feedback projections back to the OB, modulating its activity (Boyd et al., 2012, 2015).

The first section (4.2.1) characterizes the HFO rhythms observed in both the OB and PC. Subsequent sections (4.2.2 and 4.2.3) detail the effects of bidirectional communication between the OB and PC on NMDAR-dependent HFO rhythmogenesis, utilizing pharmacological agents to inhibit neural activity in these structures. For these experiments, MK801 was used as the NMDAR antagonist due to its pro-

longed effect on enhancing HFO power compared to ketamine (Hunt et al., 2006). All results presented in the following sections were obtained using freely moving rats and have been published in my recent article (Wróbel et al., 2024).

4.2.1 MK801-dependent HFO in the OB and PC

The PC serves as the primary projection target of the OB and also sends feedback projections back to the OB (Luskin and Price, 1983). To explore HFO in these both structures, I conducted simultaneous recordings from both the OB and PC in freely moving rats (N=16). The simultaneous LFPs recordings from the OB and PC following an i.p. injection of 0.15 mg/kg MK801 are illustrated in Figure 4.6 A.

Spontaneous HFO within the 130–180 Hz range appeared as a slight peak in the OB power spectra of LFPs recordings, while being largely absent in the PC. Following 0.15 mg/kg i.p. injection of MK801, distinct MK801-dependent HFO peaks became apparent in both structures (Figure 4.6 B).

Monopolar LFPs may not always originate from the recording site; they can instead passively propagate from distant regions (Kajikawa and Schroeder, 2011). To eliminate in-phase volume-conducted activity from outside the recording sites, I analysed the bipolar signal derived from two monopolar recordings with an inter-electrode distance of up to 1 mm. This analysis revealed that MK801 significantly increased the power of HFO in both the OB and PC, as shown in the onsets of Figure 4.6 B. Figure 4.6 C presents MK801-dependent HFO power, in simultaneous monopolar OB and PC recordings, approximately 30 min. after MK801 injection (Wilcoxon matched-pairs test, $p=0.0009$). To analyse the relationship between changes in HFO power in the OB and PC, I focused on the 30 min. following MK801 injection. Correlation analysis showed a positive correlation ($p<0.05$) in 15 out of 16 rats, scatter plot displays data from all individual rats (Figure 4.6 D).

Next, coherence, a mathematical method used to assess whether two or more brain regions exhibit similar neuronal oscillatory activity (Bowyer, 2016), was employed to measure functional connectivity between the OB and PC. Analysis re-

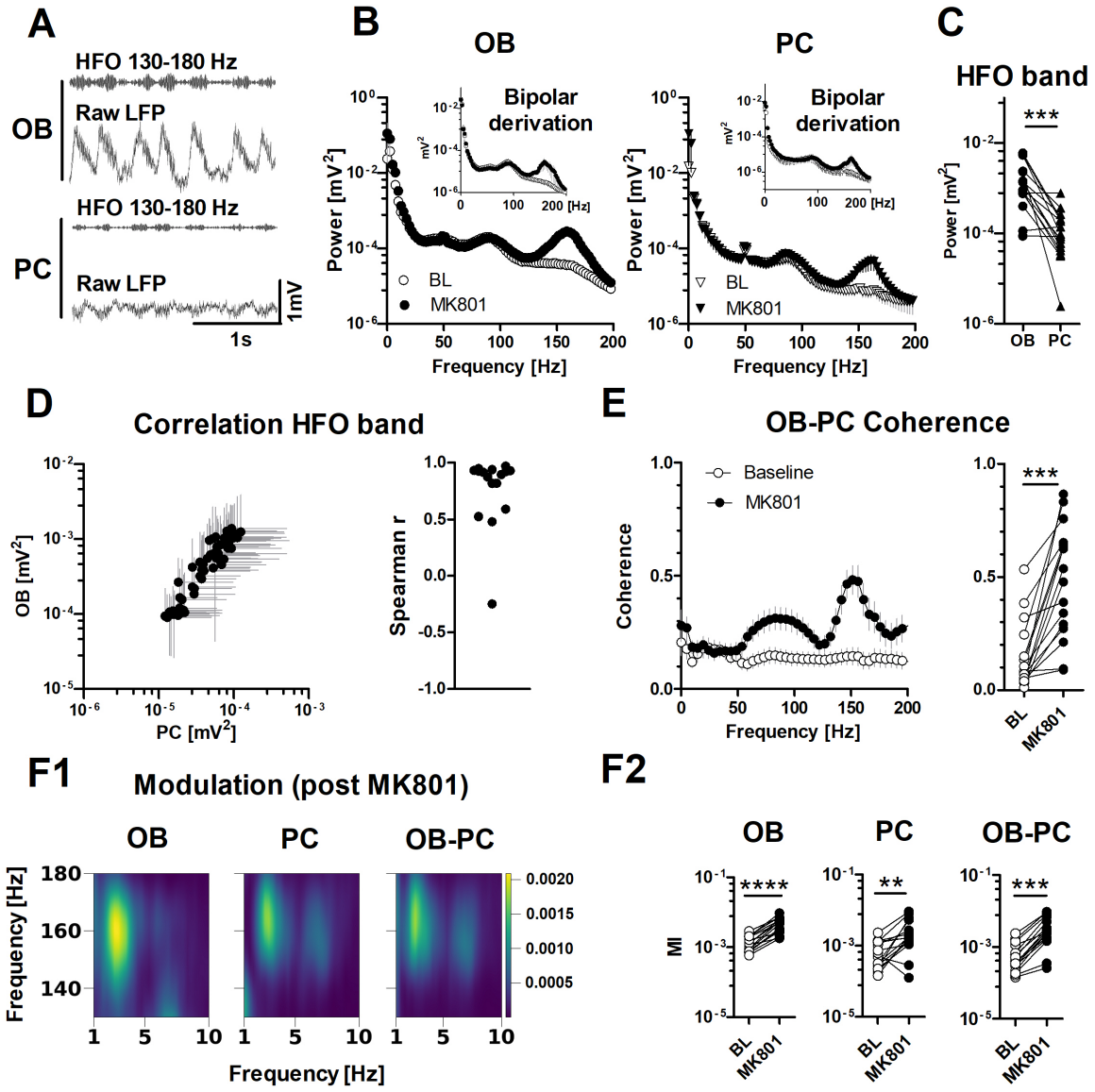

Figure 4.6: **Comparison of the power and modulation of MK801-dependent HFO recorded in the OB and PC in freely moving rats.** **(A)** 130–180 Hz filtered signals and corresponding raw LFPs from the OB and PC after 0.15 mg/kg MK801 injection. **(B)** Mean power spectra (N=16 rats) of monopolar LFPs from the OB and PC, (60s at baseline, 29–30 min. post MK801). The inserts display the bipolar-derived signal for the same data. **(C)** Comparison of HFO power in the OB and PC post MK801, ***p=0.0009. **(D)** Group mean values of HFO in the OB and PC post MK801, indicating a positive correlation, with Spearman rank values for individual rats, p<0.05. **(E)** Coherence spectra calculated at baseline and post MK801, with maximum coherence for the 130–180 Hz band at baseline and post MK801 for each rat, ***p<0.001. **(F1)** Comodulograms post MK801 with **(F2)** before-after plots show modulation of HFO by slow rhythms (1–10 Hz) in the OB (****p<0.0001), PC (**p=0.004) and OB-PC (***p=0.0002).

vealed strong coherence following MK801 injection, while coherence was weak under baseline conditions (Figure 4.6 E). The before-and-after plot displays the coherence values for each individual rat (p<0.001, paired t-test).

To investigate whether slow rhythms influence MK801-dependent HFO, CFC analysis was performed between HFO and slow oscillations (1–10 Hz). CFC refers to the coupling or correlation between the phase or amplitude of oscillations in one frequency band and those in another, playing a crucial role in coordinating neural activity and facilitating information processing in the brain (Canolty and Knight, 2010). The analysis revealed significant coupling of MK801-dependent HFO to 1-10 Hz oscillations both within the OB and PC ($p<0.0001$ for the OB and $p=0.004$ for the PC, paired t-tests). Additionally, HFO in the PC was found to be modulated by slow oscillations originating from the OB ($p=0.0002$ for the OB-PC coupling, paired t-test; see Figure 4.6 F1 and F2). Coherence and CFC analyses were conducted by Dr. Aleksandra Bramorska from the Neuroinformatics Lab.

4.2.2 Reversible inhibition of the OB reduces MK801-dependent HFO in the OB and PC

Reversible inhibition of a brain structure is commonly used by researchers to investigate its impact on connected brain regions (e.g., Majchrzak and Di Scala, 2000; Nyhuis et al., 2016). To further investigate MK801-dependent HFO in the OB and the PC, I tested the hypothesis that reversible inhibition of the OB using the GABA-A receptor agonist muscimol would decrease NMDAR-dependent HFO power in the PC. Following the infusion of muscimol into the OB, I observed an almost immediate reduction in MK801-dependent HFO power both locally within the OB and in the PC, while saline infusion showed no effect. Figures 4.7 A and B display spectrograms from a representative rat, along with the complete time-courses of the recordings.

A comparison of HFO power 5-10 min. post-infusion revealed a significant reduction in HFO power when muscimol was administered compared to saline ($p=0.0078$, Wilcoxon matched-pairs test, for both the OB and PC), a result that was consistent across all rats. Notably, reductions in HFO power in the OB were associated with changes observed in the PC.

I also sought to examine potential changes in LMA. Beam break analysis

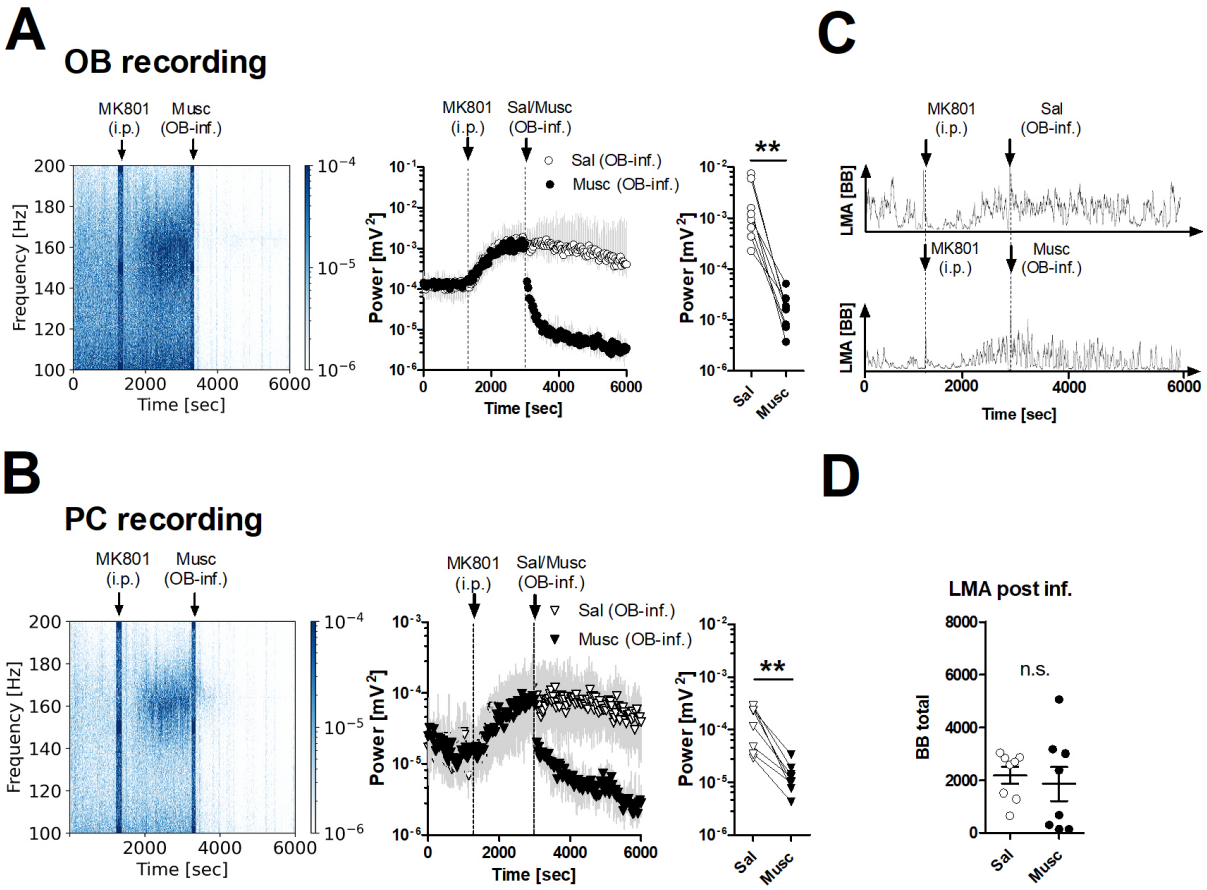

Figure 4.7: **Effect of muscimol infusion to the OB on the power of MK801-dependent HFO in the OB and PC in freely moving rats.** **(A, B)** Microinfusion of muscimol into the OB reduces MK801-dependent HFO power (130-180 Hz) in both the OB and PC. Spectrograms and time-courses demonstrate a decrease in HFO power after muscimol infusion (N=8). Before-after plots show HFO power for individual rats 5–10 min. post-musimol infusion, **p<0.01 for both. **(C)** Examples of LMA following saline or muscimol infusion. **(D)** Plot comparing total beam breaks 30 min. post infusion of saline or muscimol for individual rats; n.s. – not significant.

(Figure 4.7 C) indicated no significant differences in MK801-dependent LMA between muscimol and saline-infused controls (paired t-test, p=0.5869; Figure 4.7 D).

4.2.3 Reversible inhibition of the PC does not affect MK801-dependent HFO in the OB

To investigate the influence of the PC on the activity of the OB, I reversibly inhibited the PC using muscimol (N=10) or sodium channel blocker TTX (N=6). The infusion

of muscimol into the PC did not significantly alter the power of MK801-dependent HFO within the PC (p=0.1055, Wilcoxon matched-pairs test), nor did it impact HFO power in the OB (p=0.2754, Wilcoxon matched-pairs test), however individual data showed a considerable variability among rats. Figures 4.8 A and B display spectrograms from a representative rat, along with complete time-courses of the recordings. Towards the end of the experiment, reduction in HFO power in the PC reached statistical significance at 25 min. post-infusion (**p=0.0098, Wilcoxon matched-pairs test).

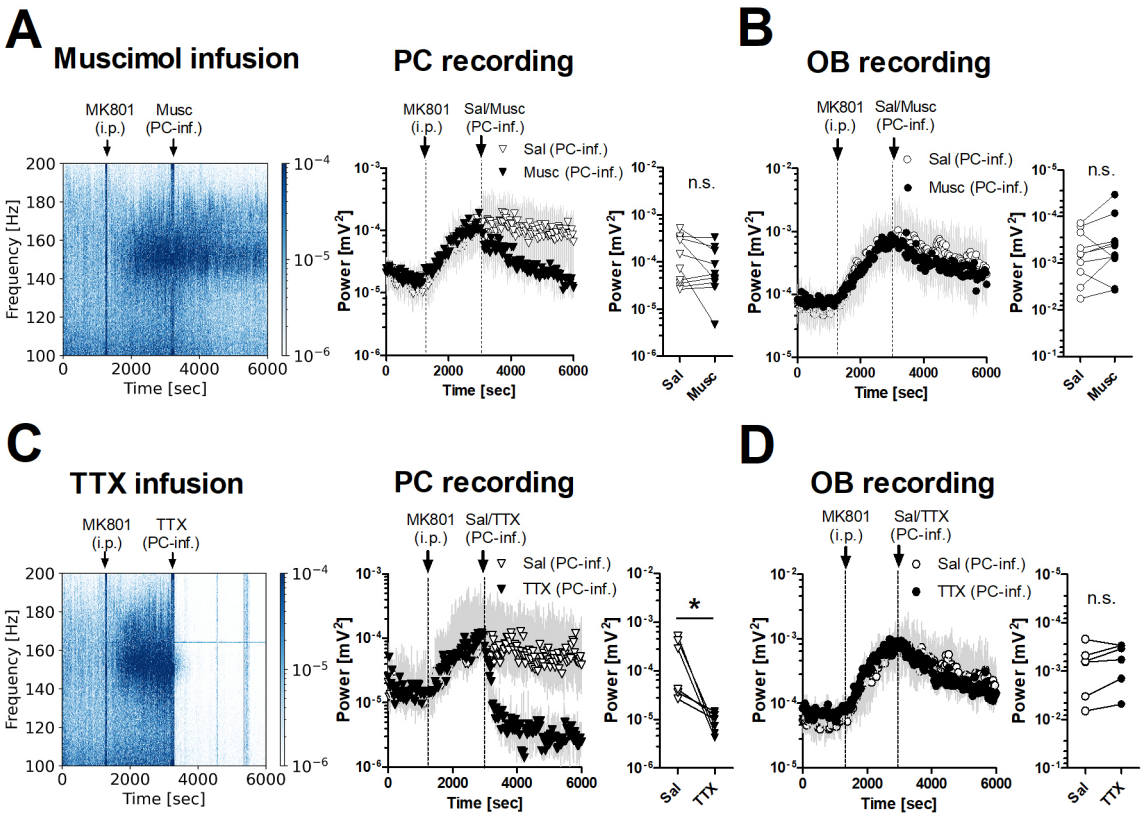

Figure 4.8: **Effect of muscimol or TTX infusion to the PC on the power of MK801-dependent HFO in the OB and PC in freely moving rats. (A, B)** Spectrogram and time-courses illustrate NMDAR-dependent HFO power in the OB and PC after muscimol infusion into PC (N=10). Plots show HFO power for individual rats 5–10 min. post-infusion. **(C, D)** Microinfusion of TTX into the PC reduces MK801-dependent HFO power (130–180 Hz) locally, but not in the OB (N=6). Spectrogram and time-courses demonstrate HFO power after TTX microinfusion in the PC and OB (N=6). Plots present HFO power for individual rats 5–10 min. after TTX or saline infusion (Wilcoxon matched-pairs test, *p<0.05 for the OB); n.s. - not significant.

To investigate the possibility that local infusion of muscimol could reduce output from the PC without significantly affecting afferent input, I next used TTX, which

blocks action potential propagation, thereby suppressing both input to the PC and its output. A subgroup of rats received TTX infusion into the PC. In contrast to the effects observed with muscimol, TTX administration resulted in an immediate reduction in MK801-dependent HFO power within the PC (p=0.0313, Wilcoxon matched-pairs test). Notably, the power of HFO in the OB remained high and was not significantly affected (p=0.0938, Wilcoxon matched-pairs test; see Figures 4.8 C and D).

4.3 Role of DA receptors in NMDAR-dependent HFO in the OB

In the previous sections, I examined the input and major output pathway of the OB. In this section, I focus on local network properties within the OB. This part of the thesis stems from my PRELUDIUM NCN grant titled *"Dopaminergic modulation of high-frequency oscillations in the rat olfactory bulb associated with the NMDA receptor hypofunction model of psychosis."*

The role of DA on NMDAR-dependent HFO in the OB has not been investigated. The OB is abundant in DA neurons and is thought to represent one of the primary sources of DA neurons in the forebrain of rodents (Björklund and Dunnett, 2007). Notably, DA receptors are expressed in mitral/tufted cells and granule cells (Coronas et al., 1997; Gutièrrez-Mecinas et al., 2005), which appear associated with HFO generation (Hunt et al., 2019; Średniawa et al., 2021). Additionally, NMDAR and DA receptors (D1R and D2R) can co-exist in the same neurons and synapses, allowing for direct interactions (Lothmann et al., 2021).

Given the importance of DA in the OB, the following subsections explore the role of DA receptors in MK801-dependent HFO. In subsections 4.3.1 and 4.3.2, I examine the effect of DA receptor stimulation on MK801-dependent HFO, followed by the impact of DA receptor inhibition in subsections 4.3.3 and 4.3.4.

4.3.1 Systemic DA receptor stimulation reduces MK801-dependent HFO frequency in the OB

First, I studied the effect of systemic administration of amphetamine (2 mg/kg) and apomorphine (2 mg/kg) on MK801-dependent HFO (N=7). Amphetamine is an indirect, non-selective agonist of DA receptors which increases the amount of DA (and other monoamines) in the synaptic cleft through various mechanisms, such as increasing DA release from the presynaptic terminals and inhibition of DA reuptake (Faraone, 2018). Apomorphine stimulates both D1R and D2R directly as a direct, non-selective agonist of DA receptors (Jenner and Katzenschlager, 2016). Example spectrogram showing the effect of 2 mg/kg systemic apomorphine injection on MK801-dependent HFO is shown in Figure 4.9 A1.

Neither amphetamine nor apomorphine affected the power of MK801-dependent HFO (Figure 4.9 B). Repeated measures 2-way ANOVA revealed no significant time×group interaction ($F_{(338,3042)}$=0.6916, p=1.0000). Administration of apomorphine, but not amphetamine, reduced the frequency of MK801-dependent HFO (Figure 4.9 C). The mean frequency 40 min. post injection was 125 Hz±0.3476 for apomorphine vs 141 Hz±0.5811 for saline. Repeated measures 2-way ANOVA revealed a significant time×group interaction ($F_{(338,3042)}$=17.35, p<0.0001). Bonferroni's *post hoc* test revealed a significant effect for apomorphine vs saline and apomorphine vs amphetamine, p<0.0001. No significant differences were found for saline vs amphetamine, p>0.05).

In a separate group of rats (N=7) I tested the effect of a D1R agonist 1 mg/kg SKF38393 and D2R agonist 1 mg/kg quinpirole to determine if a specific DA receptor may account for the change in HFO frequency after MK801. Example spectrogram showing the effect of 1 mg/kg systemic quinpirole injection on MK801-dependent HFO is shown in Figure 4.9 A2. Time-courses showing the effects of both agonists on MK801-dependent HFO power and frequency are shown in Figure 4.9 E and F, respectively. Consistent with results for apomorphine neither selective agonists affected HFO power (time×group interaction ($F_{(172,2064)}$=1.153, p=0.0925). How-

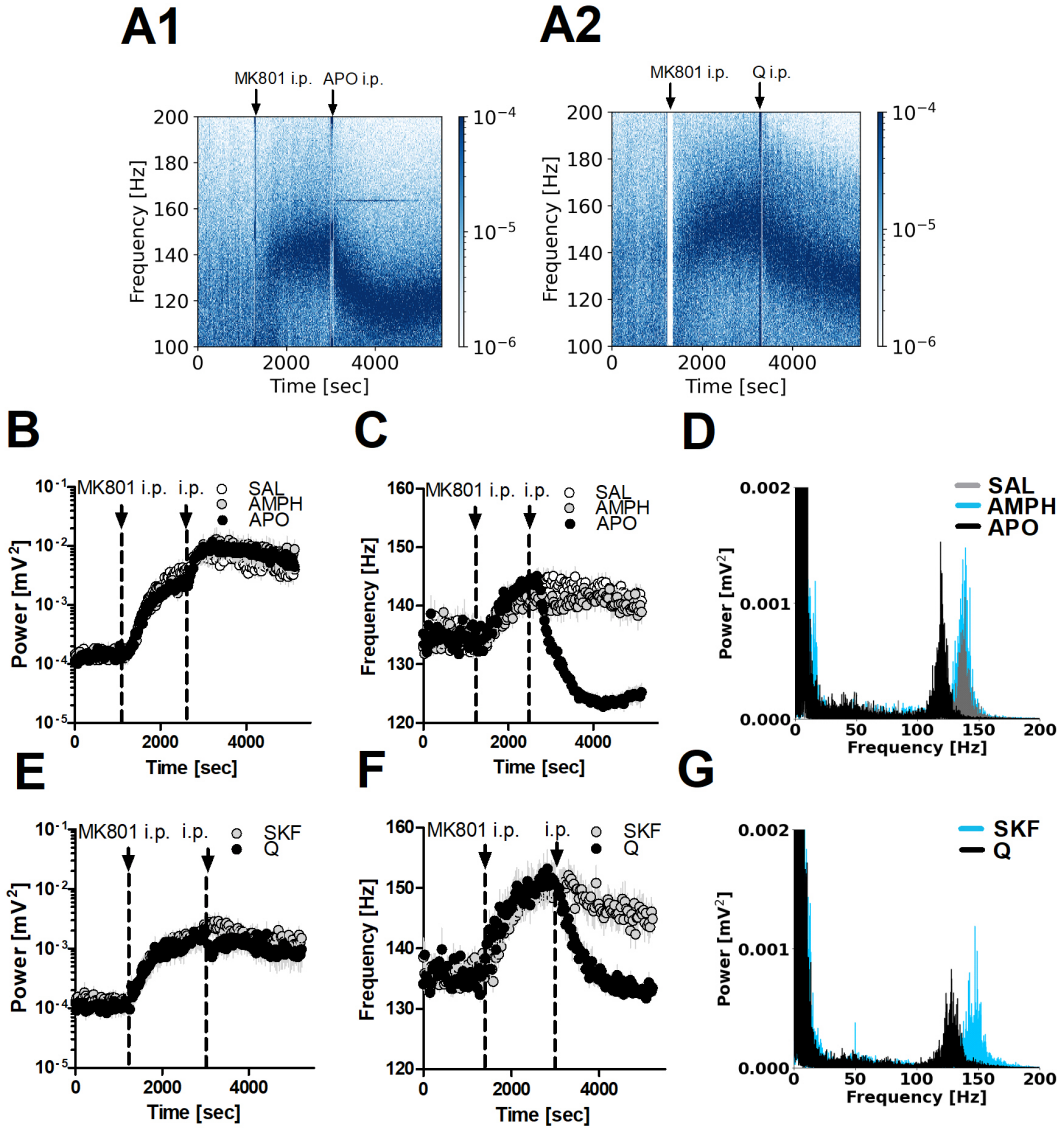

Figure 4.9: **Systemic DA receptor stimulation reduces MK801-dependent HFO frequency, but not power, in the OB *via* a D2R mechanism. (A1, A2)** Example spectrograms showing 2 mg/kg i.p. apomorphine (APO) and 1 mg/kg i.p. quinpirole (Q) effects on MK801-dependent HFO. **(B, C)** Time-courses depict the effects of 2 mg/kg amphetamine (AMPH) and APO on MK801-dependent HFO power and frequency in the OB (N=7). For power, no significant interaction; for frequency, $p<0.0001$. **(D)** Power spectra (60s) show a lower HFO frequency peak after APO compared to AMPH and saline. **(E, F)** Time-courses of Q and 1 mg/kg SKF38393 (SKF) effects on NMDAR-dependent HFO power and frequency (N=7). For power, no significant interaction; for frequency $p<0.0001$. **(G)** Power spectra (60s) indicate a shift to lower HFO frequencies with Q compared to SKF.

ever, quinpirole significantly reduced MK801-dependent HFO frequency compared with SKF38393 (Figure 4.9 F). Repeated measures 2-way ANOVA revealed a significant time×group interaction ($F_{(172,2064)}=7.363$, $p<0.0001$, Bonferroni's *post hoc* test $p<0.01$). The mean frequency 40 min. post injection after quinpirole application

was 134 Hz±0.5334 vs 144 Hz±0.3357 after SKF38393. Figures 4.9 D and G present power spectra with the NMDAR-dependent HFO frequency peak after injection of all drugs. Note that the HFO frequency peak after apomorphine and quinpirole is shifted to lower frequencies.

4.3.2 Local D2R, but not D1R, stimulation affects MK801-dependent HFO in the OB

Given that systemic injection of DA agonists affect MK801-dependent HFO recorded in the OB, I next examined the effect of direct local DA receptor stimulation in the OB. Separate groups of rats were used for D1R agonist SKF38393 at 2.5 or 5 μg/side (N=7) and D2R agonist quinpirole at 2.5 or 12.5 μg/side (N=8) (Figure 4.10).

Representative spectrograms for the higher doses of SKF38393 and quinpirole are presented in Figure 4.10 A1 and A2. Consistent with systemic injection, local infusion of D1R agonist SKF38393 did not substantially affect the power and frequency of MK801-dependent HFO (Figure 4.10 B and C). Repeated measures 2-way ANOVA revealed no significant time×group interaction for SKF38393 ($F_{(438,3942)}$=0.6310, p=1.0000 for power; $F_{(438,3942)}$=0.9856, p=0.5733 for frequency).

Local infusion of quinpirole dose-dependently reduced the power and frequency of MK801-dependent HFO, but with different temporal dynamics. Time-courses showing the effects of quinpirole infusion on MK801-dependent HFO power and frequency are shown in Figure 4.10 D and E, respectively. 2-way ANOVA of the complete time-course revealed a significant effect for HFO frequency alone (time×group interaction $F_{(428,4494)}$=2.860, p<0.0001), but not power ($F_{(428,4494)}$=1.074, p=0.1514).

Closer inspection of the time-courses revealed an apparent reduction in NMDAR-dependent HFO power associated with local infusion of the D2R agonist. I therefore analysed the data in 5 batches (fragment 0 – pre inf., fragments 1-4 post inf., each fragment=10 min.). Repeated measures 1-way ANOVA revealed effects for both power and frequency (p=0.0007 for power, p<0.0001 for frequency). Bonferroni's *post hoc* test revealed a significant effect of 12.5 μg quinpirole infusion for power

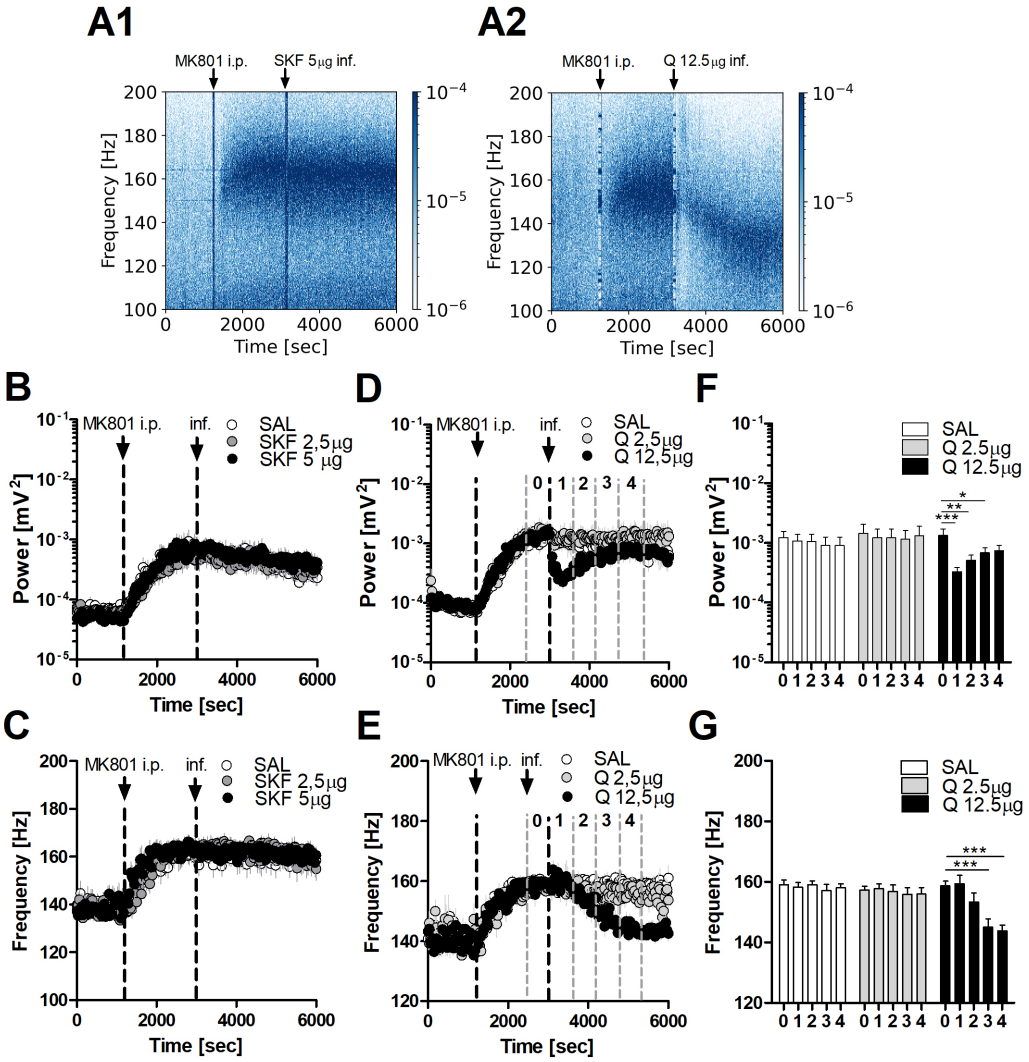

Figure 4.10: **Local infusion of quinpirole, but not SKF38393 to the OB reduces the power and frequency of MK801-dependent HFO in freely moving rats. (A1, A2)** Spectrograms showing MK810-dependent HFO after 5 μg/side D1R agonist SKF38393 (SKF) and 12.5 μg/side D2R agonist quinpirole (Q). **(B, C)** Time-courses presenting effect of 2.5 and 5 μg/side SKF (N=7) on power and frequency of MK801-dependent HFO. **(D, E)** Time-courses presenting effect of 2.5 and 12.5 μg/side Q (N=8) on power and frequency of MK801-dependent HFO. The dashed lines represent 10-min. time bins before and after infusion of Q. **(F, G)** Bar charts showing power and frequency of M801-dependent HFO after 2.5 and 12.5 μg/side Q infusion for the 10-min. bins. Repeated measures 1-way ANOVA revealed no significant effect for SAL and Q2.5 inf., but a significant effect for Q12.5 inf. ($p=0.0007$ for power, $p<0.0001$ for frequency). *$p<0.05$, **$p<0.01$, ***$p<0.001$ (Bonferroni's *post hoc* test).

($p<0.001$) and frequency ($p<0.0001$) (see Figure 4.10 F and G).

To determine the potential drug spread to regions outside the OB I infused four rats with fluorescent SKF83566-green and processed histology across the frontal regions. Analysis shows the drug is relatively well-confined to the OB 15 min. after infusion (Figure 4.11).

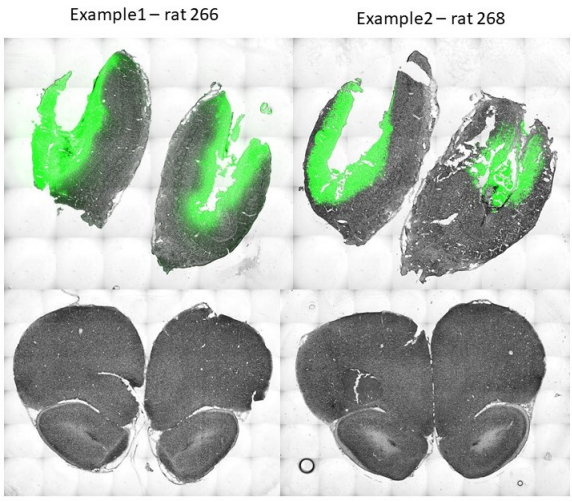

Figure 4.11: **Examples of fluorescent SKF83566-green infusion to the OB.** Please note the drug is relatively well-confined to the OB.

4.3.3 Local blockade of D1R or D2R antagonists does not affect MK801-dependent HFO in the OB

Having shown local D2R stimulation can influence the HFO rhythm in the OB, I next tested the effects D1R and D2R antagonists on HFO power and frequency in a separate groups of rats, hypothesising that these might produce effects opposite to the agonists. I tested local infusion of D1R antagonist SCH23390 at 1 or 6 μg/side (N=7) and D2R antagonist eticlopride at 2.5 or 12.5 μg/side (N=7) (Figure 4.12).

Representative spectrograms for the higher doses of SCH23390 and eticlopride are presented in Figure 4.12 A and D. Time-courses showing the effects of SCH23390 and eticlopride infusion on MK801-dependent HFO power and frequency are shown in Figure 4.12 B, C and E, F, respectively. For power repeated measures 2-way ANOVA revealed no significant time×group interaction for SCH23390 ($F_{(438,3942)}$=0.7433, p=1.0000) and for eticlopride ($F_{(438,3942)}$=0.5075, p=1.0000). Infusion of the DA antagonists had also no effects on the frequency of NMDAR-dependent HFO (SCH23390, $F_{(438,3942)}$=0.6988, p=1.0000; eticlopride, $F_{(438,3942)}$=0.7937, p=0.9991). Although there were no obvious effects on the HFO rhythm, local infusions of both D1R and D2R antagonists did reduce MK801-enhanced LMA dose-dependently (see Table 4.1 for full details).

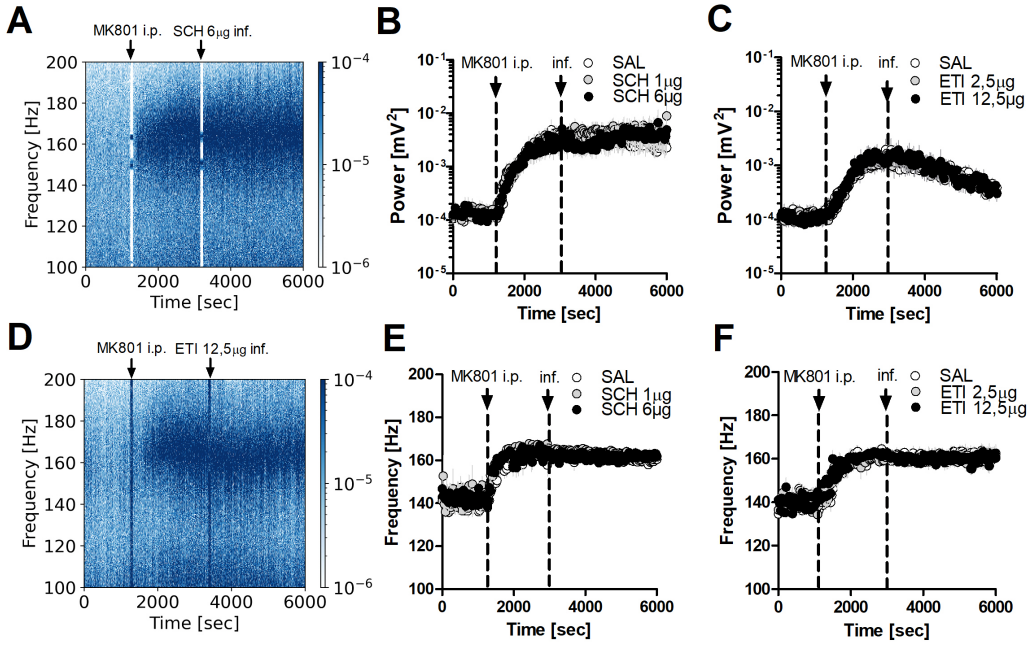

Figure 4.12: **Local OB infusion of SCH23390 or eticlopride does not affect the power or frequency of MK801-dependent HFO in freely moving rats.** **(A, D)** Spectrograms showing MK801-dependent HFO after 6 μg/side D1R antagonist SCH23390 (SCH) and 12.5 μg/side D2R antagonist eticlopride (ETI). **(B, E)** Time-courses presenting effect of 1 and 6 μg/side SCH on power and frequency of MK801-dependent HFO (N=7). **(C, F)** Time-courses presenting effect of 2.5 and 12.5 μg/side ETI on power and frequency of MK801-dependent HFO (N=7).

4.3.4 Systemic blockade of D1R and D2R does not affect MK801-dependent HFO in the OB

Next, I tested whether systemically administered DA antagonists produce effects on NMDAR-dependent HFO similar to those observed with local infusion. Rats (N=8) received coadministration of 1 mg/kg D2R antagonist eticlopride and 1 mg/kg D1R antagonist SCH23390 following 0.15 mg/kg MK801 (Figure 4.13). Example spectrogram showing the effect of eticlopride+SCH23390 systemic coadministration on MK801-dependent is shown in Figure 4.13 A. Time-courses showing the effect of eticlopride+SCH23390 coadministration on MK801-dependent HFO power, frequency and LMA are shown in Figure 4.13 B, C and D, respectively. 2-way ANOVA revealed no significant time×group interaction ($F_{(219,3066)}$=1.033, p=0.3617 for power, $F_{(219,3066)}$=0.9374, p=0.7320 for frequency) and significant time×group interaction ($F_{(220,2640)}$=9.17, p<0.0001 for LMA (Bonferroni's *post hoc* test p<0.0001).

Drug and dose	Receptor	ANOVA	Bonferroni	Significance
SCH23390: 1μg, 6μg	D1R	p=0.0071	sal vs 1μg sal vs 6μg 1μg vs 6μg	n.s. p<0.05 p<0.05
eticlopride: 2.5μg, 12.5μg	D2R	p=0.0287	sal vs 2.5μg sal vs 12.5μg 2.5μg vs 12.5μg	n.s. p<0.05 n.s.
SKF38393: 2.5μg, 5μg	D1R	p=0.1280	sal vs 2.5μg sal vs 5μg 2.5μg vs 5μg	n.s. n.s. n.s.
quinpirole: 2.5μg, 12.5μg	D2R	p=0.1255	sal vs 2.5μg sal vs 12.5μg 2.5μg vs 12.5μg	n.s. n.s. n.s.

Table 4.1: **Effect of DA agonists and antagonists on MK801-enhanced LMA.** Repeated measures 1-way ANOVA of beam break activity revealed significant effects for DA antagonists (p=0.0071 for SCH23390, p=0.0287 for eticlopride). Bonferroni's *post hoc* test, p<0.05. Repeated measures 1-way ANOVA revealed no change in beam break activity for the DA agonists (p=0.1280 for SKF38393, p=0.1255 for quinpirole); n.s. – not signifcant.

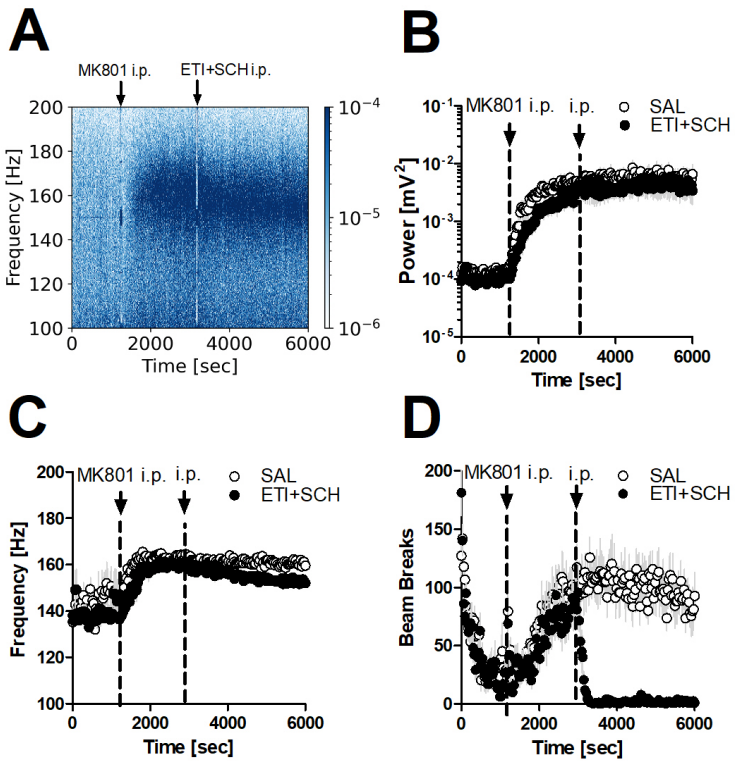

Figure 4.13: **Systemic coadministration of SCH23390 and eticlopride does not affect MK801-dependent HFO power and frequency, but reduces LMA.** **(A)** Representative spectrogram illustrating the effects of systemic injection of 1 mg/kg eticlopride+1 mg/kg SCH23390 (ETI+SCH) on MK801-dependent HFO. **(B)** Time-course presenting the effect of coadministration of ETI+SCH on MK801-dependent power. **(C)** Time-course presenting the effect of coadministration of ETI+SCH on MK801-dependent frequency. **(D)** Complete time-course presenting the effect of coadministration of ETI+SCH on MK801-enhanced LMA, p<0.0001; for all time-courses N=7.

4.4 Exploratory investigations

This chapter explores preliminary investigations that may guide future research in the HFO field. Section 4.4.1 examines the impact of local NMDAR blockade in the OB on HFO, while section 4.4.2 evaluates the effects of two antipsychotic drugs on MK801-dependent HFO in the OB.

4.4.1 Local blockade of NMDAR in the OB increases HFO power

Numerous independent research groups have shown that NMDAR blockade enhances HFO power, primarily following systemic administration. However, evidence also exists that localized infusion of MK801 in regions such as the nucleus accumbens, prefrontal cortex, or hippocampus can increase HFO power (Hunt et al., 2010, Lee et al. 2017). Whether a local NMDAR blockade in the OB alone can elevate HFO power remained an open question.

To answer this question, I examined the effects of a systemic injection of 0.15 mg/kg MK801 and a 4 μg intra-OB infusion in seven rats. Representative spectrograms displaying MK801-dependent HFO following either i.p. or local infusion are presented in Figure 4.14 A and B, respectively.

In both cases administration was associated with an increase in the power of HFO. Notably after local, but not systemic injection, I observed occasional short-lasting (50-200s) attenuation of NMDAR-dependent HFO which was associated with recovery of this rhythm at a higher frequency. Examples of 130-200 Hz HFO filtered and raw LFPs signals after systemic injection or local infusion of MK801 are shown in Figure 4.14 D and E, respectively. Associated power spectra for 60s before and after MK801 administration are shown in Figure 4.14 G and H, respectively, and were linked with increases in HFO band.

Complete time-courses showing increases in HFO power (Figure 4.14 C) and frequency (Figure 4.14 F) were comparable for systemic and local infusion of MK801.

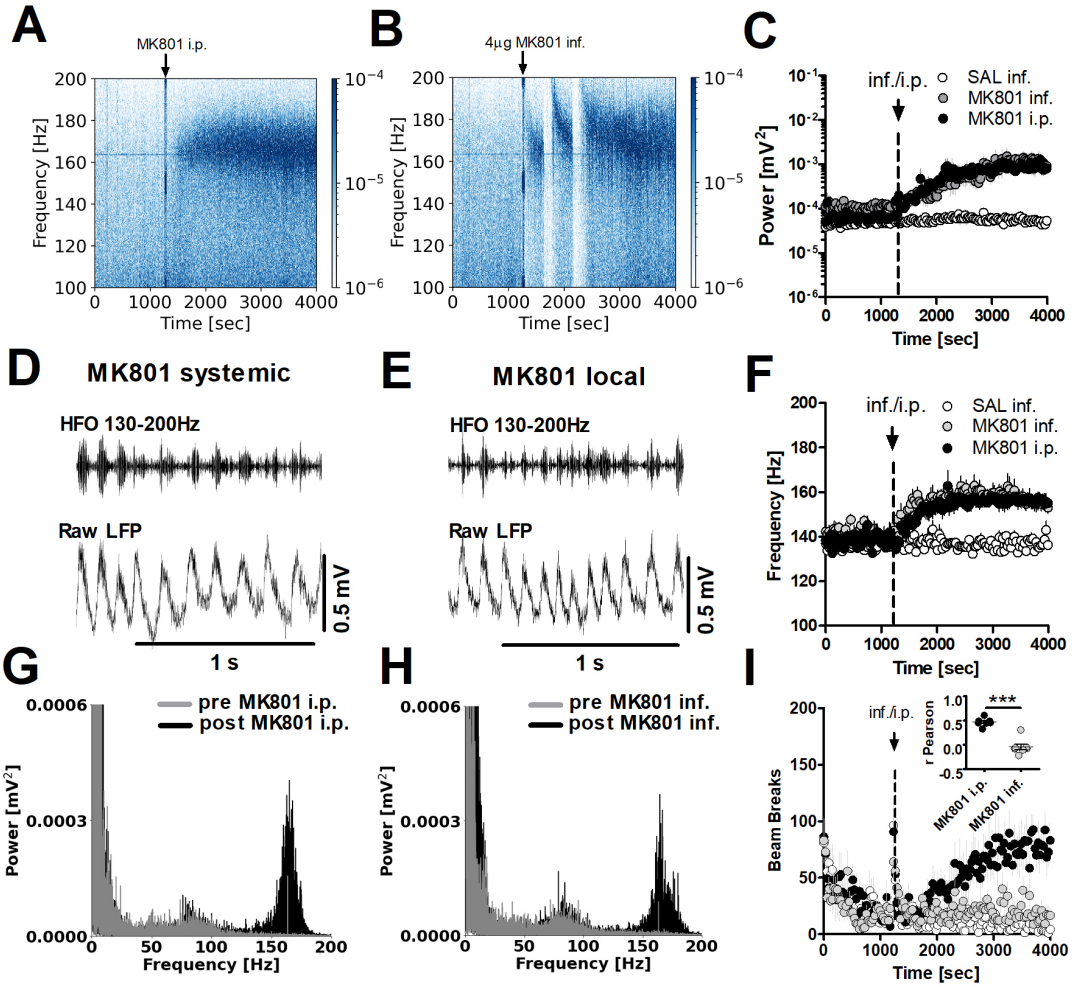

Figure 4.14: **Systemic vs local NMDAR blockade in the OB: effects on MK801-dependent HFO power and LMA.** **(A, B)** Example spectrograms show MK801-dependent HFO after systemic injection (0.15 mg/kg i.p.) and local OB infusion (4 μg/side). **(C)** Time-course of HFO power changes following MK801 i.p. or infusion, $p<0.0001$. **(D, E)** 130–200 Hz HFO filtered and raw LFPs signals after MK801 i.p. or infusion in OB reveal burst-localized HFO. **(F)** Time-course of HFO frequency changes post MK801 i.p. or infusion, $p<0.0001$. **(G, H)** Power spectra (60s) pre- and post-MK801 show an HFO peak around 170 Hz after i.p. injection or infusion. **(I)** LMA time-course following MK801 i.p. and OB infusion, $p<0.0001$, with LMA-HFO power correlation post MK801 i.p. (mean $r=0.465\pm0.031$), and after infusion (mean $r=-0.046\pm0.062$; paired t-test, $p=0.0004$); ***$p<0.001$, for all time-courses N=7.

Repeated measures 2-way ANOVA revealed a significant time×group interaction for HFO power ($F_{(318,2862)}=2.764$, $p<0.0001$) and HFO frequency ($F_{(318,2862)}=4.219$, $p<0.0001$). In both cases Bonferroni's *post hoc* test revealed a significant effect for saline vs MK801 inf., $p<0.001$; saline vs MK801 i.p., $p<0.01$ for power and saline vs MK801 inf., $p<0.0001$; saline vs MK801 i.p., $p<0.0001$ for frequency. There was no significant difference between MK801 inf. vs MK801 i.p., $p>0.05$.

Despite similar increases in HFO power and frequency, LMA, increased significantly after MK801 i.p., but not local infusion (Figure 4.14 I). Repeated measures 2-way ANOVA revealed a significant time×group interaction ($F_{(318,2862)}$=3.467, p<0.0001). Bonferroni's *post hoc* test revealed a significant effect for saline vs MK801 i.p. and MK801 i.p. vs MK801 inf., p<0.0001. There was no significant difference between saline vs MK801 inf., p>0.05. Changes in LMA correlated with HFO power after MK801 i.p. in 7/7 rats, but only 2/7 rats after local infusion. The mean Pearson r value for MK801 i.p.=0.4649±0.03112, vs MK801 infusion=-0.04591±0.06201 were significantly different paired t-test, p=0.0004 (Fig. 4.14 I, insert).

4.4.2 Differential effects of a 2^{nd} and 3^{rd} generation antipsychotic drug on MK801-dependent HFO in the OB

All antipsychotics are known to act primarily through D2R, in addition to interactions with other receptor types (Grace and Uliana, 2023). In order to explore effects of antipsychotics on MK801-dependent HFO in the OB, I examined the impact of two antipsychotic drugs: aripiprazole, a 3^{rd} generation antipsychotic which act as a partial agonist at D2R (Bymaster et al., 1996) and risperidone, a 2^{nd} generation antipsychotic shown previously to reduce HFO frequency in other brain regions (Olszewski et al., 2013b; Delgado-Sallent et al., 2022).

Representative spectrograms illustrating the effects of 3 mg/kg aripiprazole and 3 mg/kg risperidone systemic injection on MK801-dependent HFO are presented in Figure 4.15 A1 and A2. Time-courses showing the effect of aripiprazole, risperidone and control vehicle (DMSO) on MK801-dependent HFO power, frequency and LMA are shown in Figure 4.15 B, C and D, respectively (N=7). Repeated measures 2-way ANOVA revealed significant time×group interaction for power ($F_{(438,3942)}$=1.90, p<0.001), frequency ($F_{(438,3942)}$=4.38, p<0.0001) and LMA ($F_{(438,3942)}$=4.61, p<0.0001). Bonferroni's *post hoc* test revealed a significant effect for power (vehicle vs risperidone, p<0.001 and aripiprazole vs risperidone, p<0.05), frequency (vehicle vs risperidone and aripiprazole vs risperidone, both p<0.0001) and LMA (vehicle

vs risperidone, p<0.001 and aripiprazole vs risperidone, both p<0.0001), but no difference between vehicle vs aripiprazole, p>0.05, for power, frequency and LMA.

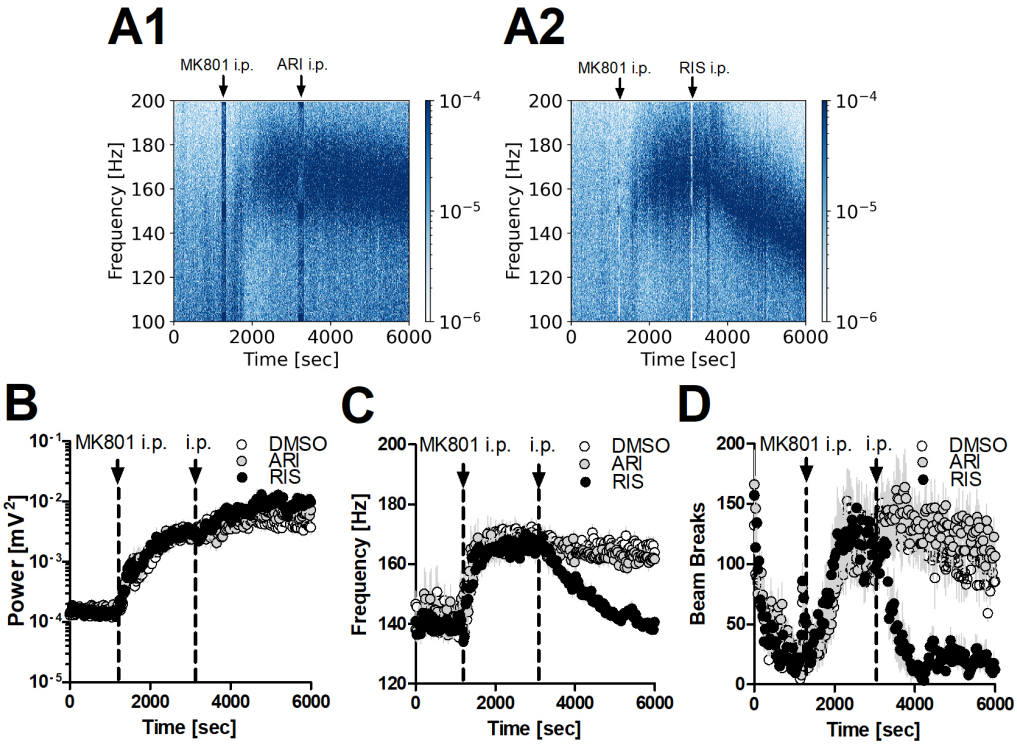

Figure 4.15: **Risperidone, but not aripiprazole, reduces MK801-dependent HFO frequency and LMA. (A1, A2)** Representative spectrograms illustrating the effects of systemic injection of 3 mg/kg aripiprazole (ARI), and 3 mg/kg risperidone (RIS) on MK801-dependent HFO. **(B)** Time-course presenting the effect of systemic injection of aripiprazole (ARI), risperidone (RIS) and control vehicle on MK801-dependent power, p<0.001. **(C)** Time-course presenting the effect of systemic ARI, RIS and control vehicle on MK801-dependent frequency, p<0.0001. **(D)** Time-course presenting the effect of systemic ARI, RIS and vehicle on MK801-enhanced LMA, p<0.0001; for all time-courses N=7.

Chapter 5

Discussion

5.1 NMDAR-dependent HFO in the brain

Ketamine, a widely used NMDAR antagonist in clinical settings, has shown diverse applications, most notably in emerging treatments for depression (Krystal et al., 2019; Glue et al., 2024), though its precise mechanisms of action remain unclear. In preclinical research, ketamine and other NMDAR antagonists are used to model psychotic-like states (Mouri et al., 2007; Manahan-Vaughan et al., 2008; Frohlich and Van Horn, 2013). NMDAR antagonists are known to affect brain rhythms broadly across animal and human models (Pinault, 2008; Hakami et al., 2009; Shaw et al., 2015). Among these rhythms, NMDAR-dependent HFO have been documented in rodents (Hunt et al., 2006), higher mammals (Yan et al., 2022, Castro-Zaballa et al., 2024), and in humans (Nottage et al, 2023) across many brain regions (see the Table A.1 in Appendix A). Recent research identified the OB as a primary generator and main source of ketamine-dependent HFO in the rat brain (Hunt et al., 2019), with further findings showing that under Ket/Xyl sedation, HFO depended on nasal input (Średniawa et al., 2021). Building on this foundation, this thesis explores NMDAR-dependent HFO with an emphasis on the OB and its input and output connections.

My results indicate that NMDAR-dependent HFO in the OB are modulated by nasal respiration, as demonstrated by their alignment with respiration rhythms

and reduction following naris blockade. The OB is essential for generating these oscillations, which are also present in the PC at a lower power, appearing to depend on the OB as a primary generator. Additionally, local NMDAR blockade in the OB enhancing HFO, emphasizing the importance of NMDAR in this rhythm. I further demonstrated that D2R stimulation in the OB affects both the power and frequency of NMDAR-dependent HFO. Reduction of NMDAR-dependent frequency was also seen with a 2^{nd} generation antipsychotic, whereas a 3^{rd} generation antipsychotic had no impact. These findings highlight the complex interaction between respiration, neurotransmitter systems, and NMDAR-dependent HFO in the olfactory system.

5.2 Generation of NMDAR-dependent HFO in the OB

My results provide strong evidence that the OB acts as a primary generator of aberrant HFO following NMDAR antagonist administration.

I demonstrated that muscimol infusion into the OB led to immediate, parallel reductions in NMDAR-dependent HFO power in both the OB and PC. This aligns with prior findings, where muscimol infusion in the OB eliminated NMDAR-dependent HFO in the OB and VS (Hunt et al., 2019). These results suggest that inhibition of this rhythm in the OB suppresses HFO in non-OB structures, supporting the idea, that NMDAR-dependent HFO observed in these areas depends on the OB as the primary generator.

However, muscimol infusion into the PC had comparatively weak effects locally and no effects in the OB. To investigate further, I used the sodium channel blocker TTX, which, unlike muscimol, blocks not only local neuronal activity but also passing fibers and axonal input to the infused area (Martin and Ghez, 1999). The immediate reduction in NMDAR-dependent HFO power following TTX infusion in the PC likely reflects its action on passing fibers, specifically by disrupting transmission at presynaptic terminals from the OB to the dendrites of pyramidal cells in

the PC. In contrast, muscimol primarily affects postsynaptic inhibition, preserving synaptic activity and allowing NMDAR antagonist-dependent HFO to maintain a high amplitude. These findings suggest that NMDAR-dependent HFO in the PC is not generated by an intrinsic PC network, as it is in the OB, but rather arises, at least in part, from axonal input originating from the OB.

The second line of evidence comes from naris block experiments. Previously, we demonstrated that unilateral naris block in Ket/Xyl-sedated rats attenuated Ket/Xyl-dependent HFO in the ipsilateral OB (Średniawa et al., 2021). Here, I demonstrated similar results in freely moving, ketamine-treated rats, free from Ket/Xyl sedation limitations. Moreover, attenuation of NMDAR-dependent HFO, parallel to the effect in the OB, was also observed in the PFC and VS, suggesting that nasal respiration is essential for sustaining this rhythm across multiple brain regions.

Commonly used monopolar recordings can introduce issues like contamination from volume-conducted rhythms and interference from activity at the reference electrode. Although the reference electrode is typically positioned at a distance, it is rarely completely inactive, which can compromise signal clarity (Holsheimer and Feenstra, 1977). To reduce volume-conducted currents, I confirmed results using bipolar recordings (Marmor et al., 2017), allowing for a more precise localization of regions generating specific activity. The clear detection of HFO at baseline and following NMDAR antagonist administration in bipolar signals from the OB supports the presence of HFO generator within this structure.

In line with this, I also showed that local infusion of MK801 into the OB alone is sufficient to elevate HFO power to levels similar to those seen with systemic administration. This suggests that NMDAR blockade within the OB can directly drive HFO increases. Notably, local infusion intermittently ceased HFO, likely due to NMDAR inhibition in mitral and tufted cells, disrupting OB rhythm generation (Schoppa, 1998). Similar waxing and waning HFO patterns were observed in the ventral striatum following high-dose MK801 administration (Hunt et al., 2010).

This finding aligns with previous work, which showed that HFO current dipoles were located near the mitral layer, mitral/tufted cells firing was phase-locked to HFO, and removal of the piriform cortex and surrounding areas did not disrupt HFO (Hunt et al., 2019; Średniawa et al., 2021). Taken together, these results suggest that the OB is likely the primary generator of HFO, though the existence of additional HFO generators outside the OB cannot be excluded.

5.3 NMDAR-dependent HFO and nasal input

Nasal respiration is essential for olfaction, enabling rodents to receive sensory information from the external environment (Alberts and May, 1980). I observed that NMDAR-dependent HFO bursts were synchronized with the respiratory rhythm, as recorded by thermocouples and in the OB. The coupling of faster and slower oscillations is thought to facilitate communication between distant brain regions (Lin et al., 2020). NMDAR blockade, which promotes the generation of HFO within local networks, in combination with nasal respiration, may provide a synchronization mechanism across brain regions. In my results, this coupling was particularly evident between the OB and PC, a structure integral to olfactory processing that serves as a primary target for OB projections (Haberly and Bower, 1989) and also provides feedback projections back to the OB, thus modulating its activity (Boyd et al., 2012, 2015). CFC analysis revealed that NMDAR-dependent HFO was coupled with slow oscillations in both the OB and PC. Additionally, slow rhythms in the OB modulated HFO in the PC, showing that they can drive NMDAR-dependent HFO in both the primary generator site and distant structures.

Based on our previous finding that an unobstructed nasal airflow is essential for Ket/Xyl-dependent HFO (Średniawa, 2021), along with suggestions about potential role for OSN, I demonstrated that this process likely depends on pressure changes in the nares rather than direct activation of olfactory receptors. Odorant molecules are detected by receptors in OSN in the nasal epithelium (Mombaerts, 1999). Signals from these receptors are transmitted directly to the OB *via* the ON, where ON's ter-

minals form synapses with mitral and tufted cells, initiating the primary processing of olfactory information (Pinching and Powell, 1971). Odours modulate oscillatory activity (including faster rhythms like gamma) within the OB and related olfactory structures (Kay, 2014; Martin and Ravel, 2014); however my findings demonstrate that none of the tested odours influenced Ket/Xyl-dependent HFO power, suggesting that direct stimulation of olfactory receptors is not essential for HFO generation. A limitation of this result is that only specific odours were tested, leaving open the possibility that other, non-tested odours could exert a different effect.

OSN are also known to respond to mechanical stimulation (Grosmaitre et al., 2007). In line with this, my findings show that manipulating air pressure in the nasal cavity, thereby mechanically stimulating OSN, increased Ket/Xyl-dependent HFO power. This result aligns with previous findings that blocking airflow attenuates Ket/Xyl-dependent HFO (Średniawa et al., 2021), suggesting that HFO generation at the sensory level may be regulated by the presence or absence of airflow, acting as a binary factor (0-1).

Taken together, these results suggest that NMDAR-dependent HFO in the OB are closely linked to the respiratory rhythm, with nasal respiration acting as a primary driver for these oscillations within the OB, the PC, and potentially other regions. These findings also support a model in which respiratory-driven mechanical stimulation of OSN, rather than odour detection, modulates HFO, highlighting the OB as the primary HFO generator in response to sensory-driven respiration.

5.4 D2R stimulation affects NMDAR-dependent HFO

The OB's primary function is to process olfactory information (Mori et al., 1999), with DA serving as one of the key neurotransmitters in this process (Escanilla et al., 2009), acting through DA receptors widely distributed throughout this structure (Gutiérrez-Mecinas et al., 2005). My results show that neither systemic nor local

blockade of D1R and D2R affected HFO generation after NMDAR blockade. This is in line with several previous studies, for example systemic D1R blockade did not affect ketamine-dependent HFO in motor cortex, striatum and hippocampus (Ye et al., 2018) or local infusion of D1R and D2R, infused separately or together in the nucleus accumbens, had no impact on HFO after ketamine (Matulewicz et al., 2010).

Surprisingly, stimulation of D2R (but not D1R) within the OB reduced the frequency of MK801-dependent HFO, accompanied by a transient reduction in power. Previously we hypothesised that HFO associated with NMDAR blockade are generated in the OB by excitatory-inhibitory interplay between mitral/tufted neurons and inhibitory neurons (Średniawa et al., 2021). DA neurons are predominantly found in glomerular layers (Pignatelli and Belluzzi, 2017), where they are thought to modulate olfactory input. *In vitro* studies have shown that D2R stimulation can reduce excitatory drive from the ON onto mitral cells (Hsia et al., 1999). Indeed, the initial short-lasting reduction of HFO power after local infusion of quinpirole could be explained by reduced drive from the ON. Consistent with this, others have shown that stimulation of D2R in the terminals could lead to a reduction in glutamate release, diminishing excitatory drive within the glomerulus (Berkowicz and Trombley, 2000; Ennis et al., 2001).

Whilst reductions in NMDAR-dependent HFO power could be explained by actions at the glomerulus, reductions in frequency are likely to be more complex. The terminals and apical dendrites of mitral/tufted cells express D2R (Coronas et al., 1997; Gutièrrez-Mecinas et al., 2005). One possible explanation is D2R-dependent change in ion channel kinetics. For example slowing of potassium channels thereby extending the refractory period of action potentials in mitral/tufted cells would be expected to slow down the NMDAR-dependent HFO rhythm (Lacey et al., 1987; Benardo and Prince, 1982; see also: Maurice et al., 2004 and Valdés-Baizabal et al., 2015).

Taken together, these results suggest that NMDAR-dependent HFO in the OB

are predominantly generated independently of DA influence. However, exogenous stimulation of D2R receptors can modulate this rhythm, likely by altering the excitatory-inhibitory balance in the OB, particularly at the glomerular level, where DA modulates olfactory input.

5.5 NMDAR-dependent HFO and behaviour

I demonstrated that ketamine induced a distinct breathing pattern in rats, characterized by continuous, stereotyped, and purposeless sniffing that persisted for nearly the entire duration of ketamine's action (approximately 15 min.). This finding aligns with the general increase in stereotypy observed following ketamine and other NMDAR antagonists (Tiedtke et al., 1990), which are linked to the activation of the DA system (Conti et al., 1997). Indeed, this behaviour was reversible by the antipsychotic haloperidol, which primarily blocks D2R (Niemegeers and Laduron, 1976) without influencing ketamine-dependent HFO.

Although an increase in HFO power is often associated with increased LMA (e.g., Ye et al., 2018; Zepeda et al., 2022; Cui et al., 2022) also dependent on DA system (Beninger, 1983), it does not necessarily indicate a functional link to movement (Hunt et al., 2006). Here, I show that muscimol inhibition of the OB attenuated MK801-dependent HFO without affecting hyperactivity, which is consistent with other studies (Olszewski et al., 2013a; Hansen, 2019) demonstrating that changes in NMDAR-dependent HFO and movement can be dissociated.

Thus, while the abberant HFO rhythm generated by the OB is not directly related to LMA, the OB itself may have important roles in LMA. Indeed, olfactory bulbectomy (OBX) rats exhibit locomotor hyperactivity, and also display increased LMA after NMDAR antagonists although at a reduced intensity (Redmond et al., 1997; Robichaud et al., 2001). This suggests that other OB networks can mediate motor control, at least in part. My work shows that MK801-dependent LMA was reduced by DA antagonists administered either intra-OB or systemically, with notable differences in effect: systemic injection typically induced continuous catalepsy,

whereas local infusion did not. DA signalling in the OB may influence LMA indirectly through broader neural circuits, particularly those related to motivation, reward, and sensory processing (Bromberg-Martin et al., 2010). Since rodents heavily depend on olfaction for exploration (Schultz and Tapp, 1973), impaired olfactory processing at D1R and D2R may underlie the reduced LMA output following MK801 injection (Escanilla et al., 2009).

Most studies examining NMDAR-dependent HFO have focused on its relevance to the NMDAR hypofunction model of psychotic-like states, which is supported by the fact that the NMDAR-dependent HFO band also interacts with antipsychotics (Olszewski et, al. 2013b; Goda et al., 2015; Hunt et al., 2015; Delgado-Sallent et al., 2021; Stan et al., 2024). Here I demonstrated that risperidone, but not aripiprazole, decreases MK801-dependent HFO frequency in the OB. I also found risperidone reduced MK801-enhanced locomotion in contrast to aripiprazole consistent with a previous reports (Su et al., 2007; Adraoui et al., 2024). Aripiprazole, a 3^{rd} generation antipsychotic, acts as a partial D2R agonist (Bymaster et al., 1996). However, when aripiprazole binds to D2R, it elicits a weaker response than the neurotransmitter DA itself (Hirose and Kikuchi, 2005; Tuplin and Holahan, 2017). This may explain the lack of effect on NMDAR-dependent HFO frequency, in contrast to full DA receptor agonists such as quinpirole and apomorphine, which have stronger affinities for DA receptors than DA itself, and may remain bound for longer (Durdagi et al., 2016), thereby reducing frequency of NMDAR-dependent HFO.

Taken together, these results suggest that NMDAR-dependent HFO in the OB are not directly linked to LMA. While the OB may not directly drive LMA, it likely plays an important role in modulating motor behaviour through broader neural circuits, particularly those involving motivation and sensory processing. These results underscore the complex interaction between NMDAR, DA signalling, and behaviour, particularly in the context of psychotic-like states.

5.6 Limitations of the study

While the findings of this thesis are compelling, several limitations should be acknowledged:

1) Odour experiment limitations. The study employed a restricted selection of odours, specifically chosen to activate different regions of the olfactory epithelium and distinct populations of olfactory sensory neurons. However, biologically significant odours for rats, such as predator scents or those associated with rewards, were not included. Additionally, all odour experiments were conducted under Ket/Xyl anesthesia rather than in freely moving conditions, limiting the ability to confirm these findings in awake rats. Pheromones were also not investigated, but they are unlikely to play a major role as they primarily target the vomeronasal organ (Pérez-Gómez et al., 2014).

2) Electrode technology. Electrophysiological recordings were conducted using twisted-wire electrodes. Although effective, the use of advanced multichannel electrodes would have enabled more detailed spatial mapping of NMDAR-dependent HFO within the studied structures, potentially yielding richer and more precise data.

3) Global measurement of LMA. Locomotion was assessed at a global level, which restricted the ability to capture specific behavioral nuances in rats following pharmacological interventions. Investigating a wider range of behaviors could reveal associations directly linked to NMDAR-dependent HFO.

4) Focus on frontal brain structures. My research concentrated exclusively on frontal brain regions, where the amplitude of NMDAR-dependent HFO is strongest. Structures such as the VS and PFC were prioritized due to their traditional association with psychoses. Investigating NMDAR-dependent HFO in more distal brain areas could offer insights into whether this rhythm shares similar characteristics across the brain. However, previous studies suggest that the power of NMDAR-dependent HFO in these regions is generally weaker compared to frontal structures.

5) Lack of single-unit recordings. The study did not include single-unit neuronal

recordings. Such data could elucidate whether NMDAR-dependent HFO is closely tied to specific neuronal firing patterns in the examined structures, offering a deeper understanding of the neural mechanisms underlying this rhythm. Addressing this limitation is the focus of an ongoing postdoctoral project in our laboratory.

5.7 Functional relevance and future work

NMDAR antagonists such as PCP and ketamine can induce symptoms that closely resemble those seen in schizophrenia (Bey and Patel, 2007; Beck et al., 2020), whereas abnormal oscillatory activity has been linked to psychiatric disorders, particularly psychotic-like states (Hunt et al., 2017; Uhlhaas and Singer, 2017). Aberrant HFO may disrupt communication between brain regions, potentially contributing to the cognitive and sensory processing deficits observed in neuropsychiatric disorders. Consequently, HFO associated with NMDAR hypofunction could represent a key neural mechanism underlying the pathophysiology of various neuropsychiatric conditions.

The HFO field presents numerous exciting avenues for exploration. For example comparative studies in different species or strains could reveal how HFO mechanisms are conserved or specialized in olfactory circuits and non-olfactory circuits. While DA role in modulating HFO has been initially explored, investigating the influence of other neuromodulatory systems like serotonin, norepinephrine, and acetylcholine could uncover additional mechanisms that affect these oscillations. From the clinical perspective studying how age and developmental stage shape aberrant HFO characteristics could highlight age-dependent plasticity, offering insights into neurodevelopmental and neurodegenerative disorders. Additionally, given the involvement of NMDAR and DA pathways in conditions like schizophrenia, future research could examine how therapeutic interventions targeting these pathways affect HFO patterns (if confirmed in psychiatric patients), potentially informing biomarkers and mechanisms underlying these disorders.

Chapter 6

Summary and conclusions

All the main research questions of this thesis were addressed, demonstrating that:

1. Nasal input likely drives NMDAR-dependent HFO primarily through the stimulation of OSN mechanoreceptors, rather than chemoreceptors. This input is essential for the generation of this rhythm. It suggests that nasal respiration, which entrains NMDAR-dependent HFO, provides an initial depolarization that modulates the neural oscillatory activity, potentially influencing sensory processing and cognitive functions.

2. NMDAR-dependent HFO in the PC is approximately tenfold lower than in the OB. Reversible inhibition of the OB reduces NMDAR-dependent HFO power both locally in the OB and in the PC, while inhibition of the PC does not significantly affect HFO power in the OB. This suggests that the OB is the primary generator of NMDAR-dependent HFO, and that HFO observed in the PC, as well as potentially in other brain areas, relies on this primary generator in the OB.

3. Although the DA system contributes to certain of the effects produced by NMDAR antagonists, such as behavioural hyperactivity, it does not markedly underlie the generation of NMDAR-dependent HFO. Despite this, local exogenous D2R stimulation in the OB influences the power and frequency of this rhythm. This suggests that non-DA networks, such as excitatory-inhibitory

circuits, underlie HFO generation in the OB, with DA playing a modulatory role.

General conclusion: NMDAR antagonists, particularly ketamine, are well-known to produce neuropsychiatric effects, but the neuronal networks affected by this class of compound are only partially understood. A growing number of studies, in a variety of mammals, have reported the existence of NMDAR-dependent HFO across multiple brain areas. This thesis demonstrates the importance of the OB and nasal respiration rhythm in the generation of HFO after NMDAR antagonists within the OB, and more widely in structurally and functionally distinct brain regions. These findings highlight olfactory networks, which are frequently overlooked in psychopharmacology research, as a potentially important site of action for this class of compounds. Future studies should be directed to understand the functional significance of this rhythm for the neuropsychiatric field.

Appendix A

HFO review table

Below is a table summarizing the findings from the NMDAR-dependent HFO review. The first column lists the types of NMDAR antagonists and their doses, the second column identifies the brain structures where NMDAR-dependent HFO were recorded, and the last column highlights the key findings, with references to the corresponding articles. The articles are arranged in chronological order.

Drug, dose	**Structures (Species)**	**Key HFO related findings (Ref.)**
10-200 mg/kg Ket, 0.1 mg/kg MK801	NAc (Rats)	Ketamine dose-dependently ↑HFO power and frequency which correlated with locomotion. ↑HFO power after MK801, but not amphetamine. (Hunt et al., 2006)
25 mg/kg Ket	NAc (Rats)	Systemic lamotrigine ↓HFO power after ketamine. Intra-NAc lamotrigine did not prevent ketamine-induced ↑HFO power. (Hunt et al, 2008)
anaesthetics + 25 mg/kg Ket	NAc (Rats)	Spontaneous HFO power greater during active waking>REM>SWS (slow-wave sleep). Ketamine-HFO attenuated by pentobarbital, urethane, and isoflurane. (Hunt et al., 2009)
2.5-5 mg/kg Ket, 0.08-0.16 mg/kg MK801	Basal ganglia (Rats)	Bursts of HFO reported in NAc, striatum, and amygdala. (Hakami et al., 2009)
1, 4 μg MK801	NAc (Rats)	Local infusion of MK801 to the NAc ↑HFO power. (Hunt et al., 2010)
25 mg/kg Ket	NAc (Rats)	Intra-NAc infusion of D1R/D2R antagonists alone or combined, did not affect ↑HFO power after ketamine. Locomotion was reduced. (Matulewicz et al., 2010)
25 mg/kg Ket	NAc, Hip, striatum (Rats)	↑HFO power after ketamine in all structures in monopolar recordings NAc>striatum>Hip. Ketamine-HFO in NAc in bipolar signals. (Hunt et al., 2011)
10-50 mg/kg Ket	Basal ganglia (Rats)	Ketamine dose-dependently ↑HFO power MotCtx>CPu>thalamus=SNr. associated with hyperlocomotion. (Nicolás et al., 2011)
SDZ220581, MK801, PCP, Ket, var. doses	MotCtx, VisCtx (Rats)	↑HFO power in model of schizophrenia after NMDAR antagonists (MotCtx>VisCtx). (Phillips et al., 2012)

Drug, dose	Structures (Species)	Key HFO related findings (Ref.)
2.5 mg/kg Ket, 0.08 mg/kg MK801	ECoG (Rats)	Low dose ketamine/MK801 ↑HFO power. (Kulikova et al., 2012)
0.1 mg/kg MK801, 25 mg/kg Ket	NAc, FrCtx, VisCtx, caudate, PFC (Rats)	Intra-NAc infusion of TTX ↓HFO power by MK801 in NAc and cortical areas. TTX infusion to PFC/caudate did not affect local HFO. HFO was coherent between regions. (Olszewski et al., 2013a)
25 mg/kg Ket, 0.1 mg/kg MK801	NAc (Rats)	Clozapine, risperidone, and sulpiride ↓HFO frequency, but ↑HFO power. Intra-NAc clozapine did not affect HFO frequency. (Olszewski et al., 2013b)
50 mg/kg Ket	Ctx (Mice)	Ketamine induced significant activity in HFO frequency range in the Sp4 hypomorphic mice compared to control mice. (Ji et al., 2013)
25 mg/kg Ket +25 mg/kg Xyl	Ctx – var. (Rats)	Coherent cortical HFO/high gamma waves near 130 Hz observed after Ket/Xyl and increased near death. (Borjigin et al., 2013)
25 mg/kg Ket	NAc (Rats)	Serotonergic psychedelics ↑HFO power and ↓HFO frequency. Serotonergic HFO increases were weaker compared to ketamine. (Goda et al., 2013)
25-75 mg/kg Ket	Hip (Rats)	Ketamine ↑HFO power in Hip which was coupled to theta rhythm. (Caixeta et al., 2013)
MK801, Mem, Ket, PCP var. doses	FrCtx (Rats)	Ketamine, PCP and MK801 ↑HFO power, all exhibiting an inverted U-shaped dose-response. (Hiyoshi et al., 2014)
100 mg/kg Ket +10 mg/kg Xyl	OB (Mice)	HFO (130 Hz) in ketamine-xylazine/meditomidine, absent during waking. Odors did not increase 100-130 Hz power. (Chery et al., 2014)
0.05-0.3 mg/kg MK801	NAc (Rats)	↑HFO power and frequency in a model of schizophrenia. Clozapine ↓HFO frequency. (Goda et al., 2015)
10-50 mg/kg Ket, 0.05-0.5 mg/kg MK801	NAc (Mice)	Ketamine and MK801 dose-dependently ↑HFO power. Clozapine, not haloperidol ↓HFO frequency. Glycine ↓HFO power and frequency. (Hunt et al., 2015)
30-80 mg/kg Ket, 0.05-0.1 mg/kg MK801	ECoG – var. (Rats)	Ketamine/MK801 ↑HFO power. Mathematical model reproduced ketamine-enhanced HFO which was non-linearly modulated by ketamine concentration. (Flores et al., 2015)
10 mg/kg Ket	Basal ganglia (Rats)	Ketamine ↑HFO power (ctx>thalamus and cauduate>SNr) and locomotion were correlated. HFO amplitude modulated by slow rhythms. (Cordon et al., 2015)
0.5 mg/kg MK801	SomCtx (Mice)	↑HFO power after MK801 observed in control and tottering (tg/tg), but not in stargazer (stg/stg) mice with AMPA defects. (Maheshwari et al., 2016)
30 mg/kg Ket	RetCtx (Mice)	Ketamine enhanced gamma power in wild-type (WT) mice. GluN2D-KO mice exhibited smaller increase in gamma power and bigger increase in HFO power. (Sapkota et al., 2016)
0.04 mg/kg Ket	PFC (Monkeys)	Power spectra no obvious increase in HFO. Behaviour test – subtle band 120 Hz after ketamine (Fig. 4). (Skoblenick et al., 2016)
0.1 mg/kg MK801, 2.5 mg/kg PCP, 10 mg/kg Ket	striatum, Hip, (Rats)	All NMDAR antagonists ↑HFO power. Power larger in striatum versus Hip. (Kealy et al., 2017)
0.16 mg/kg MK801, 5-50 μg MK801	PFC, Hip, NAc (Rats)	MK801 infusion ↑HFO power (apparent NAc>PFC>Hip) locally and in distant regions. ↑HFO power were associated with hyperactivity. (Lee et al., 2017)
25 mg/kg Ket	EEG cortical (Rats)	↑HFO coherence during emergence of isoflurane anesthesia with ketamine, but not saline. (Li et al., 2017)

Drug, dose	Structures (Species)	Key HFO related findings (Ref.)
20 mg/kg Ket	MotCtx, striatal areas, Hip (Rats)	↑Delta-HFO coupling after ketamine in dorsal striatum and ↓synchrony in Hip. D1R not involved in ketamine-HFO. (Ye et al., 2018)
0.2 mg/kg MK801	FrCtx, OccCtx, Hip (Rats)	↑HFO power after NR2A (not NR2B) antagonism replicated MK801 effects, but produced distinct phase-amplitude coupling. (Pittman-Polletta et al., 2018)
25 mg/kg Ket	OB, VS (Rats)	↑HFO power (OB>VS) after ketamine. Muscimol infusion to OB ↓HFO power in OB and VS. Multi-unit activity in OB associates with HFO. (Hunt et al., 2019)
Ket, DOI, DCS amphetamine var. doses	PFC, thalamus, ECoG vertex (Rats)	↑HFO power by 3-10 mg/kg ketamine and 100-300 mg/kg d-cycloserine. HFO power weak after 1 mg/kg DOI, but not present 1 mg/kg d-amphetamine. HFO power apparently larger in PFC>thalamus and cortex. (Hansen et al., 2019)
3-10 mg/kg Ket, 2.5-5 mg/kg PCP	PFC, thalamus (Rats)	↑HFO power after ketamine/PCP correlated with beta reduction. Similar ↑HFO power in PFC and thalamus. (Amat-Foraster et al., 2019)
0.3-1.0 mg/kg MK801	PFC, Hip (Mice)	↑HFO power after MK801 in PFC and Hip and enhanced coherence. LY379268 (GluR type 2/3 agonist) enhanced effects on HFO. (Sokolenko et al., 2019)
30 mg/kg Ket, 0.2 mg/kg MK801, 3 mg/kg PCP, 20 mg/kg Mem	RetCtx (Mice)	↑HFO power after ketamine and MK801, but not PCP or memantine in control mice. Complex effects of GluN2C and GluN2D KO mice in response to different NMDAR antagonists. (Mao et al., 2020)
2.5 mg/kg Ket, 0.1 mg/kg MK801	FrCtx, thalamus, (Rats)	↑HFO power after ketamine and MK801 in cortex and variety of thalamic nuclei. Clozapine ↓HFO power after ketamine. (Mahdavi et al., 2020)
150 mg/kg Ket	ParCtx, OccCtx, FrCtx (Rats)	Ketamine anaesthesia reduced 65-175 Hz power. HFO increase during recovery compared to anesthesia, but not waking. (Brito et al., 2020)
20 mg/kg Ket	OB, PFC, VS (Rats)	Ketamine-HFO coupled with respiratory rhythm in OB, PFC, and VS. Ipsilateral naris occlusion ↓HFO power in all three structures. (Wróbel et al., 2020)
20 mg/kg Ket, 7 or 12 mg/kg L-DOPA	MotCtx, NAc, striatum (Rat)	↑Delta-HFO and theta-HFO phase-amplitude coupling in MotCtx and striatum after ketamine in control rats but not in Parkinson's and levodopa-induced dyskinesia rats. (Ye et al., 2021)
25/200 mg/kg Ket, 100 mg Ket + 10 mg Xyl	OB (Rats); OB, VisCtx, thalamus (Cats)	Ket/Xyl-HFO recorded in the OB (not thalamus or VisCtx) of cats and reduced by naris occlusion. Ket/xyl gradually ↓HFO frequency in rats. (Średniawa et al., 2021)
25 mg/kg Ket	OB (Rats)	↑Theta-HFO phase amplitude coupling after ketamine. (Jurkiewicz et al., 2021)
5 mg/kg PCP, 10 mg/kg Ket	Ctx EEG (Mice)	Pretreatment with xanomeline (M1/M4 muscarinic agonist) ↓ketamine-HFO power. (Montani et al., 2021)
10 mg/kg PCP	PFC, Hip (Mice)	↑HFO power after PCP in PFC and Hip. 5HT2A antagonist and 5HT1A agonist ↓HFO frequency after PCP. (Delgado-Sallent et al., 2022)
0.1 mg/kg MK801	PFC, thalamus, Hip, Septal nucleus (Rats)	↑HFO power after MK801 in PFC, thalamus, medial septal nucleus, and Hip accompanied by a decrease in theta activity. (Zepeda et al., 2022)

Drug, dose	Structures (Species)	Key HFO related findings (Ref.)
3 mg/kg Ket or 0.56 mg/kg (i.v.)	SomCtx, AudCtx (Monkeys)	Ketamine increased gamma and high gamma power band activities cortical areas. (Yan et al., 2022)
10 mg/kg Ket	PFC, Nac, AudCtx, thalamus, (Rats)	↑HFO power after ketamine in NAc>PFC. Clozapine ↑ketamine-HFO power and ↓HFO frequency. Naltrexone ↓ketemine-HFO power. (Bowman et al., 2022)
0.05-0.3 mg/kg MK801	PFC, Hip (Mice)	↑HFO power in PFC and Hip after MK801. (Cui et al., 2022)
10 mg/kg Ket, 0.03 mg/kg MK801	FrCtx (Mice)	↑HFO power after ketamine. Greater increase when experimenter was male. (Georgiou et al., 2022)
0.2 mg/kg MK801	PFC, Amyg, thalamus, AudCtx, FrCtx (Rats)	↑HFO power in all regions (apparent greatest in PFC and weakest in AudCtx). General ↑HFO coherence. Baclofen did not affect HFO. (Janz et al, 2022)
25-50 mg/kg Ket, 5 mg/kg PCP, 5-HT compounds	var. brain regions (Rats)	↑HFO power by 5HT2AR and NMDAR antagonists, but not amphetamine. ↓HFO frequency after 5HT2AR. HFO phase reversal in cortical areas and VS. (Brys et al., 2023)
0.075 mg/kg MK801	ParCtx, AudCtx, PFC (Rats)	↑HFO power after MK801 with anterior-posterior gradient for cortical areas. ↑HFO in PFC, ParCtx, but weak in AudCtx. (González et al., 2023)
0.075 mg/kg MK801	PFC, Hip (Mice)	↑HFO power after MK801 in PFC and Hip. Theta-HFO modulation affected by MK801 injection in PFC, but not Hip. (Abad-Perez et al., 2023)
25-50 mg/kg Ket	var. areas (Rats)	150 Hz HFO recorded in PFC. (Nasretdinov et al., 2023)
0.5 mg/kg Ket (i.v.), 250 or 1000 mg DCS	EEG (Humans)	↑HFO power (broadband) in midline EEG after ketamine and d-cycloserine. (Nottage et al., 2023)
0.05–0.07 mg/kg MK801	var. areas (Rats)	↑HFO power in multiple structures, largest in olfactory area. Clozapine ↓HFO frequency (Stan et al., 2024)
15 mg/kg Ket	PFC, OB, PaCtx (Cats)	↑110 Hz HFO power after ketamine, OB largest increase. ↓HFO power during naris blockade. (Castro-Zaballa et al., 2024)
0.15 mg/kg MK801	OB, PC (Rats)	↑HFO power after MK801 (OB>PC). Intra-OB muscimol ↓HFO power locally and in PC. (Wróbel et al., 2024)

Table A.1: **NMDAR-dependent HFO: summary of review findings.** Legend: Amyg – amygdala, AudCtx – auditory cortex, CPu – caudate putamen, Ctx – cortex, DCS - d-cycloserine, FrCtx – frontal cortex, Hip. – hippocampus, Ket – ketamine, Mem – memantine, MotCtx – motor cortex, NAc – nucleus accumbens, OB – olfactory bulb, OccCtx – occipital cortex, ParCtx – parietal cortex, PC – piriform cortex, PFC – prefrontal cortex, RetCtx – retrosplenial cortex, SNr – substantia nigra, SomCtx – somatosensory cortex, VisCtx – visual cortex, VS – ventral striatum, Xyl – xylazine, i.v. – intravenous, var. – various, ↑ – increase, ↓ – decrease.

Appendix B

Bibliography

1. Abad-Perez P, Molina-Payá FJ, Martínez-Otero L, Borrell V, Redondo RL, Brotons-Mas JR. Theta/gamma Co-modulation Disruption After NMDAr Blockade by MK-801 Is Associated with Spatial Working Memory Deficits in Mice. Neuroscience. 2023 May 21;519:162-176. doi: 10.1016/j.neuroscience.2023.03.022. Epub 2023 Mar 28. PMID: 36990270; PMCID: PMC10229075.
2. Adraoui FW, Hettak K, Viardot G, Alix M, Guiffard S, Meot B, L'Hostis P, Maurin A, Delpy E, Drieu La Rochelle C, Carvalho K. Differential Effects of Aripiprazole on Electroencephalography-Recorded Gamma-Band Auditory Steady-State Response, Spontaneous Gamma Oscillations and Behavior in a Schizophrenia Rat Model. Int J Mol Sci. 2024 Jan 14;25(2):1035. doi: 10.3390/ijms25021035. PMID: 38256109; PMCID: PMC10815955.
3. Alberts JR, May B. Development of nasal respiration and sniffing in the rat. Physiol Behav. 1980 May;24(5):957-63. doi: 10.1016/0031-9384(80)90156-0. PMID: 7403298.
4. Amat-Foraster M, Celada P, Richter U, Jensen AA, Plath N, Artigas F, Herrik KF. Modulation of thalamo-cortical activity by the NMDA receptor antagonists ketamine and phencyclidine in the awake freely-moving rat. Neuropharmacology. 2019 Nov 1;158:107745. doi: 10.1016/j.neuropharm.2019.107745. Epub 2019 Aug 21. PMID: 31445017.
5. Aroniadou-Anderjaska V, Ennis M, Shipley MT. Glomerular synaptic responses to olfactory nerve input in rat olfactory bulb slices. Neuroscience. 1997 Jul;79(2):425-34. doi: 10.1016/s0306-4522(96)00706-3. PMID: 9200726.
6. Arvanov VL, Liang X, Russo A, Wang RY. LSD and DOB: interaction with 5-HT2A receptors to inhibit NMDA receptor-mediated transmission in the rat prefrontal cortex. Eur J Neurosci. 1999 Sep;11(9):3064-72. doi: 10.1046/j.1460-9568.1999.00726.x. PMID: 10510170.
7. Bahji A, Zarate CA, Vazquez GH. Efficacy and safety of racemic ketamine and esketamine for depression: a systematic review and meta-analysis. Expert Opin Drug Saf. 2022 Jun;21(6):853-866. doi: 10.1080/14740338.2022.2047928. Epub 2022 Mar 9. PMID: 35231204; PMCID: PMC9949988.
8. Bahr R, Lopez A, Rey JA. Intranasal Esketamine (SpravatoTM) for Use in Treatment-Resistant Depression In Conjunction With an Oral Antidepressant. P T. 2019 Jun;44(6):340-375. PMID: 31160868; PMCID: PMC6534172.
9. Bandeira ID, Lins-Silva DH , Cavenaghi VB, Dorea-Bandeira I,Faria-Guimarães D, Barouh JL, et al. Ketamine in the treatment of obsessive-compulsive disorder: a systematic review. Harv Rev Psychiatry 2022; 30: 135–45.
10. Başar E, Başar-Eroğlu C, Güntekin B, Yener GG. Brain's alpha, beta, gamma, delta, and theta oscillations in neuropsychiatric diseases: proposal for biomarker strategies. Suppl Clin Neurophysiol 2013; 62: 19-54.

11. Bathellier B, Margrie TW, Larkum ME. Properties of piriform cortex pyramidal cell dendrites: implications for olfactory circuit design. J Neurosci. 2009 Oct 7;29(40):12641-52. doi: 10.1523/JNEUROSCI.1124-09.2009. PMID: 19812339; PMCID: PMC6665100.

12. Beck K, Hindley G, Borgan F, Ginestet C, McCutcheon R, Brugger S, Driesen N, Ranganathan M, D'Souza DC, Taylor M, Krystal JH, Howes OD. Association of Ketamine With Psychiatric Symptoms and Implications for Its Therapeutic Use and for Understanding Schizophrenia: A Systematic Review and Meta-analysis. JAMA Netw Open. 2020 May 1;3(5):e204693. doi: 10.1001/jamanetworkopen.2020.4693. PMID: 32437573; PMCID: PMC7243091.

13. Bekkers JM, Suzuki N. Neurons and circuits for odor processing in the piriform cortex. Trends Neurosci. 2013 Jul;36(7):429-38. doi: 10.1016/j.tins.2013.04.005. Epub 2013 May 3. PMID: 23648377.

14. Belitski A, Panzeri S, Magri C, Logothetis NK, Kayser C. Sensory information in local field potentials and spikes from visual and auditory cortices: time scales and frequency bands. J Comput Neurosci. 2010 Dec;29(3):533-45. doi: 10.1007/s10827-010-0230-y. Epub 2010 Mar 16. PMID: 20232128; PMCID: PMC2978898.

15. Benardo and Prince. Dopamine modulates a Ca2+ -activated potassium conductance in mammalian hippocampal pyramidal cells. Nature. 1982 May 6;297(5861):76-9. doi: 10.1038/297076a0. PMID: 6280074. Epub ahead of print 1982.

16. Beninger RJ. The role of dopamine in locomotor activity and learning. Brain Res. 1983 Oct;287(2):173-96. doi: 10.1016/0165-0173(83)90038-3. PMID: 6357357.

17. Berkowicz DA, Trombley PQ. Dopaminergic modulation at the olfactory nerve synapse. Brain Res. 2000 Feb 7;855(1):90-9. doi: 10.1016/s0006-8993(99)02342-2. PMID: 10650134.

18. Berman RM, Cappiello A, Anand A, Oren DA, Heninger GR, Charney DS, et al. Antidepressant effects of ketamine in depressed patients. Biol Psychiatry 2000; 47: 351–4.

19. Beshel J, Kopell N, Kay LM. Olfactory bulb gamma oscillations are enhanced with task demands. J Neurosci. 2007 Aug 1;27(31):8358-65. doi: 10.1523/JNEUROSCI.1199-07.2007. PMID: 17670982; PMCID: PMC6673062.

20. Bey T, Patel A. Phencyclidine intoxication and adverse effects: a clinical and pharmacological review of an illicit drug. Cal J Emerg Med. 2007 Feb;8(1):9-14. PMID: 20440387; PMCID: PMC2859735.

21. Björklund A, Dunnett SB. Dopamine neuron systems in the brain: an update. Trends Neurosci. 2007 May;30(5):194-202. doi: 10.1016/j.tins.2007.03.006. Epub 2007 Apr 3. PMID: 17408759.

22. Blazing RM, Franks KM. Odor coding in piriform cortex: mechanistic insights into distributed coding. Curr Opin Neurobiol. 2020 Oct;64:96-102. doi: 10.1016/j.conb.2020.03.001. Epub 2020 May 15. PMID: 32422571; PMCID: PMC8782565.

23. Bonaventura J, Lam S, Carlton M, Boehm MA, Gomez JL, Solís O, et al. Pharmacological and behavioral divergence of ketamine enantiomers:implications for abuse liability. Mol Psychiatry 2021; 26: 6704–22.

24. Borjigin J, Lee U, Liu T, Pal D, Huff S, Klarr D, Sloboda J, Hernandez J, Wang MM, Mashour GA. Surge of neurophysiological coherence and connectivity in the dying brain. Proc Natl Acad Sci U S A. 2013 Aug 27;110(35):14432-7. doi: 10.1073/pnas.1308285110. Epub 2013 Aug 12. PMID: 23940340; PMCID: PMC3761619.

25. Bowman C, Richter U, Jones CR, Agerskov C, Herrik KF. Activity-State Dependent Reversal of Ketamine-Induced Resting State EEG Effects by Clozapine and Naltrexone in the Freely Moving Rat. Front Psychiatry. 2022 Jan 27;13:737295. doi: 10.3389/fpsyt.2022.737295. PMID: 35153870; PMCID: PMC8830299.

26. Bowyer SM. Coherence a measure of the brain networks: past and present. Neuropsychiatr Electrophysiol 2016 2, 1 https://doi.org/10.1186/s40810-015-0015-7

27. Boyd AM, Kato HK, Komiyama T, Isaacson JS. Broadcasting of cortical activity to the olfactory bulb. Cell Rep. 2015 Feb 24;10(7):1032-9. doi: 10.1016/j.celrep.2015.01.047. Epub 2015 Feb 19. PMID: 25704808; PMCID: PMC4342299.

28. Boyd AM, Sturgill JF, Poo C, Isaacson JS. Cortical feedback control of olfactory bulb circuits. Neuron. 2012 Dec 20;76(6):1161-74. doi: 10.1016/j.neuron.2012.10.020. PMID: 23259951; PMCID: PMC3725136.

29. Bragin A, Engel J Jr, Wilson CL, Fried I, Mathern GW. Hippocampal and entorhinal cortex high-frequency oscillations (100–500 Hz) in human epileptic brain and in kainic acid–treated rats with chronic seizures. Epilepsia. 1999 Feb;40(2):127-37. doi: 10.1111/j.1528-1157.1999.tb02065.x. PMID: 9952257.

30. Brea JN, Kay LM, Kopell NJ. Biophysical model for gamma rhythms in the olfactory bulb via subthreshold oscillations. Proc Natl Acad Sci U S A. 2009 Dec 22;106(51):21954-9. doi: 10.1073/pnas.0910964106. Epub 2009 Dec 8. PMID: 19996171; PMCID: PMC2799880.

31. Bresink I, Danysz W, Parsons CG, Mutschler E. Different binding affinities of NMDA receptor channel blockers in various brain regions–indication of NMDA receptor heterogeneity. Neuropharmacology. 1995 May;34(5):533-40. doi: 10.1016/0028-3908(95)00017-z. PMID: 7566488.

32. Brito MA, Li D, Mashour GA, Pal D. State-Dependent and Bandwidth-Specific Effects of Ketamine and Propofol on Electroencephalographic Complexity in Rats. Front Syst Neurosci. 2020 Aug 11;14:50. doi: 10.3389/fnsys.2020.00050. PMID: 32848642; PMCID: PMC7431468.

33. Bromberg-Martin ES, Matsumoto M, Hikosaka O. Dopamine in motivational control: rewarding, aversive, and alerting. Neuron. 2010 Dec 9;68(5):815-34. doi: 10.1016/j.neuron.2010.11.022. PMID: 21144997; PMCID: PMC3032992.

34. Brown P, Williams D. Basal ganglia local field potential activity: character and functional significance in the human. Clin Neurophysiol. 2005 Nov;116(11):2510-9. doi: 10.1016/j.clinph.2005.05.009. Epub 2005 Jul 18. PMID: 16029963.

35. Brys I, Barrientos SA, Ward JE, Wallander J, Petersson P, Halje P. 5-HT2AR and NMDAR psychedelics induce similar hyper-synchronous states in the rat cognitive-limbic cortex-basal ganglia system. Commun Biol. 2023 Jul 26;6(1):737. doi: 10.1038/s42003-023-05093-6. PMID: 37495733; PMCID: PMC10372079.

36. Burton SD. Inhibitory circuits of the mammalian main olfactory bulb. J Neurophysiol. 2017 Oct 1;118(4):2034-2051. doi: 10.1152/jn.00109.2017. Epub 2017 Jul 19. PMID: 28724776; PMCID: PMC5626887.

37. Buzsáki G, Anastassiou CA, Koch C. The origin of extracellular fields and currents–EEG, ECoG, LFP and spikes. Nat Rev Neurosci. 2012 May 18;13(6):407-20. doi: 10.1038/nrn3241. PMID: 22595786; PMCID: PMC4907333.

38. Buzsáki G. Hippocampal sharp wave-ripple: A cognitive biomarker for episodic memory and planning. Hippocampus. 2015 Oct;25(10):1073-188. doi: 10.1002/hipo.22488. PMID: 26135716; PMCID: PMC4648295.

39. Buzsáki G, Watson BO. Brain rhythms and neural syntax: implications for efficient coding of cognitive content and neuropsychiatric disease. Dialogues Clin Neurosci. 2012 Dec;14(4):345-67. doi: 10.31887/DCNS.2012.14.4/gbuzsaki. PMID: 23393413; PMCID: PMC3553572.

40. Bymaster FP, Calligaro DO, Falcone JF, Marsh RD, Moore NA, Tye NC, Seeman P, Wong DT. Radioreceptor binding profile of the atypical antipsychotic olanzapine. Neuropsychopharmacology. 1996 Feb;14(2):87-96. doi: 10.1016/0893-133X(94)00129-N. PMID: 8822531.

41. Cai M, Zhu Y, Shanley MR, Morel C, Ku SM, Zhang H, Shen Y, Friedman AK, Han MH. HCN channel inhibitor induces ketamine-like rapid and sustained antidepressant effects in chronic social defeat stress model. Neurobiol Stress. 2023 Aug 19;26:100565. doi: 10.1016/j.ynstr.2023.100565. PMID: 37664876; PMCID: PMC10468802.

42. Caixeta FV, Cornélio AM, Scheffer-Teixeira R, Ribeiro S, Tort AB. Ketamine alters oscillatory coupling in the hippocampus. Sci Rep. 2013;3:2348. doi: 10.1038/srep02348. PMID: 23907109; PMCID: PMC3731648.

43. Campbell A, Baldessarini RJ, Cremens MC. Dose-catalepsy response to haloperidol in rat: effects of strain and sex. Neuropharmacology. 1988 Nov;27(11):1197-9. doi: 10.1016/0028-3908(88)90018-4. PMID: 3205387.

44. Canolty RT, Knight RT. The functional role of cross-frequency coupling. Trends Cogn Sci. 2010 Nov;14(11):506-15. doi: 10.1016/j.tics.2010.09.001. PMID: 20932795; PMCID: PMC3359652.

45. Cansler HL, Wright KN, Stetzik LA, Wesson DW. Neurochemical organization of the ventral striatum's olfactory tubercle. J Neurochem. 2020 Feb;152(4):425-448. doi: 10.1111/jnc.14919. Epub 2020 Jan 7. PMID: 31755104; PMCID: PMC7042089.

46. Carter M., Essner R, Goldstein N, Iyer M, Chapter 4 - Electrophysiology, Editor(s): Matt Carter, Rachel Essner, Nitsan Goldstein, Manasi Iyer, Guide to Research Techniques in Neuroscience (Third Edition), Academic Press, 2022, Pages 85-113, ISBN 9780128186466,https://doi.org/10.1016/B978-0-12-818646-6.00016-6.

47. Castro-Zaballa S, González J, Cavelli M, Mateos D, Pascovich C, Tort A, Hunt MJ, Torterolo P. Cortical high-frequency oscillations (110 Hz) in cats are state-dependent and enhanced by a subanesthetic dose of ketamine. Behav Brain Res. 2025 Jan 5;476:115231. doi: 10.1016/j.bbr.2024.115231. Epub 2024 Aug 30. PMID: 39218075.

48. Chen X, Shu S, Bayliss DA. HCN1 channel subunits are a molecular substrate for hypnotic actions of ketamine. Journal of Neuroscience 2009; 29: 600–9.

49. Chery R, Gurden H, Martin C. Anesthetic regimes modulate the temporal dynamics of local field potential in the mouse olfactory bulb. J Neurophysiol. 2014 Mar;111(5):908-17. doi: 10.1152/jn.00261.2013. Epub 2013 Nov 27. PMID: 24285865.

50. Conti LH, Segal DS, Kuczenski R. Maintenance of amphetamine-induced stereotypy and locomotion requires ongoing dopamine receptor activation. Psychopharmacology (Berl). 1997 Mar;130(2):183-8. doi: 10.1007/s002130050227. PMID: 9106917.

51. Contreras PC, Monahan JB, Lanthorn TH, Pullan LM, DiMaggio DA, Handelmann GE, Gray NM, O'Donohue TL. Phencyclidine. Physiological actions, interactions with excitatory amino acids and endogenous ligands. Mol Neurobiol. 1987 Fall;1(3):191-211. doi: 10.1007/BF02936608. PMID: 2855791.

52. Cordon I, Nicolás MJ, Arrieta S, Lopetegui E, López-Azcárate J, Alegre M, Artieda J, Valencia M. Coupling in the cortico-basal ganglia circuit is aberrant in the ketamine model of schizophrenia. Eur Neuropsychopharmacol. 2015 Aug;25(8):1375-87. doi: 10.1016/j.euroneuro.2015.04.004. Epub 2015 Apr 14. PMID: 25910422.

53. Coronas V, Srivastava LK, Liang JJ, Jourdan F, Moyse E. Identification and localization of dopamine receptor subtypes in rat olfactory mucosa and bulb: a combined in situ hybridization and ligand binding radioautographic approach. J Chem Neuroanat. 1997 May;12(4):243-57. doi: 10.1016/s0891-0618(97)00215-9. PMID: 9243344.

54. Cui K, Yu Z, Xu L, Jiang W, Wang L, Wang X, Zou D, Gu J, Gao F, Zhang X, Wang Z. Behavioral features and disorganization of oscillatory activity in C57BL/6J mice after acute low dose MK-801 administration. Front Neurosci. 2022 Sep 14;16:1001869. doi: 10.3389/fnins.2022.1001869. PMID: 36188453; PMCID: PMC9515662.

55. Daly EJ, Trivedi MH, Janik A, Li H, Zhang Y, Li X, et al. Efficacy of esketamine nasal spray plus oral antidepressant treatment for relapse prevention in patients with treatment resistant depression: a randomized clinical trial. JAMA Psychiatry 2019; 76: 893–903.

56. Debarros J, Gaignon L, He S, Pogosyan A, Benjaber M, Denison T, Brown P, Tan H. Artefact-free recording of local field potentials with simultaneous stimulation for closed-loop Deep-Brain Stimulation. Annu Int Conf IEEE Eng Med Biol Soc. 2020 Jul;2020:3367-3370. doi: 10.1109/EMBC44109.2020.9176665. PMID: 33018726; PMCID: PMC7116199.

57. Delgado-Sallent C, Nebot P, Gener T, Fath AB, Timplalexi M, Puig MV. Atypical, but Not Typical, Antipsychotic Drugs Reduce Hypersynchronized Prefrontal-Hippocampal Circuits during Psychosis-Like States in Mice: Contribution of 5-HT2A and 5-HT1A Receptors. Cereb Cortex. 2022 Aug 3;32(16):3472-3487. doi: 10.1093/cercor/bhab427. PMID: 34875009.

58. Durdagi S, Salmas RE, Stein M, Yurtsever M, Seeman P. Binding Interactions of Dopamine and Apomorphine in D2High and D2Low States of Human Dopamine D2 Receptor Using Computational and Experimental Techniques. ACS Chem Neurosci. 2016 Feb 17;7(2):185-95. doi: 10.1021/acschemneuro.5b00271. Epub 2015 Dec 22. PMID: 26645629.

59. Durieux ME. Inhibition by ketamine of muscarinic acetylcholine receptor function. Anesth Analg 1995; 81(1): 57-62.

60. Economo MN, Hansen KR, Wachowiak M. Control of Mitral/Tufted Cell Output by Selective Inhibition among Olfactory Bulb Glomeruli. Neuron. 2016 Jul 20;91(2):397-411. doi: 10.1016/j.neuron.2016.06.001. Epub 2016 Jun 23. PMID: 27346531; PMCID: PMC6474342.

61. Egger V, Svoboda K, Mainen ZF. Mechanisms of lateral inhibition in the olfactory bulb: efficiency and modulation of spike-evoked calcium influx into granule cells. J Neurosci. 2003 Aug 20;23(20):7551-8. doi: 10.1523/JNEUROSCI.23-20-07551.2003. PMID: 12930793; PMCID: PMC6740749.

62. Ennis M, Zhou FM, Ciombor KJ, Aroniadou-Anderjaska V, Hayar A, Borrelli E, Zimmer LA, Margolis F, Shipley MT. Dopamine D2 receptor-mediated presynaptic inhibition of olfactory nerve terminals. J Neurophysiol. 2001 Dec;86(6):2986-97. doi: 10.1152/jn.2001.86.6.2986. PMID: 11731555.

63. Escanilla O, Yuhas C, Marzan D, Linster C. Dopaminergic modulation of olfactory bulb processing affects odor discrimination learning in rats. Behav Neurosci. 2009 Aug;123(4):828-33. doi: 10.1037/a0015855. PMID: 19634942; PMCID: PMC2766664

64. Faraone SV. The pharmacology of amphetamine and methylphenidate: Relevance to the neurobiology of attention-deficit/hyperactivity disorder and other psychiatric comorbidities. Neurosci Biobehav Rev. 2018 Apr;87:255-270. doi: 10.1016/j.neubiorev.2018.02.001. Epub 2018 Feb 8. PMID: 29428394; PMCID: PMC8063758.

65. Flores FJ, Ching S, Hartnack K, Fath AB, Purdon PL, Wilson MA, Brown EN. A PK-PD model of ketamine-induced high-frequency oscillations. J Neural Eng. 2015 Oct;12(5):056006. doi: 10.1088/1741-2560/12/5/056006. Epub 2015 Aug 13. PMID: 26268223; PMCID: PMC5764707.

66. Frohlich J, Van Horn JD. Reviewing the ketamine model for schizophrenia. J Psychopharmacol. 2014 Apr;28(4):287-302. doi: 10.1177/0269881113512909. Epub 2013 Nov 20. PMID: 24257811; PMCID: PMC4133098.

67. Gallego-Carracedo C, Perich MG, Chowdhury RH, Miller LE, Gallego JÁ. Local field potentials reflect cortical population dynamics in a region-specific and frequency-dependent manner. Elife. 2022 Aug 15;11:e73155. doi: 10.7554/eLife.73155. PMID: 35968845; PMCID: PMC9470163.

68. Gavrilovici C, D'Alfonso S, Poulter MO. Diverse interneuron populations have highly specific interconnectivity in the rat piriform cortex. J Comp Neurol. 2010 May 1;518(9):1570-88. doi: 10.1002/cne.22291. PMID: 20187146.

69. Geddes J. , Einevoll GT. , Acar E. , Stasik AJ. Multi-Linear Population Analysis (MLPA) of LFP Data Using Tensor Decompositions Frontiers in Applied Mathematics and Statistics 2020 6 DOI=10.3389/fams.2020.00041

70. Georgiou P, Zanos P, Mou TM, An X, Gerhard DM, Dryanovski DI, Potter LE, Highland JN, Jenne CE, Stewart BW, Pultorak KJ, Yuan P, Powels CF, Lovett J, Pereira EFR, Clark SM, Tonelli LH, Moaddel R, Zarate CA Jr, Duman RS, Thompson SM, Gould TD. Experimenters' sex modulates mouse behaviors and neural responses to ketamine via corticotropin releasing factor. Nat Neurosci. 2022 Sep;25(9):1191-1200. doi: 10.1038/s41593-022-01146-x. Epub 2022 Aug 30. PMID: 36042309; PMCID: PMC10186684.

71. Glue P, Loo C, Fam J, Lane HY, Young AH, Surman P; BEDROC study investigators. Extended-release ketamine tablets for treatment-resistant depression: a randomized placebo-controlled phase 2 trial. Nat Med. 2024 Jul;30(7):2004-2009. doi: 10.1038/s41591-024-03063-x. Epub 2024 Jun 24. PMID: 38914860; PMCID: PMC11271411.

72. Goda SA, Olszewski M, Piasecka J, Rejniak K, Whittington MA, Kasicki S, Hunt MJ. Aberrant high frequency oscillations recorded in the rat nucleus accumbens in the methylazoxymethanol acetate neurodevelopmental model of schizophrenia. Prog Neuropsychopharmacol Biol Psychiatry. 2015 Aug 3;61:44-51. doi: 10.1016/j.pnpbp.2015.03.016. Epub 2015 Apr 7. PMID: 25862088.

73. Goda SA, Piasecka J, Olszewski M, Kasicki S, Hunt MJ. Serotonergic hallucinogens differentially modify gamma and high frequency oscillations in the rat nucleus accumbens. Psychopharmacology (Berl). 2013 Jul;228(2):271-82. doi: 10.1007/s00213-013-3057-1. Epub 2013 Mar 23. PMID: 23525524; PMCID: PMC3693439.

74. Gonzalez-Burgos I, Bainier M, Gross S, Schoenenberger P, Ochoa JA, Valencia M, Redondo RL. Glutamatergic and GABAergic Receptor Modulation Present Unique Electrophysiological Fingerprints in a Concentration-Dependent and Region-Specific Manner. eNeuro. 2023 Apr 20;10(4):ENEURO.0406-22.2023. doi: 10.1523/ENEURO.0406-22.2023. PMID: 36931729; PMCID: PMC10124153.

75. Gourévitch B, Kay LM, Martin C. Directional coupling from the olfactory bulb to the hippocampus during a go/no-go odor discrimination task. J Neurophysiol. 2010 May;103(5):2633-41. doi: 10.1152/jn.01075.2009. Epub 2010 Feb 17. PMI

76. Grace AA, Uliana DL. Insights into the Mechanism of Action of Antipsychotic Drugs Derived from Animal Models: Standard of Care versus Novel Targets. Int J Mol Sci. 2023 Aug 3;24(15):12374. doi: 10.3390/ijms241512374. PMID: 37569748; PMCID: PMC10418544.

77. Greer, CA. Structural organization of the olfactory system. In Smell and Taste in Health and Disease 1991 T.V. Getchell, R.L. Doty, L.M. Bartoshuk and J.B. Snow Jr., eds (New York, Raven), pp. 65–81.

78. Grosmaitre X, Santarelli LC, Tan J, Luo M, Ma M. Dual functions of mammalian olfactory sensory neurons as odor detectors and mechanical sensors. Nat Neurosci. 2007 Mar;10(3):348-54. doi: 10.1038/nn1856. Epub 2007 Feb 18. PMID: 17310245; PMCID: PMC2227320.

79. Grunebaum MF, Galfalvy HC, Liu J, Huang YY, Marcott S, Burke AK, et al. Opioid receptor μ-1 and ketamine effects in a suicidal depression trial: a post hoc exploration. J Clin Psychopharmacol 2020; 40: 420–2.

80. Gutièrrez-Mecinas M, Crespo C, Blasco-Ibáñez JM, Gracia-Llanes FJ, Marqués-Marí AI, Nácher J, Varea E, Martínez-Guijarro FJ. Distribution of D2 dopamine receptor in the olfactory glomeruli of the rat olfactory bulb. Eur J Neurosci. 2005 Sep;22(6):1357-67. doi: 10.1111/j.1460-9568.2005.04328.x. PMID: 16190891.

81. Haberly LB, Bower JM. Olfactory cortex: model circuit for study of associative memory? Trends Neurosci. 1989 Jul;12(7):258-64. doi: 10.1016/0166-2236(89)90025-8. PMID: 2475938.

82. Hakami T, Jones NC, Tolmacheva EA, Gaudias J, Chaumont J, Salzberg M, O'Brien TJ, Pinault D. NMDA receptor hypofunction leads to generalized and persistent aberrant gamma oscillations independent of hyperlocomotion and the state of consciousness. PLoS One. 2009 Aug 25;4(8):e6755. doi: 10.1371/journal.pone.0006755. PMID: 19707548; PMCID: PMC2727800.

83. Hammer LH, Kochanski RB, Starr PA, Little S. Artifact Characterization and a Multipurpose Template-Based Offline Removal Solution for a Sensing-Enabled Deep Brain Stimulation Device. Stereotact Funct Neurosurg. 2022;100(3):168-183. doi: 10.1159/000521431. Epub 2022 Feb 7. PMID: 35130555; PMCID: PMC9064887.

84. Hansen IH, Agerskov C, Arvastson L, Bastlund JF, Sørensen HBD, Herrik KF. Pharmacoelectroencephalographic responses in the rat differ between active and inactive locomotor states. Eur J Neurosci. 2019 Jul;50(2):1948-1971. doi: 10.1111/ejn.14373. Epub 2019 Apr 1. PMID: 30762918; PMCID: PMC6806018.

85. Hansen KB, Yi F, Perszyk RE, Menniti FS, Traynelis SF. NMDA Receptors in the Central Nervous System. Methods Mol Biol. 2017;1677:1-80. doi: 10.1007/978-1-4939-7321-71. PMID: 28986865; PMCID: PMC7325486.

86. Harper AA, Rimmer K, Dyavanapalli J, McArthur JR, Adams DJ. Ketamine inhibits synaptic transmission and nicotinic acetylcholine receptor-mediated responses in rat intracardiac ganglia in situ. Neuropharmacology 2020; 165: 107932.

87. Herreras O. Local Field Potentials: Myths and Misunderstandings. Front Neural Circuits. 2016 Dec 15;10:101. doi: 10.3389/fncir.2016.00101. PMID: 28018180; PMCID: PMC5156830.

88. Herweg NA, Solomon EA, Kahana MJ. Theta Oscillations in Human Memory. Trends Cogn Sci. 2020 Mar;24(3):208-227. doi: 10.1016/j.tics.2019.12.006. Epub 2020 Feb 3. PMID: 32029359; PMCID: PMC8310425.

89. Hirose T, Kikuchi T. Aripiprazole, a novel antipsychotic agent: dopamine D2 receptor partial agonist. J Med Invest. 2005 Nov;52 Suppl:284-90. doi: 10.2152/jmi.52.284. PMID: 16366516.

90. Hiyoshi T, Kambe D, Karasawa J, Chaki S. Differential effects of NMDA receptor antagonists at lower and higher doses on basal gamma band oscillation power in rat cortical electroencephalograms. Neuropharmacology. 2014 Oct;85:384-96. doi: 10.1016/j.neuropharm.2014.05.037. Epub 2014 Jun 5. PMID: 24907590.

91. Holsheimer J, Feenstra BW. Volume conduction and EEG measurements within the brain: a quantitative approach to the influence of electrical spread on the linear relationship of activity measured at different locations. Electroencephalogr Clin Neurophysiol. 1977 Jul;43(1):52-8. doi: 10.1016/0013-4694(77)90194-8. PMID: 68872.

92. Hsia AY, Vincent JD, Lledo PM. Dopamine depresses synaptic inputs into the olfactory bulb. J Neurophysiol. 1999 Aug;82(2):1082-5. doi: 10.1152/jn.1999.82.2.1082. PMID: 10444702.

93. Hunt MJ, Adams NE, Średniawa W, Wójcik DK, Simon A, Kasicki S, Whittington MA. The olfactory bulb is a source of high-frequency oscillations (130-180 Hz) associated with a subanesthetic dose of ketamine in rodents. Neuropsychopharmacology. 2019 Jan;44(2):435-442. doi: 10.1038/s41386-018-0173-y. Epub 2018 Aug 8. PMID: 30140046; PMCID: PMC6300534.

94. Hunt MJ, Falinska M, Kasicki S. Local injection of MK801 modifies oscillatory activity in the nucleus accumbens in awake rats. J Psychopharmacol. 2010 Jun;24(6):931-41. doi: 10.1177/0269881109102539. Epub 2009 Mar 27. PMID: 19329548.

95. Hunt MJ, Falinska M, Łeski S, Wójcik DK, Kasicki S. Differential effects produced by ketamine on oscillatory activity recorded in the rat hippocampus, dorsal striatum and nucleus accumbens. J Psychopharmacol. 2011 Jun;25(6):808-21. doi: 10.1177/0269881110362126. Epub 2010 Apr 22. PMID: 20413405.

96. Hunt MJ, Garcia R, Large CH, Kasicki S. Modulation of high-frequency oscillations associated with NMDA receptor hypofunction in the rodent nucleus accumbens by lamotrigine. Prog Neuropsychopharmacol Biol Psychiatry. 2008 Jul 1;32(5):1312-9. doi: 10.1016/j.pnpbp.2008.04.009. Epub 2008 Apr 20. PMID: 18514376.

97. Hunt MJ, Kopell NJ, Traub RD, Whittington MA. Aberrant Network Activity in Schizophrenia. Trends Neurosci. 2017 Jun;40(6):371-382. doi: 10.1016/j.tins.2017.04.003. Epub 2017 May 14. PMID: 28515010; PMCID: PMC5523137.

98. Hunt MJ, Matulewicz P, Gottesmann C, Kasicki S. State-dependent changes in high-frequency oscillations recorded in the rat nucleus accumbens. Neuroscience. 2009 Dec 1;164(2):380-6. doi: 10.1016/j.neuroscience.2009.08.047. Epub 2009 Aug 28. PMID: 19716859.

99. Hunt MJ, Olszewski M, Piasecka J, Whittington MA, Kasicki S. Effects of NMDA receptor antagonists and antipsychotics on high frequency oscillations recorded in the nucleus accumbens of freely moving mice. Psychopharmacology (Berl). 2015 Dec;232(24):4525-35. doi: 10.1007/s00213-015-4073-0. Epub 2015 Oct 8. PMID: 26446869; PMCID: PMC4646921.

100. Hunt MJ, Raynaud B, Garcia R. Ketamine dose-dependently induces high-frequency oscillations in the nucleus accumbens in freely moving rats. Biol Psychiatry. 2006 Dec 1;60(11):1206-14. doi: 10.1016/j.biopsych.2006.01.020. Epub 2006 May 2. PMID: 16650831.

101. Imamura F, Ito A, LaFever BJ. Subpopulations of Projection Neurons in the Olfactory Bulb. Front Neural Circuits. 2020 Aug 28;14:561822. doi: 10.3389/fncir.2020.561822. PMID: 32982699; PMCID: PMC7485133.

102. Janz P, Nicolas MJ, Redondo RL, Valencia M. GABAB R activation partially normalizes acute NMDAR hypofunction oscillatory abnormalities but fails to rescue sensory processing deficits. J Neurochem. 2022 Jun;161(5):417-434. doi: 10.1111/jnc.15602. Epub 2022 Mar 25. PMID: 35253214.

103. Javitt DC. Negative schizophrenic symptomatology and the PCP (phencyclidine) model of schizophrenia. Hillside J Clin Psychiatry 1987; 9(1): 12-35.

104. Jenner P, Katzenschlager R. Apomorphine - pharmacological properties and clinical trials in Parkinson's disease. Parkinsonism Relat Disord. 2016 Dec;33 Suppl 1:S13-S21. doi: 10.1016/j.parkreldis.2016.12.003. Epub 2016 Dec 13. PMID: 27979722.

105. Ji B, Wang X, Pinto-Duarte A, Kim M, Caldwell S, Young JW, Behrens MM, Sejnowski TJ, Geyer MA, Zhou X. Prolonged Ketamine Effects in Sp4 Hypomorphic Mice: Mimicking Phenotypes of Schizophrenia. PLoS One. 2013 Jun 18;8(6):e66327. doi: 10.1371/journal.pone.0066327. PMID: 23823008; PMCID: PMC3688895.

106. Johnson DM, Illig KR, Behan M, Haberly LB. New features of connectivity in piriform cortex visualized by intracellular injection of pyramidal cells suggest that "primary" olfactory cortex functions like "association" cortex in other sensory systems. J Neurosci. 2000 Sep 15;20(18):6974-82. doi: 10.1523/JNEUROSCI.20-18-06974.2000. PMID: 10995842; PMCID: PMC6772836.

107. Jurkiewicz GJ, Hunt MJ, Żygierewicz J. Addressing Pitfalls in Phase-Amplitude Coupling Analysis with an Extended Modulation Index Toolbox. Neuroinformatics. 2021 Apr;19(2):319-345. doi: 10.1007/s12021-020-09487-3. PMID: 32845497; PMCID: PMC8004528.

108. Kajikawa Y, Schroeder CE. How local is the local field potential? Neuron. 2011 Dec 8;72(5):847-58. doi: 10.1016/j.neuron.2011.09.029. PMID: 22153379; PMCID: PMC3240862.

109. Kapur S, Seeman P. NMDA receptor antagonists ketamine and PCP have direct effects on the dopamine D2 and serotonin 5-HT2 receptors - implications for models of schizophrenia. Mol Psychiatry 2002; 7: 837–44.

110. Kay LM, Beshel J, Brea J, Martin C, Rojas-Líbano D, Kopell N. Olfactory oscillations: the what, how and what for. Trends Neurosci. 2009 Apr;32(4):207-14. doi: 10.1016/j.tins.2008.11.008. Epub 2009 Feb 23. PMID: 19243843; PMCID: PMC3389991.

111. Kay LM. Circuit oscillations in odor perception and memory. Prog Brain Res. 2014;208:223-51. doi: 10.1016/B978-0-444-63350-7.00009-7. PMID: 24767485.

112. Kay LM. Two species of gamma oscillations in the olfactory bulb: dependence on behavioral state and synaptic interactions. J Integr Neurosci. 2003 Jun;2(1):31-44. doi: 10.1142/s0219635203000196. PMID: 15011275.

113. Kealy J, Commins S, Lowry JP. The effect of NMDA-R antagonism on simultaneously acquired local field potentials and tissue oxygen levels in the brains of freely-moving rats. Neuropharmacology. 2017 Apr;116:343-350. doi: 10.1016/j.neuropharm.2017.01.006. Epub 2017 Jan 11. PMID: 28087359.

114. Kepecs A, Uchida N, Mainen ZF. Rapid and precise control of sniffing during olfactory discrimination in rats. J Neurophysiol. 2007 Jul;98(1):205-13. doi: 10.1152/jn.00071.2007. Epub 2007 Apr 25. PMID: 17460109.

115. Kim B, Haney S, Milan AP, Joshi S, Aldworth Z, Rulkov N, Kim AT, Bazhenov M, Stopfer MA. Olfactory receptor neurons generate multiple response motifs, increasing coding space dimensionality. Elife. 2023 Jan 31;12:e79152. doi: 10.7554/eLife.79152. PMID: 36719272; PMCID: PMC9925048.

116. Kim J, Gulati T, Ganguly K. Competing Roles of Slow Oscillations and Delta Waves in Memory Consolidation versus Forgetting. Cell. 2019 Oct 3;179(2):514-526.e13. doi: 10.1016/j.cell.2019.08.040. PMID: 31585085; PMCID: PMC6779327.

117. Kohrs R, Durieux ME. Ketamine: teaching an old drug new tricks. Anesthesia and Analgesia 1998; 87(5): 1186-1193.

118. Kostka JK, Hanganu-Opatz IL. Olfactory-driven beta band entrainment of limbic circuitry during neonatal development. J Physiol. 2023 Aug;601(16):3605-3630. doi: 10.1113/JP284401. Epub 2023 Jul 11. PMID: 37434507.D: 20164392; PMCID: PMC2867565.

119. Kovacic P, Somanathan R. Clinical physiology and mechanism of dizocilpine (MK-801): electron transfer, radicals, redox metabolites and bioactivity. Oxid Med Cell Longev. 2010 Jan-Feb;3(1):13-22. doi: 10.4161/oxim.3.1.10028. PMID: 20716924; PMCID: PMC2835885.

120. Krystal JH, Abdallah CG, Sanacora G, Charney DS, Duman RS. Ketamine: A Paradigm Shift for Depression Research and Treatment. Neuron. 2019 Mar 6;101(5):774-778. doi: 10.1016/j.neuron.2019.02.005. PMID: 30844397; PMCID: PMC6560624.

121. Krystal JH, Kavalali ET, Monteggia LM. Ketamine and rapid antidepressant action: new treatments and novel synaptic signaling mechanisms. Neuropsychopharmacology. 2024 Jan;49(1):41-50. doi: 10.1038/s41386-023-01629-w. Epub 2023 Jul 24. PMID: 37488280; PMCID: PMC10700627.

122. Kulikova SP, Tolmacheva EA, Anderson P, Gaudias J, Adams BE, Zheng T, Pinault D. Opposite effects of ketamine and deep brain stimulation on rat thalamocortical information processing. Eur J Neurosci. 2012 Nov;36(10):3407-19. doi: 10.1111/j.1460-9568.2012.08263.x. Epub 2012 Aug 29. PMID: 22928838.

123. Kumar A, Schiff O, Barkai E, Mel BW, Poleg-Polsky A, Schiller J. NMDA spikes mediate amplification of inputs in the rat piriform cortex. Elife. 2018 Dec 21;7:e38446. doi: 10.7554/eLife.38446. PMID: 30575520; PMCID: PMC6333441.

124. Lacey MG, Mercuri NB, North RA. Dopamine acts on D2 receptors to increase potassium conductance in neurones of the rat substantia nigra zona compacta. J Physiol. 1987 Nov;392:397-416. doi: 10.1113/jphysiol.1987.sp016787. PMID: 2451725; PMCID: PMC1192311.

125. Lee G, Zhou Y. NMDAR Hypofunction Animal Models of Schizophrenia. Front Mol Neurosci. 2019 Jul 31;12:185. doi: 10.3389/fnmol.2019.00185. PMID: 31417356; PMCID: PMC6685005.

126. Lee J, Hudson MR, O'Brien TJ, Nithianantharajah J, Jones NC. Local NMDA receptor hypofunction evokes generalized effects on gamma and high-frequency oscillations and behavior. Neuroscience. 2017 Sep 1;358:124-136. doi: 10.1016/j.neuroscience.2017.06.039. Epub 2017 Jul 1. PMID: 28676240.

127. Lepousez G, Lledo PM. Odor discrimination requires proper olfactory fast oscillations in awake mice. Neuron. 2013 Nov 20;80(4):1010-24. doi: 10.1016/j.neuron.2013.07.025. Epub 2013 Oct 17. PMID: 24139818.

128. Leung LS, Gill RS, Shen B, Chu L. Cholinergic and behavior-dependent beta and gamma waves are coupled between olfactory bulb and hippocampus. Hippocampus. 2024 Sep;34(9):464-490. doi: 10.1002/hipo.23622. Epub 2024 Jul 1. PMID: 38949057.

129. Li D, Hambrecht-Wiedbusch VS, Mashour GA. Accelerated Recovery of Consciousness after General Anesthesia Is Associated with Increased Functional Brain Connectivity in the High-Gamma Bandwidth. Front Syst Neurosci. 2017 Mar 24;11:16. doi: 10.3389/fnsys.2017.00016. PMID: 28392760; PMCID: PMC5364164.

130. Liljequist S, Ossowska K, Grabowska-Andén M, Andén NE. Effect of the NMDA receptor antagonist, MK-801, on locomotor activity and on the metabolism of dopamine in various brain areas of mice. Eur J Pharmacol. 1991 Mar 19;195(1):55-61. doi: 10.1016/0014-2999(91)90381-y. PMID: 1829683.

131. Lin A, Liu KKL, Bartsch RP, Ivanov PC. Dynamic network interactions among distinct brain rhythms as a hallmark of physiologic state and function. Commun Biol. 2020 Apr 27;3(1):197. doi: 10.1038/s42003-020-0878-4. Erratum in: Commun Biol. 2020 May 21;3(1):266. doi: 10.1038/s42003-020-0998-x. PMID: 32341420; PMCID: PMC7184753.

132. Lisman JE, Jensen O. The theta-gamma neural code. Neuron. 2013 Mar 20;77(6):1002-16. doi: 10.1016/j.neuron.2013.03.007. PMID: 23522038; PMCID: PMC3648857.

133. Liu S. Dopaminergic Modulation of Glomerular Circuits in the Mouse Olfactory Bulb. Front Cell Neurosci. 2020 Jun 12;14:172. doi: 10.3389/fncel.2020.00172. PMID: 32595457; PMCID: PMC7304284.

134. Lockmann ALV, Laplagne DA, Tort ABL. Olfactory bulb drives respiration-coupled beta oscillations in the rat hippocampus. Eur J Neurosci. 2018 Oct;48(8):2663-2673. doi: 10.1111/ejn.13665. Epub 2017 Sep 14. PMID: 28833629.

135. López-Gil X, Jiménez-Sánchez L, Campa L, Castro E, Frago C, Adell A. Role of serotonin and noradrenaline in the rapid antidepressant action of ketamine. ACS Chem Neurosci 2019; 10: 3318–26.

136. Lothmann K, Amunts K, Herold C. The Neurotransmitter Receptor Architecture of the Mouse Olfactory System. Front Neuroanat. 2021 Apr 23;15:632549. doi: 10.3389/fnana.2021.632549. PMID: 33967704; PMCID: PMC8102831.

137. Luskin MB, Price JL. The laminar distribution of intracortical fibers originating in the olfactory cortex of the rat. J Comp Neurol. 1983 May 20;216(3):292-302. doi: 10.1002/cne.902160306. PMID: 6863605.

138. Łęski S, Kublik E, Swiejkowski DA, Wróbel A, Wójcik DK. Extracting functional components of neural dynamics with Independent Component Analysis and inverse Current Source Density. J Comput Neurosci. 2010 Dec;29(3):459-73. doi: 10.1007/s10827-009-0203-1. Epub 2009 Dec 22. PMID: 20033271.

139. Magri C, Mazzoni A, Logothetis NK, Panzeri S. Optimal band separation of extracellular field potentials. J Neurosci Methods. 2012 Sep 15;210(1):66-78. doi: 10.1016/j.jneumeth.2011.11.005. Epub 2011 Nov 9. PMID: 22101145.

140. Mahdavi A, Qin Y, Aubry AS, Cornec D, Kulikova S, Pinault D. A single psychotomimetic dose of ketamine decreases thalamocortical spindles and delta oscillations in the sedated rat. Schizophr Res. 2020 Aug;222:362-374. doi: 10.1016/j.schres.2020.04.029. Epub 2020 Jun 5. PMID: 32507548.

141. Maheshwari A, Akbar A, Wang M, Marks RL, Yu K, Park S, Foster BL, Noebels JL. Persistent aberrant cortical phase-amplitude coupling following seizure treatment in absence epilepsy models. J Physiol. 2017 Dec 1;595(23):7249-7260. doi: 10.1113/JP274696. Epub 2017 Sep 19. PMID: 28901011; PMCID: PMC5709336.

142. Majchrzak M, Di Scala G. GABA and muscimol as reversible inactivation tools in learning and memory. Neural Plast. 2000;7(1-2):19-29. doi: 10.1155/NP.2000.19. PMID: 10709211; PMCID: PMC2565374.

143. Manahan-Vaughan D, von Haebler D, Winter C, Juckel G, Heinemann U. A single application of MK801 causes symptoms of acute psychosis, deficits in spatial memory, and impairment of synaptic plasticity in rats. Hippocampus. 2008;18(2):125-34. doi: 10.1002/hipo.20367. PMID: 17924525.

144. Mandal S, Sinha VK, Goyal N. Efficacy of ketamine therapy in the treatment of depression. Indian J Psychiatry. 2019 Sep-Oct;61(5):480-485. doi: 10.4103 psychiatry.Indian J Psychiatry 484 18. PMID: 31579184; PMCID: PMC6767816.

145. Mao Z, He S, Mesnard C, Synowicki P, Zhang Y, Chung L, Wiesman AI, Wilson TW, Monaghan DT. NMDA receptors containing GluN2C and GluN2D subunits have opposing roles in modulating neuronal oscillations; potential mechanism for bidirectional feedback. Brain Res. 2020 Jan 15;1727:146571. doi: 10.1016/j.brainres.2019.146571. Epub 2019 Nov 28. PMID: 31786200; PMCID: PMC7193694.

146. Marmor O, Valsky D, Joshua M, Bick AS, Arkadir D, Tamir I, Bergman H, Israel Z, Eitan R. Local vs. volume conductance activity of field potentials in the human subthalamic nucleus. J Neurophysiol. 2017 Jun 1;117(6):2140-2151. doi: 10.1152/jn.00756.2016. Epub 2017 Feb 15. PMID: 28202569; PMCID: PMC5454468.

147. Martin C, Ravel N. Beta and gamma oscillatory activities associated with olfactory memory tasks: different rhythms for different functional networks? Front Behav Neurosci. 2014 Jun 23;8:218. doi: 10.3389/fnbeh.2014.00218. PMID: 25002840; PMCID: PMC4066841.

148. Martin LL, Bouchal RL, Smith DJ. Ketamine inhibits serotonin uptake in vivo. Neuropharmacology. 1982 Feb;21(2):113-8. doi: 10.1016/0028-3908(82)90149-6. PMID: 6460944.

149. Martin JH, Ghez C. Pharmacological inactivation in the analysis of the central control of movement. J Neurosci Methods. 1999 Jan;86(2):145-59. doi: 10.1016/s0165-0270(98)00163-0. PMID: 10065983.

150. Mathews D. F., Rat Olfactory Nerve Responses To Odor, Chemical Senses, 1974, Volume 1, Issue 1, January Pages 69–76, https://doi.org/10.1093/chemse/1.1.69

151. Matsutani S, Yamamoto N. Centrifugal innervation of the mammalian olfactory bulb. Anat Sci Int. 2008 Dec;83(4):218-27. doi: 10.1111/j.1447-073X.2007.00223.x. PMID: 19159349.

152. Matulewicz P, Kasicki S, Hunt MJ. The effect of dopamine receptor blockade in the rodent nucleus accumbens on local field potential oscillations and motor activity in response to ketamine. Brain Res. 2010 Dec 17;1366:226-32. doi: 10.1016/j.brainres.2010.09.088. Epub 2010 Oct 1. PMID: 20888326.

153. Maurice N, Mercer J, Chan CS, Hernandez-Lopez S, Held J, Tkatch T, Surmeier DJ. D2 dopamine receptor-mediated modulation of voltage-dependent Na+ channels reduces autonomous activity in striatal cholinergic interneurons. J Neurosci. 2004 Nov 17;24(46):10289-301. doi: 10.1523/JNEUROSCI.2155-04.2004. PMID: 15548642; PMCID: PMC6730305.

154. Mion G, Villevieille T. Ketamine Pharmacology: an update (pharmacodynamics and molecular Aspects, recent findings). CNS Neurosci Ther 2013; 19: 370–80.

155. Miyasaka M, Domino EF. Neuronal mechanisms of ketamine induced anesthesia. Neuropharmacology 1968; 7(6): 557-73. Mombaerts P. Seven-transmembrane proteins as odorant and chemosensory receptors. Science. 1999 Oct 22;286(5440):707-11. doi: 10.1126/science.286.5440.707. PMID: 10531047.

156. Mombaerts P. Molecular biology of odorant receptors in vertebrates. Annu Rev Neurosci. 1999;22:487-509. doi: 10.1146/annurev.neuro.22.1.487. PMID: 10202546.

157. Monaghan DT and Jane DE. Chapter 12 Pharmacology of NMDA Receptors in Biology of the NMDA Receptor. 2009 Van Dongen AM, editor. Boca Raton (FL): CRC Press/Taylor and Francis.

158. Montani C, Canella C, Schwarz AJ, Li J, Gilmour G, Galbusera A, Wafford K, Gutierrez-Barragan D, McCarthy A, Shaw D, Knitowski K, McKinzie D, Gozzi A, Felder C. The M1/M4 preferring muscarinic agonist xanomeline modulates functional connectivity and NMDAR antagonist-induced changes in the mouse brain. Neuropsychopharmacology. 2021 May;46(6):1194-1206. doi: 10.1038/s41386-020-00916-0. Epub 2020 Dec 20. PMID: 33342996; PMCID: PMC8115158.

159. Mori K, Manabe H, Narikiyo K, Onisawa N. Olfactory consciousness and gamma oscillation couplings across the olfactory bulb, olfactory cortex, and orbitofrontal cortex. Front Psychol. 2013 Oct 16;4:743. doi: 10.3389/fpsyg.2013.00743. PMID: 24137148; PMCID: PMC3797617.

160. Mori K, Nagao H, Yoshihara Y. The olfactory bulb: coding and processing of odor molecule information. Science. 1999 Oct 22;286(5440):711-5. doi: 10.1126/science.286.5440.711. PMID: 10531048.

161. Mouri A, Noda Y, Enomoto T, Nabeshima T. Phencyclidine animal models of schizophrenia: approaches from abnormality of glutamatergic neurotransmission and neurodevelopment. Neurochem Int. 2007 Jul-Sep;51(2-4):173-84. doi: 10.1016/j.neuint.2007.06.019. Epub 2007 Jun 27. PMID: 17669558.

162. Murthy VN, Fetz EE. Synchronization of neurons during local field potential oscillations in sensorimotor cortex of awake monkeys. J Neurophysiol. 1996 Dec;76(6):3968-82. doi: 10.1152/jn.1996.76.6.3968. PMID: 8985893.

163. Nagayama S, Homma R, Imamura F. Neuronal organization of olfactory bulb circuits. Front Neural Circuits. 2014 Sep 3;8:98. doi: 10.3389/fncir.2014.00098. PMID: 25232305; PMCID: PMC4153298.

164. Nasretdinov A, Barrientos SA, Brys I, Halje P, Petersson P. Systems-level analysis of local field potentials reveals differential effects of lysergic acid diethylamide and ketamine on neuronal activity and functional connectivity. Front Neurosci. 2023 May 23;17:1175575. doi: 10.3389/fnins.2023.1175575. PMID: 37287794; PMCID: PMC10242129.

165. Ni L, Xu Y, Dong S, Kong Y, Wang H, Lu G, et al. The potential role of the HCN1 ion channel and BDNF-mTOR signaling pathways and synaptic transmission in the alleviation of PTSD. Transl Psychiatry 2020; 10(1): 101.

166. Nicol AU, Morton AJ. Characteristic patterns of EEG oscillations in sheep (Ovis aries) induced by ketamine may explain the psychotropic effects seen in humans. Sci Rep. 2020 Jun 11;10(1):9440. doi: 10.1038/s41598-020-66023-8. PMID: 32528071; PMCID: PMC7289807.

167. Nicolás MJ, López-Azcárate J, Valencia M, Alegre M, Pérez-Alcázar M, Iriarte J, Artieda J. Ketamine-induced oscillations in the motor circuit of the rat basal ganglia. PLoS One. 2011;6(7):e21814. doi: 10.1371/journal.pone.0021814. Epub 2011 Jul 29. PMID: 21829443; PMCID: PMC3146469.

168. Niemegeers CJ, Laduron PM. Pharmacology and biochemistry of haloperidol. Proc R Soc Med. 1976;69 suppl 1(Suppl 1):3-8. PMID: 14331; PMCID: PMC1863606.

169. Nikolin S, Rodgers A, Schwaab A, Bahji A, Zarate C Jr, Vazquez G, Loo C. Ketamine for the treatment of major depression: a systematic review and meta-analysis. EClinicalMedicine. 2023 Aug 3;62:102127. doi: 10.1016/j.eclinm.2023.102127. PMID: 37593223; PMCID: PMC10430179.

170. Nottage JF, Gabay A, De Meyer K, Herrik KF, Bastlund JF, Christensen SR, Gijsen S, Mehta MA. The effect of ketamine and D-cycloserine on the high frequency resting EEG spectrum in humans. Psychopharmacology (Berl). 2023 Jan;240(1):59-75. doi: 10.1007/s00213-022-06272-9. Epub 2022 Nov 19. PMID: 36401646; PMCID: PMC9816261.

171. Nyhuis TJ, Masini CV, Taufer KL, Day HE, Campeau S. Reversible inactivation of rostral nucleus raphe pallidus attenuates acute autonomic responses but not their habituation to repeated audiogenic stress in rats. Stress. 2016;19(2):248-59. doi: 10.3109/10253890.2016.1160281. Epub 2016 Mar 21. PMID: 26998558; PMCID: PMC4957647.

172. Oliva A, Fernández-Ruiz A, Fermino de Oliveira E, Buzsáki G. Origin of Gamma Frequency Power during Hippocampal Sharp-Wave Ripples. Cell Rep. 2018 Nov 13;25(7):1693-1700.e4. doi: 10.1016/j.celrep.2018.10.066. PMID: 30428340; PMCID: PMC6310484.

173. Olney JW, Farber NB. Glutamate receptor dysfunction and schizophrenia. Arch Gen Psychiatry 1995; 52(12): 998-1007.

174. Olszewski M, Dolowa W, Matulewicz P, Kasicki S, Hunt MJ. NMDA receptor antagonist-enhanced high frequency oscillations: are they generated broadly or regionally specific? Eur Neuropsychopharmacol. 2013 Dec;23(12):1795-805. doi: 10.1016/j.euroneuro.2013.01.012. Epub 2013 Mar 5. PMID: 23466347.

175. Olszewski M, Piasecka J, Goda SA, Kasicki S, Hunt MJ. Antipsychotic compounds differentially modulate high-frequency oscillations in the rat nucleus accumbens: a comparison of first- and second-generation drugs. Int J Neuropsychopharmacol. 2013 Jun;16(5):1009-20. doi: 10.1017/S1461145712001034. Epub 2012 Nov 21. PMID: 23171738.

176. Orser BA, Pennefather PS, MacDonald JF. Multiple mechanisms of ketamine blockade of N-methyl-D-aspartate receptors. Anesthesiology. 1997 Apr;86(4):903-17. doi: 10.1097/00000542-199704000-00021. PMID: 9105235.

177. Ozaki I, Hashimoto I. Exploring the physiology and function of high-frequency oscillations (HFOs) from the somatosensory cortex. Clin Neurophysiol. 2011 Oct;122(10):1908-23. doi: 10.1016/j.clinph.2011.05.023. Epub 2011 Jul 2. PMID: 21724458.

178. Paoletti P. Molecular basis of NMDA receptor functional diversity. Eur J Neurosci. 2011 Apr;33(8):1351-65. doi: 10.1111/j.1460-9568.2011.07628.x. Epub 2011 Mar 14. PMID: 21395862.

179. Park CJ, Hong SB. High Frequency Oscillations in Epilepsy: Detection Methods and Considerations in Clinical Application. J Epilepsy Res. 2019 Jun 30;9(1):1-13. doi: 10.14581/jer.19001. PMID: 31482052; PMCID: PMC6706641.

180. Paxinos G., Watson C. The Rat Brain in Stereotaxic Coordinates. 1998 4th Edition, Academic Press, San Diego.

181. Pérez-Gómez A, Stein B, Leinders-Zufall T, Chamero P. Signaling mechanisms and behavioral function of the mouse basal vomeronasal neuroepithelium. Front Neuroanat. 2014 Nov 26;8:135. doi: 10.3389/fnana.2014.00135. PMID: 25505388; PMCID: PMC4244706.

182. Peters JA, Malone HM, Lambert JJ. Ketamine potentiates 5-HT3 receptor-mediated currents in rabbit nodose ganglion neurones. Br J Pharmacol 1991; 103: 1623–5.

183. Phillips KG, Cotel MC, McCarthy AP, Edgar DM, Tricklebank M, O'Neill MJ, Jones MW, Wafford KA. Differential effects of NMDA antagonists on high frequency and gamma EEG oscillations in a neurodevelopmental model of schizophrenia. Neuropharmacology. 2012 Mar;62(3):1359-70. doi: 10.1016/j.neuropharm.2011.04.006. Epub 2011 Apr 19. PMID: 21521646.

184. Pignatelli A, Belluzzi O. Dopaminergic Neurones in the Main Olfactory Bulb: An Overview from an Electrophysiological Perspective. Front Neuroanat. 2017 Feb 14;11:7. doi: 10.3389/fnana.2017.00007. PMID: 28261065; PMCID: PMC5306133.

185. Pinault D. N-methyl d-aspartate receptor antagonists ketamine and MK-801 induce wake-related aberrant gamma oscillations in the rat neocortex. Biol Psychiatry. 2008 Apr 15;63(8):730-5. doi: 10.1016/j.biopsych.2007.10.006. Epub 2007 Nov 26. PMID: 18022604.

186. Pinching AJ, Powell TP. The neuropil of the glomeruli of the olfactory bulb. J Cell Sci. 1971 Sep;9(2):347-77. doi: 10.1242/jcs.9.2.347. PMID: 4108057.

187. Pitchford B, Arnell KM. Resting EEG in alpha and beta bands predicts individual differences in attentional breadth. Conscious Cogn. 2019 Oct;75:102803. doi: 10.1016/j.concog.2019.102803. Epub 2019 Aug 28. PMID: 31472420.

188. Pittman-Polletta B, Hu K, Kocsis B. Subunit-specific NMDAR antagonism dissociates schizophrenia subtype-relevant oscillopathies associated with frontal hypofunction and hippocampal hyperfunction. Sci Rep. 2018 Aug 2;8(1):11588. doi: 10.1038/s41598-018-29331-8. PMID: 30072757; PMCID: PMC6072790.

189. Price JL, Powell TP. The mitral and short axon cells of the olfactory bulb. J Cell Sci. 1970 Nov;7(3):631-51. doi: 10.1242/jcs.7.3.631. PMID: 5492279.

190. Price JL, Powell TP. The morphology of the granule cells of the olfactory bulb. J Cell Sci. 1970 Jul;7(1):91-123. doi: 10.1242/jcs.7.1.91. PMID: 5476864.

191. Purves D, Augustine GJ, Fitzpatrick D, et al., editors. Neuroscience. 2nd edition. Sunderland (MA): Sinauer Associates; 2001. The Olfactory Epithelium and Olfactory Receptor Neurons. Available from: https://www.ncbi.nlm.nih.gov/books/NBK10896/

192. Ravel N, Caille D, Pager J. A centrifugal respiratory modulation of olfactory bulb unit activity: a study on acute rat preparation. Exp Brain Res. 1987;65(3):623-8. doi: 10.1007/BF00235985. PMID: 3556489.

193. Ray S, Crone NE, Niebur E, Franaszczuk PJ, Hsiao SS. Neural correlates of high-gamma oscillations (60-200 Hz) in macaque local field potentials and their potential implications in electrocorticography. J Neurosci. 2008 Nov 5;28(45):11526-36. doi: 10.1523/JNEUROSCI.2848-08.2008. PMID: 18987189; PMCID: PMC2715840.

194. Ray S, Niebur E, Hsiao SS, Sinai A, Crone NE. High-frequency gamma activity (80-150Hz) is increased in human cortex during selective attention. Clin Neurophysiol. 2008 Jan;119(1):116-33. doi: 10.1016/j.clinph.2007.09.136. Epub 2007 Nov 26. PMID: 18037343; PMCID: PMC2444052.

195. Redmond AM, Kelly JP, Leonard BE. Behavioural and neurochemical effects of dizocilpine in the olfactory bulbectomized rat model of depression. Pharmacol Biochem Behav. 1997 Oct;58(2):355-9. doi: 10.1016/s0091-3057(97)00259-1. PMID: 9300592.

196. Robichaud M, Beauchemin V, Lavoie N, Dennis T, Debonnel G. Effects of bilateral olfactory bulbectomy on N-methyl-D-aspartate receptor function: autoradiographic and behavioral studies in the rat. Synapse. 2001 Nov;42(2):95-103. doi: 10.1002/syn.1105. PMID: 11574946.

197. Rodriguez CI, Kegeles LS, Flood P, Simpson HB. Rapid resolution of obsessions after an infusion of intravenous ketamine in a patient with treatment-resistant obsessive-compulsive disorder. Journal of Clinical Psychiatry 2011; 72: 567–9.

198. Rojas-Líbano D, Kay LM. Olfactory system gamma oscillations: the physiological dissection of a cognitive neural system. Cogn Neurodyn. 2008 Sep;2(3):179-94. doi: 10.1007/s11571-008-9053-1. Epub 2008 Jun 19. PMID: 19003484; PMCID: PMC2518753.

199. Salimi M, Tabasi F, Nazari M, Ghazvineh S, Salimi A, Jamaati H, Raoufy MR. The olfactory bulb modulates entorhinal cortex oscillations during spatial working memory. J Physiol Sci. 2021 Jun 30;71(1):21. doi: 10.1186/s12576-021-00805-1. PMID: 34193043; PMCID: PMC10717170.

200. Sapkota K, Mao Z, Synowicki P, Lieber D, Liu M, Ikezu T, Gautam V, Monaghan DT. GluN2D N-Methyl-d-Aspartate Receptor Subunit Contribution to the Stimulation of Brain Activity and Gamma Oscillations by Ketamine: Implications for Schizophrenia. J Pharmacol Exp Ther. 2016 Mar;356(3):702-11. doi: 10.1124/jpet.115.230391. Epub 2015 Dec 16. PMID: 26675679; PMCID: PMC4767398.

201. Sartiani L, Mannaioni G, Masi A, Novella Romanelli M, Cerbai E. The Hyperpolarization-Activated Cyclic Nucleotide-Gated Channels: from Biophysics to Pharmacology of a Unique Family of Ion Channels. Pharmacol Rev. 2017 Oct;69(4):354-395. doi: 10.1124/pr.117.014035. PMID: 28878030.

202. Schoppa NE, Kinzie JM, Sahara Y, Segerson TP, Westbrook GL. Dendrodendritic inhibition in the olfactory bulb is driven by NMDA receptors. J Neurosci. 1998 Sep 1;18(17):6790-802. doi: 10.1523/JNEUROSCI.18-17-06790.1998. PMID: 9712650; PMCID: PMC6792983.

203. Schuh FT. Influence of ketamine on human plasma cholinesterase. Br J Anaesth. 1975 Dec;47(12):1315-9. doi: 10.1093/bja/47.12.1315. PMID: 1218172.

204. Schultz EF, Tapp JT. Olfactory control of behavior in rodents. Psychol Bull. 1973 Jan;79(1):21-44. doi: 10.1037/h0033817. PMID: 4567728.

205. Shao Z, Puche AC, Liu S, Shipley MT. Intraglomerular inhibition shapes the strength and temporal structure of glomerular output. J Neurophysiol. 2012 Aug 1;108(3):782-93. doi: 10.1152/jn.00119.2012. Epub 2012 May 16. PMID: 22592311; PMCID: PMC3424091.

206. Shaw AD, Saxena N, E Jackson L, Hall JE, Singh KD, Muthukumaraswamy SD. Ketamine amplifies induced gamma frequency oscillations in the human cerebral cortex. Eur Neuropsychopharmacol. 2015 Aug;25(8):1136-46. doi: 10.1016/j.euroneuro.2015.04.012. Epub 2015 May 27. PMID: 26123243.

207. Sheriff A, Pandolfi G, Nguyen VS, Kay LM. Long-Range Respiratory and Theta Oscillation Networks Depend on Spatial Sensory Context. J Neurosci. 2021 Dec 1;41(48):9957-9970. doi: 10.1523/JNEUROSCI.0719-21.2021. Epub 2021 Oct 19. PMID: 34667070; PMCID: PMC8638692.

208. Siapas AG, Wilson MA. Coordinated interactions between hippocampal ripples and cortical spindles during slow-wave sleep. Neuron. 1998 Nov;21(5):1123-8. doi: 10.1016/s0896-6273(00)80629-7. PMID: 9856467.

209. Silva Pereira V, Elfving B, Joca SRL, Wegener G. Ketamine and aminoguanidine differentially affect Bdnf and Mtor gene expression in the prefrontal cortex of adult male rats. Eur J Pharmacol 2017; 815: 304–11.

210. Simola, N. Experimental Psychopharmacology. In: Riederer, P., Laux, G., Nagatsu, T., Le, W., Riederer, C. (eds) NeuroPsychopharmacotherapy 2022 Springer, Cham. https://doi.org/10.1007/978-3-030-62059-23

211. Skoblenick KJ, Womelsdorf T, Everling S. Ketamine Alters Outcome-Related Local Field Potentials in Monkey Prefrontal Cortex. Cereb Cortex. 2016 Jun;26(6):2743-2752. doi: 10.1093/cercor/bhv128. Epub 2015 Jun 3. PMID: 26045564; PMCID: PMC4869811.

212. Sleigh, J.W., Harvey, M., Voss, L.J., Denny, B. Ketamine – More mechanisms of action than just NMDA blockade. Trends in Anaesthesia and Critical Care, 2014, 4, 76-81.

213. Sokolenko E, Hudson MR, Nithianantharajah J, Jones NC. The mGluR2/3 agonist LY379268 reverses NMDA receptor antagonist effects on cortical gamma oscillations and phase coherence, but not working memory impairments, in mice. J Psychopharmacol. 2019 Dec;33(12):1588-1599. doi: 10.1177/0269881119875976. Epub 2019 Oct 3. PMID: 31580222.

214. Sorrenti V, Cecchetto C, Maschietto M, Fortinguerra S, Buriani A, Vassanelli S. Understanding the Effects of Anesthesia on Cortical Electrophysiological Recordings: A Scoping Review. Int J Mol Sci. 2021 Jan 28;22(3):1286. doi: 10.3390/ijms22031286. PMID: 33525470; PMCID: PMC7865872.

215. Średniawa W, Wróbel J, Kublik E, Wójcik DK, Whittington MA, Hunt MJ. Network and synaptic mechanisms underlying high frequency oscillations in the rat and cat olfactory bulb under ketamine-xylazine anesthesia. Sci Rep. 2021 Mar 18;11(1):6390. doi: 10.1038/s41598-021-85705-5. PMID: 33737621; PMCID: PMC7973548.

216. Stan TL, Ronaghi A, Barrientos SA, Halje P, Censoni L, Garro-Martínez E, Nasretdinov A, Malinina E, Hjorth S, Svensson P, Waters S, Sahlholm K, Petersson P. Neurophysiological treatment effects of mesdopetam, pimavanserin and clozapine in a rodent model of Parkinson's disease psychosis. Neurotherapeutics. 2024 Mar;21(2):e00334. doi: 10.1016/j.neurot.2024.e00334. Epub 2024 Feb 16. PMID: 38368170; PMCID: PMC10937958.

217. Su CY, Menuz K, Carlson JR. Olfactory perception: receptors, cells, and circuits. Cell. 2009 Oct 2;139(1):45-59. doi: 10.1016/j.cell.2009.09.015. PMID: 19804753; PMCID: PMC2765334.

218. Su YA, Si TM, Zhou DF, Guo CM, Wang XD, Yang Y, Shu L, Liang JH. Risperidone attenuates MK-801-induced hyperlocomotion in mice via the blockade of serotonin 5-HT 2A/2C receptors. Eur J Pharmacol. 2007 Jun 14;564(1-3):123-30. doi: 10.1016/j.ejphar.2007.02.031. Epub 2007 Feb 27. PMID: 17395179.

219. Subramanian S, Haroutounian S, Palanca BJA, Lenze EJ. Ketamine as a therapeutic agent for depression and pain: mechanisms and evidence. J Neurol Sci. 2022 Mar 15;434:120152. doi: 10.1016/j.jns.2022.120152. Epub 2022 Jan 14. PMID: 35092901.

220. Tiedtke PI, Bischoff C, Schmidt WJ. MK-801-induced stereotypy and its antagonism by neuroleptic drugs. J Neural Transm Gen Sect. 1990;81(3):173-82. doi: 10.1007/BF01245040. PMID: 1975747.

221. Tort AB, Komorowski RW, Manns JR, Kopell NJ, Eichenbaum H. Theta-gamma coupling increases during the learning of item-context associations. Proc Natl Acad Sci U S A. 2009 Dec 8;106(49):20942-7. doi: 10.1073/pnas.0911331106. Epub 2009 Nov 23. PMID: 19934062; PMCID: PMC2791641.

222. Trejo DH, Ciuparu A, da Silva PG, Velasquez CM, Rebouillat B, Gross MD, Davis MB, Muresan RC, Albeanu DF. Fast updating feedback from piriform cortex to the olfactory bulb relays multimodal reward contingency signals during rule-reversal. bioRxiv [Preprint]. 2023 Sep 13:2023.09.12.557267. doi: 10.1101/2023.09.12.557267. PMID: 37745564; PMCID: PMC10515864.

223. Tufo C, Poopalasundaram S, Dorrego-Rivas A, Ford MC, Graham A, Grubb MS. Development of the mammalian main olfactory bulb. Development. 2022 Feb 1;149(3):dev200210. doi: 10.1242/dev.200210. Epub 2022 Feb 11. PMID: 35147186; PMCID: PMC8918810.

224. Tuplin EW, Holahan MR. Aripiprazole, A Drug that Displays Partial Agonism and Functional Selectivity. Curr Neuropharmacol. 2017 Nov 14;15(8):1192-1207. doi: 10.2174/1570159X15666170413115754. PMID: 28412910; PMCID: PMC5725548.

225. Uhlhaas PJ, Singer W. Abnormal neural oscillations and synchrony in schizophrenia. Nat Rev Neurosci. 2010 Feb;11(2):100-13. doi: 10.1038/nrn2774. PMID: 20087360.

226. Valdés-Baizabal C, Soto E, Vega R. Dopaminergic modulation of the voltage-gated sodium current in the cochlear afferent neurons of the rat. PLoS One. 2015 Mar 13;10(3):e0120808. doi: 10.1371/journal.pone.0120808. PMID: 25768433; PMCID: PMC4359166.

227. Wang L, Li X, Chen F, Liu Q, Xu F. Organizational Principles of the Centrifugal Projections to the Olfactory Bulb. Int J Mol Sci. 2023 Feb 26;24(5):4579. doi: 10.3390/ijms24054579. PMID: 36902010; PMCID: PMC10002860.

228. Ward LM. Synchronous neural oscillations and cognitive processes. Trends Cogn Sci. 2003 Dec;7(12):553-9. doi: 10.1016/j.tics.2003.10.012. PMID: 14643372.

229. Weickert CS, Fung SJ, Catts VS, Schofield PR, Allen KM, Moore LT, et al. Molecular evidence of N-methyl-D-aspartate receptor hypofunction in schizophrenia. Mol Psychiatry 2013; 18: 1185–92.

230. Wesson DW, Verhagen JV, Wachowiak M. Why sniff fast? The relationship between sniff frequency, odor discrimination, and receptor neuron activation in the rat. J Neurophysiol. 2009 Feb;101(2):1089-102. doi: 10.1152/jn.90981.2008. Epub 2008 Dec 3. PMID: 19052108; PMCID: PMC2657070.

231. Wickenden AD. Overview of Electrophysiological Techniques. Curr Protoc Pharmacol. 2014 Mar 3;64:11.1.1-17. doi: 10.1002/0471141755.ph1101s64. PMID: 26344208.

232. Wilson MA, McNaughton BL. Reactivation of hippocampal ensemble memories during sleep. Science. 1994 Jul 29;265(5172):676-9. doi: 10.1126/science.8036517. PMID: 8036517.

233. Wimmer K, Ramon M, Pasternak T, Compte A. Transitions between Multiband Oscillatory Patterns Characterize Memory-Guided Perceptual Decisions in Prefrontal Circuits. J Neurosci. 2016 Jan 13;36(2):489-505. doi: 10.1523/JNEUROSCI.3678-15.2016. PMID: 26758840; PMCID: PMC4710772.

234. Wróbel J, Hunt M, Podolecka W: Beyond anesthesia: uses and actions of ketamine. Med Sci Pulse 2024; 18(1): 57-66. https://doi.org/10.5604/01.3001.0054.4952.

235. Wróbel J, Średniawa W, Bramorska A, Dovgialo M, Wójcik DK, Hunt MJ. NMDA receptor antagonist high-frequency oscillations are transmitted via bottom-up feedforward processing. Sci Rep. 2024 Sep 19;14(1):21858. doi: 10.1038/s41598-024-71749-w. PMID: 39300126; PMCID: PMC11413191.

236. Wróbel J, Średniawa W, Jurkiewicz G, Żygierewicz J, Wójcik DK, Whittington MA, Hunt MJ. Nasal respiration is necessary for ketamine-dependent high frequency network oscillations and behavioral hyperactivity in rats. Sci Rep. 2020 Nov 4;10(1):18981. doi: 10.1038/s41598-020-75641-1. PMID: 33149202; PMCID: PMC7642442.

237. Yamaguchi K, Kumakura S, Murakami T, Someya A, Inada E, Nagaoka I. Ketamine suppresses the substance P-induced productionof IL-6 and IL-8 by human U373MG glioblastoma/astrocytoma cells. Int J Mol Med 2017; 39: 687–92.

238. Yan T, Suzuki K, Kameda S, Maeda M, Mihara T, Hirata M. Electrocorticographic effects of acute ketamine on non-human primate brains. J Neural Eng. 2022 Apr 11;19(2). doi: 10.1088/1741-2552/ac6293. PMID: 35354131.

239. Yavi M, Lee H, Henter ID, Park LT, Zarate CA Jr. Ketamine treatment for depression: a review. Discov Ment Health. 2022;2(1):9. doi: 10.1007/s44192-022-00012-3. Epub 2022 Apr 15. PMID: 35509843; PMCID: PMC9010394.

240. Ye T, Bartlett MJ, Schmit MB, Sherman SJ, Falk T, Cowen SL. Ten-Hour Exposure to Low-Dose Ketamine Enhances Corticostriatal Cross-Frequency Coupling and Hippocampal Broad-Band Gamma Oscillations. Front Neural Circuits. 2018 Aug 13;12:61. doi: 10.3389/fncir.2018.00061. PMID: 30150926; PMCID: PMC6099120.

241. Ye T, Bartlett MJ, Sherman SJ, Falk T, Cowen SL. Spectral signatures of L-DOPA-induced dyskinesia depend on L-DOPA dose and are suppressed by ketamine. Exp Neurol. 2021 Jun;340:113670. doi: 10.1016/j.expneurol.2021.113670. Epub 2021 Mar 2. PMID: 33662379; PMCID: PMC9191762.

242. Zepeda NC, Crown LM, Medvidovic S, Choi W, Sheth M, Bergosh M, Gifford R, Folz C, Lam P, Lu G, Featherstone R, Liu CY, Siegel SJ, Lee DJ. Frequency-specific medial septal nucleus deep brain stimulation improves spatial memory in MK-801-treated male rats. Neurobiol Dis. 2022 Aug;170:105756. doi: 10.1016/j.nbd.2022.105756. Epub 2022 May 16. PMID: 35584727; PMCID: PMC9343054.

243. Zhang K, Xu T, Yuan Z, Wei Z, Yamaki VN, Huang M, et al. Essential roles of AMPA receptor GluA1 phosphorylation and presynaptic HCN channels in fast-acting antidepressant responses of ketamine. Sci Signal 2016; 9(458): 123.

244. Zhou W, Wang N, Yang C, Li XM, Zhou ZQ, Yang JJ. Ketamine-induced antidepressant effects are associated with AMPA receptors-mediated upregulation of mTOR and BDNF in rat hippocampus and prefrontal cortex. European Psychiatry 2014; 29: 419–23.

Appendix C

Publications of the PhD candidate

1. **Wróbel J**, Średniawa W, Bramorska A, Dovgialo M Wójcik DK, Hunt MJ. NMDA receptor antagonist high-frequency oscillations are transmitted via bottom-up feedforward processing. Sci. Rep. 2024 14:21858 doi.org/10.1038/s41598-024-71749-w.

2. **Wróbel J**, Podolecka W, Hunt M. Beyond anesthesia: uses and actions of ketamine. Med Sci Pulse 2024;18(1):57-66. doi: 10.5604/01.3001.0054.4952.

3. Średniawa W, **Wróbel J**, Kublik E, Wójcik DK, Whittington MA, Hunt MJ. Network and synaptic mechanisms underlying high frequency oscillations in the rat and cat olfactory bulb under ketamine-xylazine anesthesia. Sci Rep. 2021 Mar 18;11(1):6390. doi: 10.1038/s41598-021-85705-5.

4. **Wróbel J**, Średniawa W, Jurkiewicz G, Żygierewicz J, Wójcik DK, Whittington MA, Hunt MJ. Nasal respiration is necessary for ketamine-dependent high frequency network oscillations and behavioral hyperactivity in rats. Sci Rep. 2020 Nov 4;10(1):18981. doi: 10.1038/s41598-020-75641-1.

5. **Wróbel J**, Wójcik DK, Hunt MJ. D2 receptor activation modulates NMDA receptor antagonist-enhanced high-frequency oscillations in the olfactory bulb of freely moving rats (research article, manuscript under review at *Psychopharmacology*).

6. Hunt MJ and **Wróbel** J. Ketamine-dependent fast brain oscillations (review article, manuscript submitted to the *Journal of Psychopharmacology*).